QATAR UNIVERSITY

COLLEGE OF ENGINEERING

DESIGN OF FULLY POROUS FUNCTIONALLY GRADED TI-6AL-4V FEMORAL

STEM FOR STRESS SHIELDING AND IMPLANT'S STABILITY

BY

NASER FAWZI KHALED AL ZOUBI

A Dissertation Submitted to

the College of Engineering

in Partial Fulfillment of the Requirements for the Degree of

Doctorate of Philosophy in Materials Science and Engineering

June 2022

COMMITTEE PAGE

The members of the Committee approve the Dissertation of
Naser Fawzi Khaled Al Zoubi defended on Tuesday, 10/05/2022.

_____

Prof. Faris Tarlochan
Thesis/Dissertation Supervisor

_____

Dr. Hassan Mehboob
Thesis/Dissertation Co-Supervisor

_____

Dr. Asan Abdul Muthalif
Committee Member

_____

Dr. MD Anwarul Hasan
Committee Member

_____

Prof. Risby Mohammad Sohaimi
Committee Member (External Examiner)

Approved:

_____

Khalid Kamal Naji, Dean, College of Engineering

ABSTRACT

AL ZOUBI, NASER, AL ZOUBI, Doctorate June:[2022],

Doctorate of Philosophy in Materials Science and E

Title: Design Of Fully Porous Functionally Graded Ti-6al-4v Femoral Stem For Stress Shielding And Implant's Stability

Supervisor of Dissertation: Prof. Faris Tarlochan.

The main objective of this study is to design titanium alloy femoral stems with cubic porous structures that will be able to reduce stress-shielding and promote stem stability. Stress-shielding is one of the factors that contributes toward aseptic loosening, which eventually leads to the failure of implants. These porous structure designs were accommodated into the titanium alloy femoral stem as homogeneous and functionally graded porous structures. First, the cubic cellular structures were simulated under compressive loading to measure the yield and modulus of elasticity for various porosity ranges. This allowed the selection of porosity range to design the femoral stems having stiffness in compressive loading identical to that of an intact femur bone. This was done to reduce the stress shielding effects. Based on the selected porosity range, fifteen different arrangements of radial geometrical functionally graded (FG) designs were developed with average porosities of 30, 50, and 70% respectively. The finite element models developed with physiological loads presenting three different walking speeds (1, 3, and 5 km/hrs.), where the average human body weight was assumed. Stresses at the bone Gruen zones were measured to check the percentage of stress transfer to the bone for each porous stem design and were compared with the bulk/dense stem. Micromotion for each design was measured to find the acceptable designs that enable the bone tissue ingrowth (stability of implant). It was found that stems with 70% average porosity had similar stiffness to the intact bone. Besides this, the functionally

graded (FG) porous stems tend to transfer higher stress values to the bone compared to bulk/dense stems for all physiological loads associated with three studied walking speeds. Micromotion values increased as the porosity and physiological loads / walking speed increased, creating a constraint on the amount of porosity that can be introduced in the stem design. Finally, the Fatigue factor of safety of the designed stems was calculated at the studied walking speeds to find the appropriate designs for hip implants. Several FG stems designs were shortlisted as recommended candidates for hip implants.

DEDICATION

Thank you to my academic adviser who guided me in this process and kept me on

track.

Many thanks to my family who inspired me to pursue my doctoral degree.

For the souls of my father and mother, may God have mercy on them

ACKNOWLEDGMENTS

TABLE OF CONTENTS

LIST OF TABLES

LIST OF FIGURES

LIST OF ABBREVIATIONS

Abbreviation	Definition
3D	Three dimensional
3D Printing	Three-Dimensional Printing
316L - SS	316L Stainless Steel
ABAQUS	Finite Element Analysis Software
AM	Additive Manufacturing
Al	Aluminum
BW	Body Weight
CAD	Computer-Aided Design
C3D10 element (in ABAQUS)	General Purpose Tetrahedral Element
CoCrMo	Cobalt Chromium Molybdenum
CPU	Central Processing Unit
DMLS	Direct Metal Laser Sintering
D	Design
G	Gruen Zone
H	Homogeneous
ISO	International Organization for Standardization
L	Layer in Stem Radial Direction
LCCA	Life Cycle Cost Analysis
E	Modulus of Elasticity
EOS	Electro Optical Systems
FEA	Finite Element Analysis
FG	Functionally Graded
FEM	Finite Element Model

FGM	Functionally Graded Material
Nf	Factor of Safety
THA	Total Hip Arthroplasty
THR	Total Hip Replacement
Se,	Endurance Limit
SF	Stem's Failure
Su	Ultimate Tensile Strength,
Sys	Yield Strength,
Ti-4Al-6V	Ti Alloy
Ti	Titanium
TM	Traditional Manufacturing
USA	United States of America
V	Vanadium
VP	Volumetric Porosity

CHAPTER 1: INTRODUCTION

1.1 Research Background

Osteoarthritis and osteoporosis can affect any joint in the body, but it is more common in the hip and knee joints which can be secondary to trauma, avascular necrosis, some metabolic diseases, infection, or alteration of the joint morphology such as hip dysplasia [1]. Many adults and elderly people with severe osteoporosis end up with bone fractures, especially hip fractures, due to small falls [2]. There is no curative treatment for hip joints, and in severe cases, total hip arthroplasty (THA) is the only choice. Besides this, accidents are another factor for the loss of functionality in the hip joint due to fractures which are also treated by THA. According to the epidemiological projections, by 2050 the total number of THA globally will reach 6.26 million [3]. THA in the USA is expected to increase from 930,575 in 2020 to 1,537,422 in 2050 with an annual growth rate of 1.7% [4]. The revision of hip replacement surgery after 20 years varies from 40% for patients less than 50 years old, 30% for ages between 50 and 59 years old, and 15% for ages between 60 and 75 years old [4]. Early hip arthroplasty revisions with the diagnosis of infection and inflammatory reaction, fracture, instability, other mechanical complications, and aseptic loosening over the years 2012 to 2019 are 32.5%, 24.3%, 21,7%, 4.8%, and 4.2% respectively [5], [6].

To treat this enormous number of patients, metallic femoral stem biomaterials like stainless steel, cobalt-chrome alloy, and titanium alloy are conventionally employed in THA. The stiffness of these materials is 4-12 fold greater than the stiffness of the bone [7]–[10]. The high stiffness value of the bulk / dense femoral stems in comparison with femur bone causes numerous complications such as aseptic loosening and stress shielding which may lead to poor bone ingrowth, stem failure, and undesirable revision surgery [7]–[11]. The revision rate of THA performed in the

United States is about 6% after 5 years, 12% after 10 years, and 18% between 10 and 20 years of the initial surgery [12]–[14]. The risk of revision surgeries is higher for young adults (35%), due to an active lifestyle [15], [16].

To treat the THA, initially, the femoral stem was made of stainless steel and its alloy, especially 316L, was used extensively, However, the usage of stainless steel has decreased tremendously primarily due to corrosion issues [17]. Stainless steel stems are replaced by titanium and cobalt chrome alloys, but the recipients of cobalt chrome alloy stems reported more pain compared with those receiving titanium-based stems [18]. This is because the stiffness of cobalt chrome alloy is almost twice that of titanium alloy, which promotes stress shielding, a phenomenon that causes loosening of the femoral stem. Accordingly, in this study, titanium alloy (Ti-6Al-4V) was selected for the stem material because of its light weight, bio-compatibility, good strength, corrosion resistance, and flexibility [19], [20]. But the stiffness of bulk / dense Ti-6Al-4V alloy (114 GPa) is still 6 - 11 times that of cortical bone (10-18 GPa) which may cause stress shielding. The stress shielding is where the stiffer femoral stem takes more bodyweight with insufficient load sharing with the femur bone. As a result, the density of the bone close to the implant starts to decrease [13], [14], [21], [22]. The consequence of this is aseptic loosening of the stem [23]–[25], which is one of the major factors for revision surgeries for THA [13], [14].

Due to their inherent limitations, conventional manufacturing of femoral stems such as casting, and machining is incapable of producing femoral stems with porous cellular architecture to reduce the stiffness and unique shape for stability. It is also costly and time-consuming to produce specifically- customized implants for patients using these traditional manufacturing processes. Introducing cellular porous structures with different porosities is used to customize the stiffness of the femoral stem for

mimicking the bone properties [7]–[11]. Additive manufacturing (AM) technology allows the manufacturing of such cellular geometrical structures and provides flexibility to control the shapes and geometries as needed for each particular patient. Thus, AM can produce porous stems with the desired stiffness to meet the biomechanical and clinical criteria for THA [26]–[28] to overcome the aforementioned problems.

This study introduces a functionally graded porous structure in the radial direction of the femoral stem. A previous study [29] has investigated longitudinal functionally graded stems. Hence, to complete the understanding of functionally graded stems, it is vital to investigate the radial direction. This is important to mimic the mechanical properties of the femur bone, which is split up into two parts: cortical, and cancellous (trabecular) bones, and as the mechanical properties of each type are depending on the mineral density in the mineral matrix, the bone can be considered as functionally graded in the radial direction. Computational analysis will be utilized here as it is an accepted means of investigating the performance of implant-related devices [30]–[33]. These functionally graded structures are designed to have average porosities of 30%, 50% and 70% in radial layers. A total of fifteen designs were generated and these designs were subjected to physiological loads mimicking three walking speeds, namely 1 km/hr., 3 km/hr., and 5 km/hr. The commercially available finite element software ABAQUS was used to simulate the stems using three different walking speeds. The stresses in stem layers and proximal bone were calculated to estimate the life of the stem, micromotion, and stress shielding, respectively.

1.2 Research Problem Statement

Failure of the hip joint is a familiar problem that occurs because of degenerative diseases such as osteoarthritis and osteoporosis. Osteoarthritis is due to the wear and tear of arthritis. Obesity can be considered as one of the causes that increases osteoarthritis among older people. Osteoporosis is the status of the bone when its density becomes less. It occurs due to a low estrogen level, especially in women, which can lead to mineral deficiencies (i.e., Calcium), and then the bone density becomes less with an inactive lifestyle. Also, several types of accidents can cause hip failures, such as traffic, slip and drop, sports, and other reasons that may cause a strong impact.

Total Hip Arthroplasty (THA) is a surgical procedure in which the injured femoral head is replaced with a metal femoral stem to reinstate the hip joint functionality. However, premature femoral stem failure due to stress shielding, micromotions, and fatigue is the main problem of the available femoral stems that leads to total hip arthroplasty another time. The stress shielding effect could be avoided if the elastic modulus of the femoral stem material is close to the femur bone's elastic modulus. One of the reasons is the unavailability of manufacturing technology to allow the manufacturing of functionally graded materials to mimic the human bone's elastic modulus.

In this study, a comprehensive investigation for designing lightweight Ti-4Al-6V alloy femoral stems by introducing porosity of cubic cellular structure that can be manufactured using additive manufacturing methods such as Direct Metal Laser Sintering (DMLS). Different fully porous geometrical designs were employed to generate innovative cellular structures having mechanical properties that are significantly closer to the femur bone properties using the computation finite element method. Three-dimensional (3D) finite element models were established to study the

4

stress shielding, micromotions, and fatigue behaviors of different fully porous homogeneous and functionally graded (FG) femoral stems presenting various stiffness arrangements under unique physiological loading conditions associated with selected walking speeds using commercially available finite element analysis software (ABAQUS).

1.3 Impact of the Study

Total hip replacement is a common surgery globally. The number of THA may reach six million globally by 2050. Around $6 - 12\%$ of these patients will need to undergo revision surgery due to aseptic loosening after $5 - 10$ years of the initial surgery. Aseptic loosening is caused by stress shielding, a phenomenon where the bone density reduces because the femoral implant takes the body load (stiffer implant). This phenomenon can be reduced if the femoral stem has stiffness matching that of the femur bone. One of the ways to achieve this is to introduce porosity in the stem design. Functionally graded porosity is a viable option to lower stress shielding by reducing the stem stiffness and density without compromising strength. Besides this, customized stem geometry can offer the patient the best available solution. The difficulty of bringing this idea to life is the limitation of traditional manufacturing techniques.

1.4 Objectives of the Study

The main objective of this proposed study is to design, develop, and make ready to fabricate a lightweight - porous titanium alloy femoral stem from Direct Metal Laser Sintering (DMLS), with sufficient reduction in stress shielding, micromotion, and acceptable fatigue factor of safety. This objective is supported by the following scopes:

a) To design fully porous homogeneous and functionally graded femoral stems to promote stability and a significant reduction in stress shielding.

5

b) To study the influence of unique physiological loading conditions on the stem's micromotion, and stress shielding.

c) To investigate the fatigue behavior of functionally graded and fully dense Titanium alloy femoral stems at different stress levels associated with different physiological loading conditions.

1.5 Methodology

The research design and methods were developed systematically by tasks to address the objectives of this study. There are a total of four (4) tasks in this proposed study, each explained in detail in the following sub-sections.

a) Design of porous cellular structures to mimic the stiffness of the human femur bone.

b) Design of the femoral stems with a range of volumetric porosities that can be grouped under three average porosities, namely, 30%, 50% and 70% with different porosity arrangements in the stem's radial direction.

c) Performance evaluation of the designed stems under three physiological loading conditions associated with walking speeds of 1Km/hr., 3Km/hr., and 5Km/hr.

d) Life Cycle Cost Analysis (LCCA) of adopting AM for producing the proposed stems.

1.6 limitation of the study

a) Bone mechanical properties of the femur are not unique and differ from one patient to another following the patient's bone status, geometry, age, sex, and the mineral availability in the mineral matrix. However, in this

study, the bone (cortical and cancellous) material properties used are fixed for all cases.

b) The simplified materials assignment for the stems in the finite element model is used instead of the actual porous ones, however, the simplified model is justified and validated, and there should be some deviation in the results from the accurate ones.

c) The square pore cellular structure was considered oriented vertically similar to the designed cubes. It is required during the manufacturing to have the same orientation within the stem's structure vs the loading direction.

d) This study only focuses on immediate postoperative conditions of the implanted stems, but the long-term osseointegration and bone remodelling were not taken into consideration.

e) The fatigue analysis was done using static loading conditions and fatigue analysis using dynamic loading conditions was not conducted. This shall be part of the future work to provide greater accuracy.

f) The proposed designs were assessed using computation analysis, manufacturing the proposed designs using additive manufacturing technology and subjecting the manufactured samples to physical mechanical testing is desired to compare the results and proper validation of the designs.

g) Manufacturing the proposed porous stems using additive manufacturing methods deems to be sustainable in terms of environmental, social, carbon footprint, and considerable cost saving.

CHAPTER 2: LITERATURE REVIEW

2.1 Introduction

Osteoarthritis and osteoporosis are degenerative diseases that are quite common in the world, especially among the elderly. Osteoarthritis, or degenerative joint disease, is a process that causes progressive wear and tear on the joint with impaired function and pain. Osteoarthritis can affect any joint in the body, but it is most common in the hip and knee. Hip osteoarthritis can occur as a result of trauma, avascular necrosis, certain metabolic disorders, infection, or changes in joint morphology such as hip dysplasia. The cause of primary coxarthrosis is unknown, but there are several predisposing factors such as obesity, family history (genetic background), lifestyle, and occupation. There is no cure for hip osteoarthritis and hip replacement is the most suitable option in severe cases. Osteoporosis is a condition in which the bones become weak and brittle. This is due to the reduction in bone density, which is a normal aging process. However, for some, this process can be profoundly serious. Many older people with severe osteoporosis have fractures, especially hip fractures from small falls [2].

However, some teenagers and young adults may suffer from a condition called hip dysplasia, which is a kind of illness causing a lack of usual development of the hip joint [34]. One of the consequences of these diseases is loss of functionality and excruciating pain in the hip joint. In addition, accidents (quite common in young adults) are another factor in the loss of function of the hip joint due to a fracture. In either case, in the event of illness and accident, the hip joint must undergo total hip arthroplasty (THA), a surgical procedure wherein a damaged joint is replaced by artificial components.

With THA (also called total hip replacement - THR), the damaged hip joint (bone and cartilage) is taken away and replaced with hip implants (prosthesis). In THA, the hip joint is removed (the femoral head with its neck is excised, and the acetabulum reamed) and the joint is replaced with an artificial joint or prosthesis. The prosthesis consists of two main components, the femoral part (stem and head) and the acetabular part (cup and liner). Figures 2.1 and 2.2 depict the hip implants as well as the various components that make up the implant. Most of these implants are made of either a titanium alloy (highest bio-compatibility) or cobalt-chromium. The densities of these materials are 2-4 times greater than bone density, making these implants relatively stiffer when inserted into the femur. The traditional fabrication of femoral stems such as casting and machining due to their inherent limitations has limited the study of new hip implants with tailorable stiffness and unique shape for stability. It is also expensive and time consuming to use these traditional manufacturing techniques to produce specific and tailor-made implants for patients.

In joint replacement operations such as hip replacement, one of the most important criteria for success is the need for revision surgery. From the data collected [12], it has been reported that the recovery rates for THA are around 6% after 5 years and 12% after 10 years of surgery. According to the epidemiologic projections, by 2050 the total number of THA globally will reach 6.26 million [3]. THA in the USA is expected to increase from 930,575 in 2020 to 1,537,422 in 2050 with annual growth rate of 1.7% [4]. There will be 20,000 to 40,000 revision surgeries 5 to 10 years after the first replacement surgery in the USA alone. As the annual number of THA increases, revision surgeries also increase [4], [13]. This can be corroborated by the World Health Organization prognosis that osteoarthritis will be the fourth leading cause

of disability by 2020 due to increased life expectancy [35]. Since osteoarthritis is one of the contributing factors to THA, it will increase the number of hip replacement surgeries and the number of revision surgeries. Revision surgeries are expensive and carry a high risk of complications [36], [37].
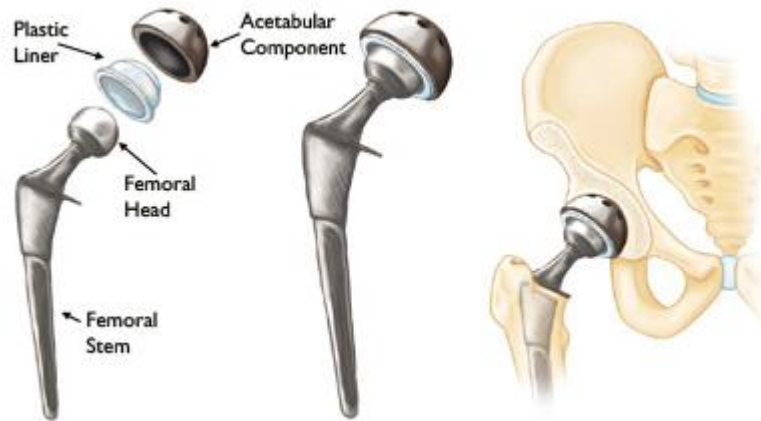
Figure 2.1. Hip prosthetic [Source: http://orthoinfo.aaos.org]

Figure 2.2 Components of the hip prosthetic [Source:http://www.tri-stateorthopaedics.com/total-hip-joint.html]

The hip joint and the femur bone carry the weight of a person. Bone growth and density depend on load carrying capacity. Wolff's Law is a theory created by Julius

Wolff (1836-1902), the German anatomist and surgeon; in this theory, bones adapt to loads. The load stimulates bone remodeling and becomes stronger over time. When physical activity decreases, the bone becomes weak [22]. People who exercise have denser bones than those who do not. The hip joint and femur carry a person's weight. Due to its function as the main load standing structure of the body, the femoral bone is very dense [38]. Over time, the density of the femoral bone (proximal femur part specifically) in patients with hip implants decreases due to phenomena known as stress shielding [14], [24], [25], [29]. In stress shielding, the stiffer femoral stem takes on the role of supporting the body's weight, with only a small share of the load being on the femoral bone itself. This causes a poor distribution of mechanical stresses on the femoral bone. As a result, bone density near the implant begins to decrease [7], [13], [14]. This results in aseptic loosening of the hip joint [7], [24], [29], which is one of the main factors in revision surgery for PTH [7]–[11]. This can be easily explained with the help of figure 2.3.

(a)   (b)
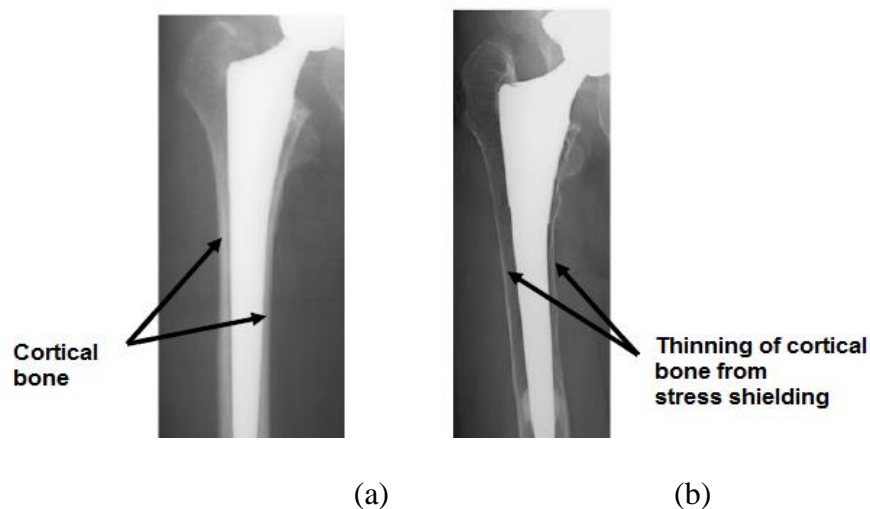
Figure 2.3 Radiographs of femur bone depicting stress shielding. (a) 1 month after surgery (b) 5 years after surgery. (Source: Nishino et al. [19])

In summary, the design of the femoral stem should include the means to reduce stress shielding. This can be achieved by adapting the stiffness of the femoral stem [7]–[11], [39]. With the intention to increase the implant stability, the shape of the femoral stem and the addition of porosity to the stem surface to promote bone growth (osseointegration) must be taken seriously [40]. Therefore, the introduction of functionally gradated porosity into the femoral stem could reduce stress shielding and improve stability. This therefore, justifies focusing this study on the femoral stem.

2.2 The hip joints

The medical definition of a hip joint is acetabular femoral joint. It is basically a ball and socket joint as illustrated in Figure 2.4.
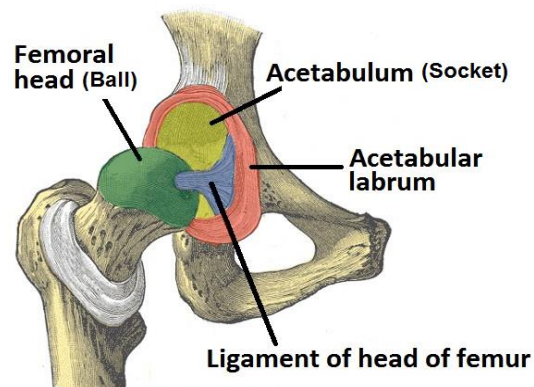
Figure 2.4 Acetabulo femoral joint

[Source: http://teachmeanatomy.info/lower-limb/joints/the-hip-joint/]

The ball consists of the femoral head, which is naturally spherical. The socket, on the other hand, is the acetabulum. The ball fits into the socket to allow articulation around the hip joint. There are many muscles involved in the movement of the hip joint. In principle, the hip joint has 6 degrees of freedom. The main movement consists of

rotations along three different axes, with very few translations along these axes. The forces exerted in the hip joint vary with the level of activity [41]. During normal walking, the average maximum reaction force of the hip joint is approximately 2.5 times body weight [41].

2.3 Material properties of the femur bone

The bone's mechanical properties and quality play an important role in successful arthroplasty surgical operation and implant stability [42]. The mechanical property of the bone varies with sex, age, location, and type and orientation of the loads applied. The bone as a living organ has two types of bone structures, namely, cortical, and cancellous / trabecular bone. Yvonne Haba et al [43] studied the relationship between the mechanical properties of the femoral bone and the mineral density and found that the mechanical properties of the bone are linearly correlated to the bone mineral densities. This is valuable for the proper treatment of each specific patient, specifically, to provide a proper selection and design for the total hip arthroplasty / replacement based on the particular bone quality [43]–[45].

To avoid fracture under any physiological activities and normal loading conditions, it is vital to have strong enough bone. The bone mechanical properties depend on the mineral availability in the mineral matrix. The femur bone is split into two parts: cortical, and cancellous (trabecular) bones. The bone material properties are heterogeneous and anisotropic. However, cancellous bone has been considered homogeneous for the simplicity of the analysis [46]. Cortical bone has several Young's moduli and Poisson's ratio that have been utilized in three

orthogonal directions as shown in table 3.3 [7], [10], [29], [47] which shows that the cortical bone demonstrates an anisotropic material behaviour.

Bone structure adapts to the applied mechanical loading and the environment in which it resides. Hence, the bone architecture and mass are adjusted based on the applied mechanical stresses [22], [38], [48]. So, remodelling of the bone is a crucial issue required for femoral stem design and performance analysis.

2.4 Materials of femoral stem and classifications design

The materials of the femoral stem are called orthopedic materials and these materials must be bio-compatible. The first material used for femoral stems was stainless steel. The alloy, in particular 316L, has been widely used until recently [17]. However, the use of stainless steel has declined dramatically due to corrosion problems [17]. Stainless steel stems are gradually being replaced by titanium and cobalt-chromium alloys. However, cobalt-chromium alloy stems have been reported to cause twice as much pain in the thigh as titanium-based stems [18]. In fact, the rigidity (stiffness) of cobalt-chromium is twice that of titanium, which promotes stress shielding, a phenomenon that causes loosening of the femoral stem. Titanium alloy (Ti-6Al-4V) is therefore the preferred stem material due to its low weight, bio-compatibility, strength, corrosion resistance, and flexibility (less stiff)[19], [20].

Femoral stems have two designs, namely Monoblock (one-piece) and modular (Figure 2.5). With the Monoblock construction, the stem and head are made in one piece. With the modular design, the stem and stem head are manufactured separately and connected to each other by a mechanical taper connection. Modular stem designs are the most preferred among orthopedic surgeons because they allow a degree of

customization and have successful clinical records [14], [49]. The femoral stems can be fixed in the femoral bone by two methods, cementless or cemented, as shown in Figure 2.6. The type of fixation used depends on the patient and the condition of the femoral bone, but in general, cementless fixation is gaining popularity [50]. The advantage of cementless fixation is that it promotes bone ingrowth and the long-term stability of stems with rough, porous surfaces [29].

Figure 2.5 Modular vs. Monoblock femoral stem designs

[Source: http://www.stanmoreimplants.com/custom-hip-implants.php]
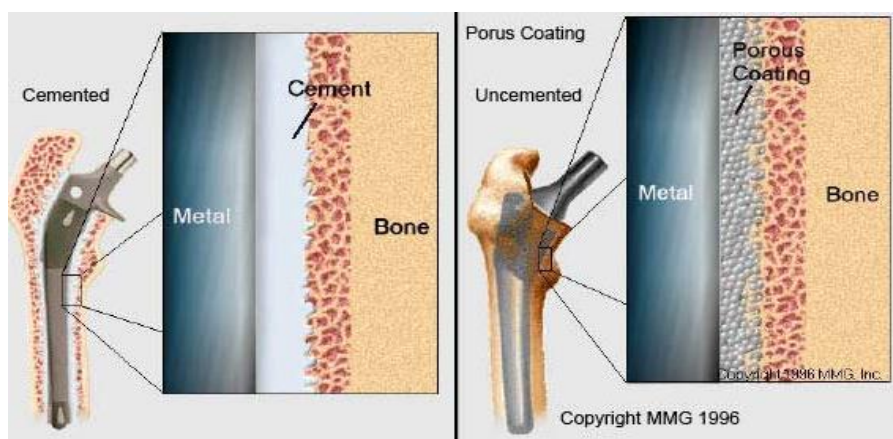
Figure 2.6 Cemented vs. cementless femoral stem fixations

[Source: http://www.healthpages.org/surgical-care/hip-joint-replacement-surgery/]

2.5 Failure in femoral stem and design of materials

Failure of total hip arthroplasty (THA) due to the femoral stem fracture is a critical clinical challenge with various complications. In the past, cases of such fractures have been reported by various research groups examining removed implants for causes of failure[51]–[53]. These possibilities could be linked to design intricacies, manufacturing processes, surgery methods, or even the patient's body weight and the level of activities of an individual [3]. In fact, fatigue has been defined previously as a mechanism that compromises the survival of THA [54]–[56] and remains a problem even for relatively new adapted material generations such as Cobalt – Chrome and Titanium alloys.

Various research groups have produced several research results on possible failure mechanisms depending on the influence of composition, microstructure, fractographic patterns, engineering designs, etc. [9], [10].

Although the fracture patterns vary with the designs, surface characteristics (coated and uncoated), the initial microstructure, and the type of processes used to construct the femoral stem, as well as the load distributions, the signatures of such failures are characterized by a medially located open microcrack and surface roughness. This microcrack can be caused by the effect of high compressive stresses cyclically generated by additional compression load and mediolateral femoral stem bending and can indicate a larger number of these medially developed cracks. Such patterns, on the other hand, are established fatigue process indicators.

In recent years, a popular approach to changing THA has been based on modular prostheses utilization [55], [57]. In most cases, tapered cones are used for metal-to-metal connections along the femoral stem. These arrangements make it easier to restore

the patient's anatomy by the surgeon through biomechanical repair of leg offset and length. The filling of the proximal and distal canals can be flexibly adjusted. In addition, preservation of the soft tissue structures is attained, and problems associated with the bone loss and the deformations of the femur during the surgical operation can be controlled [55], [57]. Also, other issues related to differences in the femur length, instability and offset can be controlled during the surgical operation [58]. Modular central rod connection had been offered to overcome the issues associated with the differences in bone conditions between the patients, this allows the proximal and distal body designs to be independently selected [59]. It can also be seen that in the modular type of stem, the fit failure begins to occur at contact ends of the distal and proximal conical stem point, where the cross-sectional reduction is available in the distal stem end [58]. The coupling is not an ideal one in this area, which promotes micro-movements that lead to increased wear and roughness. The extent of the unstable crack expansion of the fracture area indicates that fatigue fracture occurred at high cycles and low rated loads, as evidenced by the ratchet micromechanics, beach marks and poor formation quality of the striations which covers a minimum of 75 % of the surface [60]. The fracture is made up of 2-oblique and 1-transverse planes, that is occurred due to the cracks - propagation direction changes at the time of loading [58], [59].

In general, femoral stem fixation failure is attributed to many reasons, Figure 2.7 shows some of these popular causes; however, the aseptic loosening is considered as a mean reason. Aseptic loosening can be caused by Stress shielding of periprosthetic bone, implant wear, and relative micromotion at the bone - femoral stem interface.
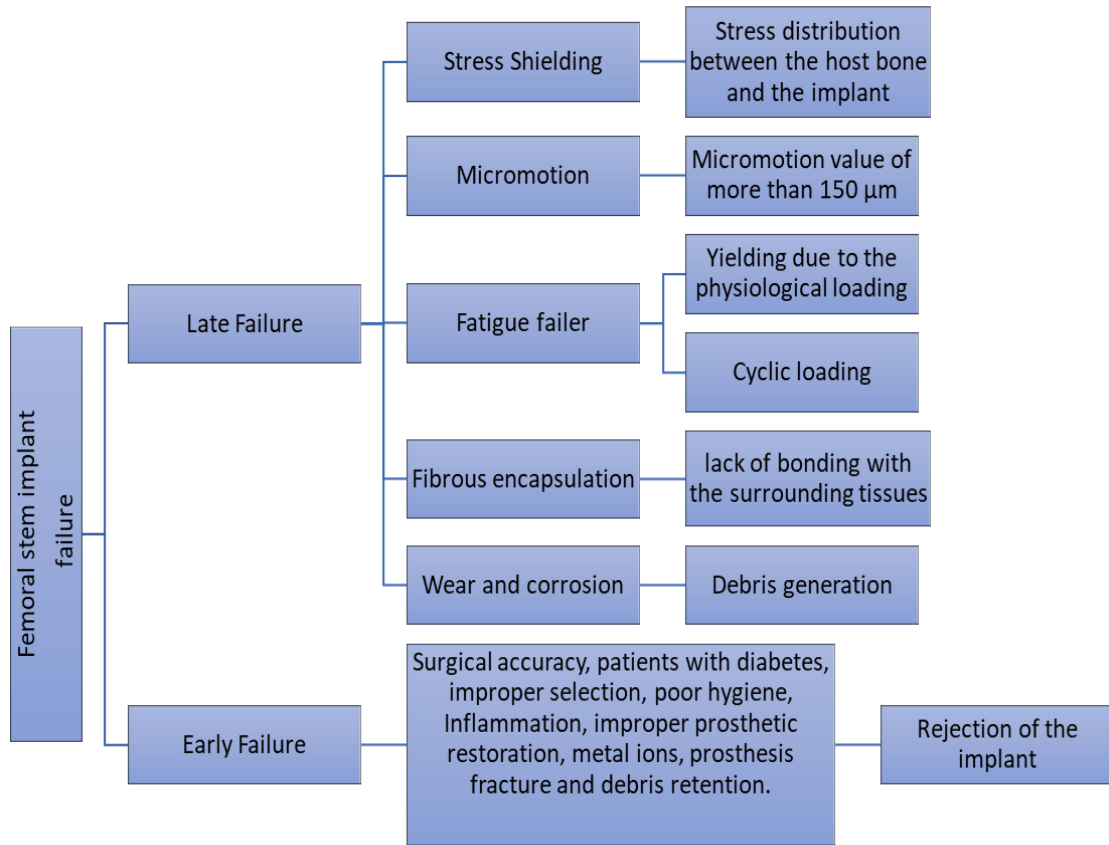
Figure 2.7. Implant failure reasons leading to revision surgery [61]

2.5.1 Stress shielding

Stress shielding is an observable mechanical fact that may lead to poor bone ingrowth, and stem failure due to the loosening of the femoral stem [9]–[11], [62]–[64]. The stress shielding is where the stiffer femoral stem takes more bodyweight, with insufficient load sharing with the femur bone. As a result, the density of the bone close to the implant starts to decrease [13], [14], [22], [35], [62]. The consequence of this is aseptic loosening of the stem [24], [25], [29], [62], which is one of the major factors for revision surgeries for THA [13], [14], [62].

Femoral stems made of metallic biomaterials such as stainless-steel, cobalt-chrome alloy, and titanium alloy are conventionally used in THA. The stiffness of these materials is 4-12 folds greater than the stiffness of the bone authors [9], [10], [63], [64].

The high stiffness of the bulk / dense stems in comparison to the femur bone causes various complications such as aseptic loosening and stress shielding [9]–[11], [24], [62]–[64]. The revision rate of THA performed in the United States is about 6% after 5 years, 12% after 10 years, and 18% between 10 and 20 years of the initial surgery [12]–[14]. The risk of revision surgeries is higher for young adults (35%), due to an active lifestyle [15], [16]. The stiffness of the stem materials is a main factor in ensuring load and stress transfer to the adjacent bone. A stiffer stem shows more stress shielding as less load is transferred to the bone. Hence, Titanium alloy (Ti-6Al-4V) can be a suitable candidate for the stem material because of its light weight, bio-compatibility, good strength, corrosion resistance, and flexibility [19], [20]. But the stiffness of bulk / dense Ti-6Al-4V alloy (114 GPa) is still 5 - 10 folds of cortical bone (10-18 GPa) which may cause stress shielding [62]. Producing a femoral stem with porous cellular architecture with a unique shape to reduce the stiffness and enhance the stability can be the best choice to overcome the stress shielding dilemma.

The stress shielding can be assessed by evaluating the performance of the stems based on stress distribution along the Gruen Zones resulting from the loads transfer from the implanted stem to the femur bone (Figure 2.8). [62]
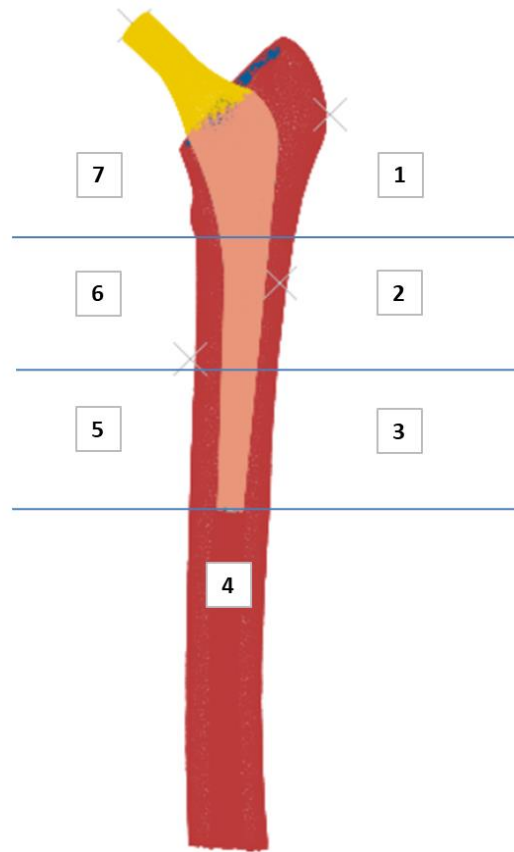
Figure 2.8. Gruen zones for measuring the stress distribution resulting from the loads transfer from the implanted stem to the femur bone

Gruen zones is the commonly used for evaluation of the remodeling following the implantation of femoral stems. These zones were developed by Gruen et al in 1979 to study the modes of failure of the femoral stems using radiographic evaluation method [65]. Zones 1 and 7 were defined at the distal area of the stem-femur interaction, zones 2–3 and 5–6 respectively the lateral and medial zones, and zone 4 represents the overall bone region distally from the stem's tip. [66].

Gruen et al described the modes of failures of the femoral stems which were divided into 4 modes as illustrated in Figure 2.9 [65].

I	Ia	Pistoning: stem within cement	
	Ib	Pistoning: stem within bone	
II		Medial midstem pivot	
III		Calcar pivot	
IV		Bending cantilever (fatigue)	

Figure 2.9. Gruen et al Modes of femoral stem failures [65]

2.5.2 Micromotion at the stem–femur interface

Micromotion is the relative movement between the femoral stem surface and the host bone in relevant to the applied physiological loads. Micromotion assessment is vital to evaluate the bone tissue ingrowth; micromotion value of more than 150 µm is considered excessive and causes instability of the implant [9], [11], [62].

The stem–bone stability can be classified as primary, and secondary [67]. Primary stability refers to the stem–bone stability just after the stem insertion surgery [67], [68]

that can be affected by many factors such as surgical accuracy, method of fixation, patients with diabetes, improper femoral stem selection, poor oral hygiene, inflammation, improper prosthetic restoration, and debris retention [61], [62]. Secondary stability refers to the biological stability after bone tissue ingrowth of the cementless implant fixation. In order to attain secondary stability, it is vital to establish a perfect primary stability and to have a stem design that promotes bone tissue ingrowth which can be achieved by designing a stem with a porous structure [67], [69], [70]. Cancellous bone microstructure quality is also important to achieve secondary stability [42].

2.5.3 Femoral stem wear debris

Wear resistance of the femoral stem material is vital for a safe implant lifetime. Wear debris can cause undesired biological consequences on the density of the femoral bone and implant stability leading to a lessening in the expected femoral stem lifespan and revision surgery [71].

The wear debris that builds up can also cause harmful consequences such as the release of harmful enzymes, inflammation, osteolysis, pain, infection, and implant loosening [67], [71]. The most commonly used material for implants is Ti-6Al-4V, this is attributed to its excellent bio-compatibility, excellent mechanical properties, corrosion, and wear resistance.

2.5.4 Fatigue

Fatigue is a material failure which occurs due to cyclic loading exposure normally below the yield strength limit of the material leading to material lifespan or life cycle reduction. It can be affected by several factors such as maximum and minimum stress,

endurance limit, yield strength, surface finish, heat treatment, and material quality. Sustaining the maximum required fatigue life cycle represents a superior design. This can be evaluated during the design phase either by physical fatigue testing or via fatigue analysis using the finite element analysis method.

Fatigue fracture is one of the major problems associated with femoral stem failures [72], [73]. Femoral stems fracture may occur due to several factors, including, but not limited to, high loading on the stem due to activity levels or patient age, sex and weight, stem alignment inside the femur, femoral stem geometry, material mechanical properties, and fabrication defects [46], [74], [75].

Porous cellular microstructures were reported to have a fatigue strength fraction of the effective yield strength of $0.3\sigma_{Ys}$ approximate [7], [9], [76]–[78]. However, this strength value is also affected by many factors such as stress ratio (R), the percentage of the volumetric porosity, and the type of porosity unit cell [79], [80]. The cubic unit cell structure shows superior performance in fatigue in relation to the other unit cell types such as diamond [79].

Yavari et al. [81] carried out a fatigue study on different porous Ti-4Al-6V alloy structure types with different volumetric porosities ranging from 63% to 89%. The samples were manufactured using selective laser additive manufacturing method, and fatigue was mechanically tested under compression with stress ration of 0.1 and sinusoidal shape with 15Hz frequency. The results of this study shows none of the cubic porous structure specimens failed under fatigue testing even at maximum load of 80% of the relevant porous structure yield strength ($0.8\sigma_Y$) applied. These porous cubic structures reached 10^6 loading cycles without signs of failure. This is attributed to the vertical struts performing better than the diagonal and horizontal ones in compression loading conditions [81], [82].

The fatigue life of the diamond unit cell porous Ti-4Al-6V alloy structure fatigue life depends on the volumetric porosity induced to the designed structure, i.e. as the volumetric porosity increased the fatigue life decreased as reported by Yavari et al. [81]. Hence, the cubic unit cell structure shows superior performance in fatigue over the diamond structure. Due to that, the cubic unit cell structure was selected to be used in the current study.

However, it is necessary to have a balance between the required reduction in porous structure stiffness and an acceptable fatigue limit. So, it is desired to ensure the designs are safe under certain physiological loading conditions based on the yield strength of the porous structure and the Fatigue Factor of Safety limit ($N_f > 1.0$) [62], [83]. In many studies, the factor of safety was calculated for femoral stem designs using Soderberg Approach. This approach is efficient for estimating the fatigue limit for the moral stem under high cyclic loading conditions [9], [54], [56], [62], [72], [83].

The fatigue life can be calculated using several methods such as Gerber, Soderberg, and Goodman [83]. The calculations associated with each method are represented in the following equations which all are associated with the mean stress σ_m, and the alternating stress σ_a:

$$\sigma_m = \frac{(\sigma_{max.} + \sigma_{min.})}{2} \tag{2.1}$$

$$\sigma_a = \frac{(\sigma_{max.} - \sigma_{min.})}{2} \tag{2.2}$$

Where σ_{max} and σ_{min} represent the maximum stresses and the minimum stresses. Gerber's approach is defined as follows:

$$\left(\frac{N\sigma_a}{S_e}\right) + \left(\frac{N\sigma_m}{S_u}\right)^2 = 1 \qquad\qquad (2.3)$$

Goodman's approach is defined as follows:

$$\left(\frac{\sigma_a}{S_e}\right) + \left(\frac{\sigma_m}{S_u}\right) = \frac{1}{N} \qquad\qquad (2.4)$$

Soderberg's approach is defined as follows:

$$\left(\frac{\sigma_a}{S_e}\right) + \left(\frac{\sigma_m}{S_{ys}}\right) = \frac{1}{N} \qquad\qquad (2.5)$$

Where S_e, S_u S_{ys}, and N represent the endurance limit, ultimate tensile strength, yield strength, and factor of safety respectively.

Senalp et al. [83] studied different bulk / dense Ti-4Al-6V alloy femoral stem designs with different shapes under static and dynamic loading using finite element analysis to calculate the fatigue factors of safety based on Gerber, Goodman, and Soderberg approaches as illustrated in tables 2.1 and 2.2. The main findings in the study are that there are differences in the factor of safety in reference to each calculation approach with the lowest values reported in the Soderberg approach. The second finding is that the calculated factors of safety in dynamic loading conditions are less than those for static loading conditions for all designs and calculation approaches.

Table 2.1 Factor of safety based on static analysis for bulk /dense Ti-4Al-6V alloy stems [83]

Fatigue theories	Minimum safety factor				
	Charnley	Stem-1	Stem-2	Stem-3	Stem-4
Mean stress curve	2.74	2.94	3.08	3.27	3.24
Goodman	2.23	2.41	2.54	2.67	2.65
Soderberg	2.18	2.37	2.49	2.62	2.60
Gerber	2.65	2.85	2.98	3.16	3.14

Table 2.2 Factor of safety based on dynamic analysis for bulk /dense Ti-4Al-6V alloy stems [83]

Fatigue theories	Minimum safety factor				
	Charnley	Stem-1	Stem-2	Stem-3	Stem-4
Mean stress curve	2.20	2.35	2.46	2.61	2.59
Goodman	1.78	1.92	2.03	2.13	2.10
Soderberg	1.74	1.90	1.99	2.10	2.08
Gerber	2.12	2.28	2.38	2.54	2.51

In the study, static analysis was employed based on the Soderberg approach as this approach provides the worst-case scenario among the other approaches as detailed in the Senalp et al. [83] study.

2.6 Finite element analysis

Finite Element Analysis (FEA) is an effective and powerful tool that has been employed and widely applied in implant performance, and bio-mechanical studies. Mechanical design is deemed faster and more cost-effective than mechanical testing. FEA is a robust tool which provides complete mechanical data and mechanical properties throughout the design structure, thus allowing designers to

evaluate the design and make necessary modifications before prototyping and performing physical-mechanical testing. Since the early 1970s, FEM has been adopted for human bone stress assessment and evaluation, particularly for hip modeling [46].

Due to the limitations of the mechanical testing of the bio-mechanical structures by in-vivo or in-vitro such as ethical constraints, time, excessive cost, and elevated level of testing variability, FEA is considered the ultimate solution for preclinical analysis. Several studies were carried out for modelling of the hip stems using FEA to investigate the effectiveness of the design on stress shielding, micromotion, and stem life cycle under different loading conditions [7]–[11], [24], [29], [84].

Several aspects and parameters need to be considered for modelling the Total Hip Arthroplasty (THA) that influences the implant performance, as the following.

2.6.1 Material properties

The prefabricated femoral stem design enables the use of various bio-compatible materials with properties that meet the functional requirements [85], [86] and increase the expectations to last longer than previously. Studies have proven that Ti-6Al-4V (Ti-6Al-4V alloy) is a perfect bio-medical material for hip implants in terms of strength, bio-compatibility, corrosion resistance, light weight, and flexibility [87]–[89]. The stiffness of the Ti-6Al-4V alloy is 5 -10 times stiffer than that of the femur bone [88], [90]. For that reason, stems with porous structure designs have been developed to reduce the stiffness, improve the trabecular bone tissue ingrowth that facilitates the integration of the implanted stem with the hosting bone [91], and significantly reduce the stress shielding [90]. The forces exerted on the implanted stem depend on various human activities such as stair climbing,

running, jogging, and walking at various speeds, generating dynamic stresses leading to fatigue fracture [54]. Many researchers in their studies have focused on transferring part of the applied stresses on the stem to the femur bone in order to reduce the stress shielding and micromotion without taking into account the fatigue failure due to the dynamic stresses. Most of the previous studies have shown to predict the fatigue limit using FEA for bulk / dense stems under concentrated compression loads, while few studies have been performed for stems with a porous structure [51], [52]. No literature was found to calculate the fatigue life for porous stems using different physiological loads.

Assigning proper material properties for the model simulation is important to achieve sufficient accuracy in the finite element analysis. The elastic–plastic data of the bulk / dense Ti-6Al-4V alloy with 115GPa elastic modulus were utilized to assign the material properties for the different types of the proposed porous structures [8]–[10], [92]. The use of a cubic porous cellular structure provides outstanding mechanical performance and relatively isotropic mechanical properties [7], [62].

To avoid fracture under any physiological loads, it is necessary to have strong bone. The bone mechanical properties depend on the mineral availability in the mineral matrix. The femur bone is divided into two parts, namely, cortical, and cancellous (trabecular) bones. The bone material properties are heterogeneous and anisotropic. However, cancellous bone has been considered homogeneous for the simplicity of the analysis [46]. For cortical bone, several Young's moduli and Poisson's ratio have been utilized in three orthogonal directions as shown in table 3.3 [7], [10], [29], [47].

2.6.2 Bone - femoral stem interaction

The bone – stem surface to surface interface is required to achieve the required transfer of the physiological load and to avoid loosening of the implanted stem[24], [39], [41]. Different interface modelling methods to simulate the surface contact between two parts that can be applied using the FEA software as node to node, surface to node, and surface to surface. For more accuracy of the hip implants, surface to surface contact is utilized [46], [68].

2.6.3 Applying muscular loads

Different loading scenarios were applied in the literature for the hip implants. Several in vitro analyses of the hip implants were done concentrating on hip contact force only where the load is applied on the centre of the femoral stem head [47], [54], [87]. Such load is not appropriate for fixation stability and actual in vivo condition evaluation of the Total Hip Arthroplasty (THA). Bergmann et al. measured muscular loads generated due to different human daily activities such as walking at low, normal, and high speeds, up stairs, down stairs, etc. and a simplified loading profile was calculated and developed for preclinical of the femoral stem [41], [93]. The hip contact force acting on the femoral stem head at the origin of the coordinate system is labeled as P0. Labeled P1 to P3 are the muscles forces attached to the femur (figure 3.6 – a).

2.6.4 Size and type of the meshing elements

Meshing is commonly performed to split the model into cells to perform a simulation analysis or to execute a digital model. Mesh size influences the computation time and accuracy. For example, small mesh size provides more accuracy and needs more computational time required for model simulation [94]. The number of nodes required for a small mesh size becomes high and hence requires a high CPU capacity to accomplish the simulation with less time [95], [96], particularly for complex models simulations such as hip implants. It is not logical to spend extra hours running the FEA simulation with a fine mesh if a coarser mesh can provide the same results, hence, a convergence / sensitivity study is performed to obtain the required accuracy.
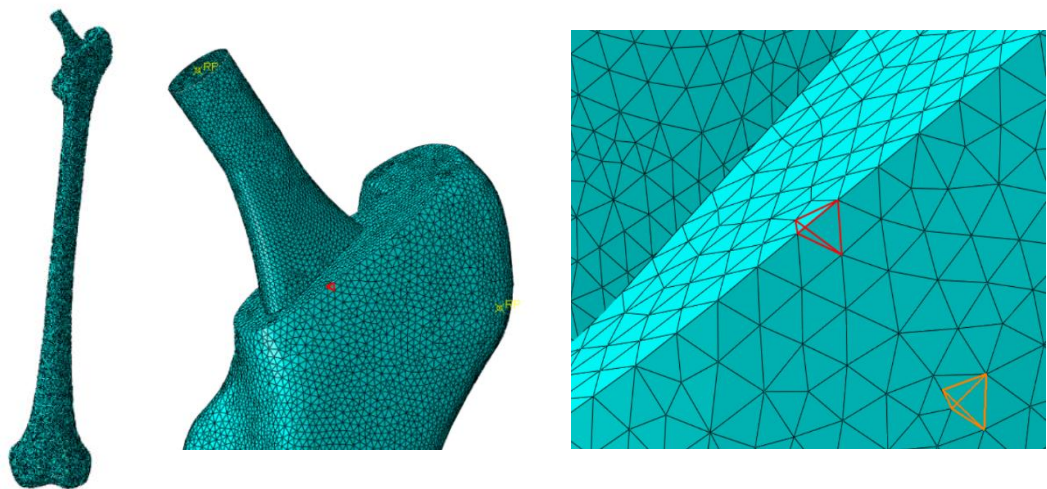
Figure 2.10. Tetrahedron mesh type of femoral stem assembly[62]

There are several mesh element types available. The basic types for the three-dimensional models are tetrahedron (4 vertices, 6 edges) (Figure 2.10), hexahedron (8 vertices, 12 edges), pyramid (5 vertices, 8 edges), and triangular prism (6 vertices, 9 edges). Mathur et al. (2012) evaluated the effect of two commonly used element types on two different proximal femurs. The femurs were meshed with

30

tetrahedron and hexahedron 3D mesh types and subjected to 100N force. Load – displacement curves generated from the FEA show similar results for both mesh types [97].

However, it was found in the current study that the tetrahedron mesh type required more run time, but it is easy to generate with fewer running errors.

2.7 Validation of simplified finite element model

To reduce the porous stems design complexity and finite element analysis time, a simplified model can be employed where the effective porous stem's mechanical properties are used for the bulk / dense Ti-6Al-4V alloy stem in the finite element analysis software (ABAQUS) instead of utilizing the designed porous structures [9], [10], [24]. Hasan et al. [9] and Sami et al. [10] simulated both models of the actual porous and the simplified effective stems in ABAQUS and validated the models using force – displacement output obtained from applying a load of 1200N in ten increments at the stem's head (figure 2.11). The obtained force–displacement results show a strong agreement between both models.
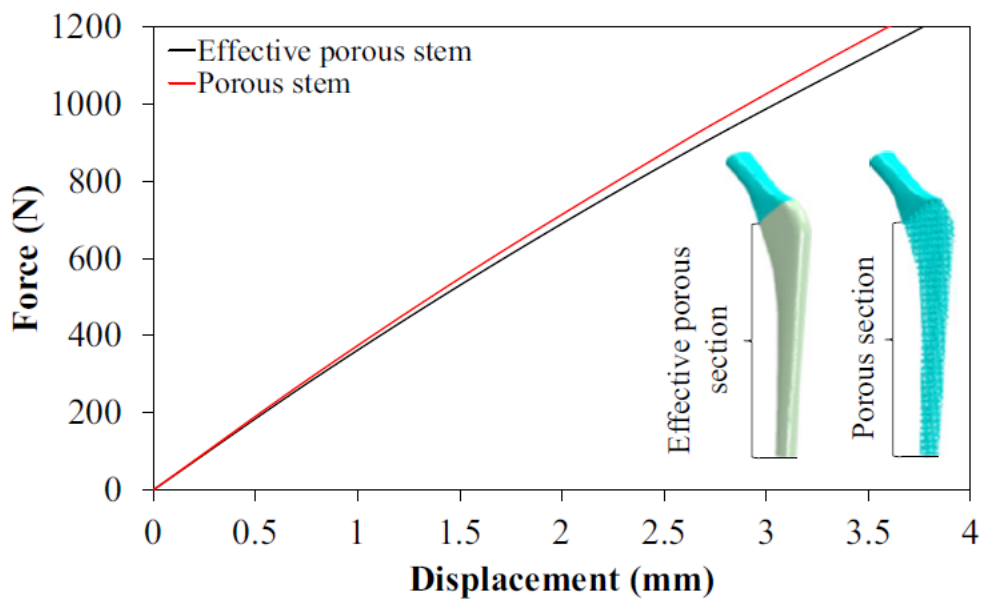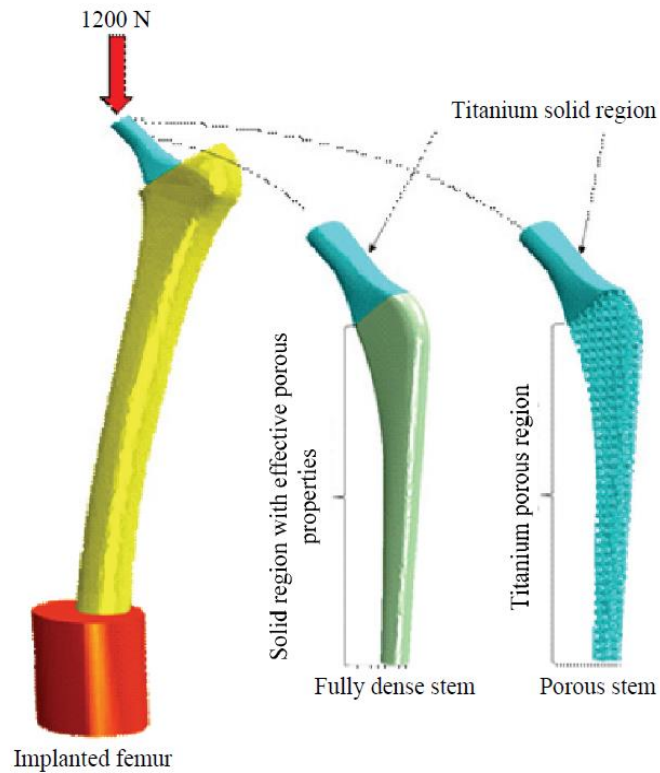
Figure 2.11 Validation of porous and simplified effective porous stems [9], [10]

2.8 Contribution to the knowledge

Previous studies investigated the functionally graded porous structures in the longitudinal direction. to complete the understanding of functionally graded porous

structure stems, but it is vital to investigate the functionally graded porosity in the radial direction. Hence, the aim of this study is to investigate the performance of functionally graded porous structures in the radial direction of the femoral stem, focusing on mechanical performance, fatigue performance, stress shielding, and micromotions to have the most ideal design that can be recommended for the surgeon based on the patient's condition.

The hypothesis in this study is that such radial functionally graded porous structure will provide optimum designs that can reduce the stress-shielding, promote stem stability, and survive under high cyclic loading focusing on the level of porosity in the stems required to achieve good biomechanical performance. These functionally graded structures in this study were designed to have average porosities of 30%, 50% and 70% in radial layers. A total of fifteen designs were generated and these designs were subjected to physiological loads mimicking three walking speeds, namely 1 km/hr, 3 km/hr, and 5 km/hr. The commercially available finite element software ABAQUS was used to simulate the stems using these three different walking speeds. The stresses within the stem's porous layers and proximal bone were measured and assessed to verify and estimate the life of the stems, stress shielding, and micromotion, respectively. Computational analysis will be utilized here as it is an accepted means of investigating the performance of implant related devices [30], [32], [33], [98].

2.9 Additive manufacturing sustainability

Additive manufacturing (also known as 3D printing) is one of the most innovative technologies nowadays. The possible applications range from the food industry[99], and bioscience to the manufacturing of jet engines and the

construction of buildings and bridges [100]. Additive manufacturing technologies have many different advantages over classical technologies. One of them is the ability to join operations that were typically done by different processes. This means that one machine might be enough to produce extraordinarily complex parts and that the production processes can be sped up and brought closer to the end-user.

In general, additive manufacturing technology provides a high potential for increasing efficiency, responsiveness, and sustainability of upcoming supply chains, as it has the potential to lead to a strong increase in local manufacturing of limited batches of different types of products, or even fully customized products[101]. The fact that NASA launched, in June 2014, a "zero gravity" 3D printer into space to print spare parts for the International Space Station (ISS), shows that this innovative technology is already practically useful. Some components are already printed for airplanes and engines [101], [102]. Opportunities for application are facilitated by a rapid increase in technological possibilities. Already at this point in time, industrial 3D printers achieve a high resolution, support many materials, and costs are decreasing quickly [101].

Additive manufacturing (AM) of metal components is a relatively new and novel manufacturing technique. The idea comes from 3-D printing (rapid prototyping). AM allows complex, net-shaped components to be fabricated in successive layers [103], depositing material only where it is needed. Because the idea is based on rapid prototyping, design changes are easily incorporated [103]. Since AM works on the principle of addition of material rather than removal (traditional machining), material cost and scrap can be reduced [103]–[105]. Additive manufacturing can produce parts that are more environmentally friendly, with an impact reduction of up to 70% for titanium based components [104].

34

Besides saving material, cost, and being environmentally friendly, AM is capable of producing customized products. This helps lower the inventory risk and improves the working capital management [105]. In summary, AM has the potential to minimize energy, material, and waste scrap production besides giving the flexibility for innovative design in the most efficient manner.

The use of additive manufacturing (3D printing) has a significant impact on the environment by reducing the need for consumables, minimizing tooling, and enabling large reductions in energy consumption compared to traditional manufacturing processes besides reducing the transportation required for moving the parts to different geographical locations [106].

Additive Manufacturing is a very competitive manufacturing process in terms of production speed and operational cost which has led to a large number of prototypes that can be produced and evaluated at the product development phase; this is important for improving the properties of the product either by improving the quality of the powder, binding material, and binding technique or by improving the post manufacturing treatment of the product such as infiltration and/or sintering. Studying the ability for producing functionally graded materials, which are widely used in orthopaedic implants using a suitable CAD model, in turn, will have a high impact on reducing lead time and cost of parts procurement. Table 2.3 summarizes the existing studies of Life Cycle Analysis and issues related to the sustainability of AM technology. Energy saving, cost analysis, environmental and societal impacts have been studied for different industrial applications.

Table 2.3 Qualitative literature on AM sustainability processes and applications

#	Author(s)	Date	Aim	Information provided
1	Huang et al.	2016	Energy and emissions saving potential of additive manufacturing	The adoption of AM components in aircraft has the potential to provide significant energy savings, The LCI analysis of cradle-to-gate energy mass reductions estimate by material and component system through AM replacement
2	Schrödera et al.	2015	Evaluation of Cost Structures of Additive Manufacturing Processes Using a New Business Model	Analysis of the most important process steps in additive manufacturing is presented. A new business model for additive manufacturing technologies is introduced afterwards including the implementation of this business model in a software tool. Case studies for different product types and produc quantities are explained and detailed values for process costs are provided. Sensitivity analysis is done to find the most important parameters (cost drivers) for those case studies.
3	Ford et al.	2016	Exploratory study of the advantages and challenges	Impacts of additive manufacturing on sustainability in terms of the sources of innovation, business models, and the configuration of value chains.
4	Hapuwatte et al.	2016	Total Life Cycle Sustainability Analysis of Additive Manufactured Products	Sustainability concerns in manufacturing of AM products. Product sustainability Index methodology
5	Burkharta et al.	2015	Predict the environmental impact of additive manufacturing in the product life cycle.	Inventory consideration LCA life cycle impact assessment (LCIA) to determine the effect of the quantified inputs and outputs on human health and the ecosystem

2.9.1 Aspects for improving the sustainability of AM femoral stem

Product life cycles which include preproduction, production, use, and post-use stages should be studied comprehensively to have a complete understanding of the total product life cycle [107]. Hapuwatte et al.[108] proposed a methodology for product sustainability improvement. Product quality, quantity, complexity of the design, and functional/material requirements are the main concerns for product sustainability improvement during the early design stage. A comprehensive methodology and review of the product sustainability evaluation which includes three sub-indices of society, economy, and environment based on weighting depending on the importance of the sub-cluster data on sustainability was developed and adopted for comprehensive evaluation of sustainability for each component under study. Cost sustainability will be comprehensively studied to evaluate the adoption of additive manufacturing for femoral stem manufacturing.

Improving additively manufactured product quality is required to maintain sustainability; improving the stem surface finish, achieving the required mechanical properties, i.e., stress, strain, fatigue, stiffness, ductility, and microstructure by controlling the printing machine parameters, besides using good powder quality, and introducing post-process treatments, are important quality aspects to positively impact sustainability.

2.9.2 Cost of utilizing Ti4Al6V – Additive Manufacturing For medical and industrial applications

Additive manufacturing presents a sustainable resolution to the issues of waste during the production cycle. This is because the steps used in the production of the initial product will not be repeated, but the product will be duplicated as it is. Therefore, the amount of wastage that may occur at every cycle is avoided [109],

given that the global market for 3D printing will be approximately $50 billion US dollars by 2025. This figure is expected to be at least four times the value that was recorded in 2014. The life cycle cost of utilizing additive manufacturing is expected to be very low considering the fact that it ensures materials efficiency and the use of fewer processing procedures [109]. Therefore, 3D printing has gained prominence due to the economic benefits it is expected to have.

However, there is a difference in the costs of the materials used for additive manufacturing. Titanium alloys are among the most important advanced materials which have managed to improve performance in aerospace, medical and industrial systems. Unfortunately, when compared to competing materials, titanium alloys are more costly (Table 2.4). The extremely high costs are a result of high extraction costs and high processing costs [110].

Table 2.4 Cost comparison of Titanium versus steel and aluminum [110]

| Item | Material (US $/pound) | | |
	Steel	Aluminium	Titanium
Metal	0.10	1.10	5.44
Ingot	0.15	1.15	9.07
Sheet	0.30-0.60	1.00-5.00	15.00-50.00
powder	1.00-3.00	4.94- 8.47	90.90-181.81

2.9.3 Life Cycle Inventory of additive manufacturing

AM is prepared to transform various aspects of manufacturing, distribution, the supply chain, organizations, and the international economy [111], Inventory is expected to be impacted such that a company will never have too few stored products and raw materials. The amount of inventory is expected to be enough to satisfy the demand of the population. This is because the typical 3D printer has the capability of producing most product parts or even the main products given that the materials used in the printer have adequate properties [111]. It also depends on the

size of the product which becomes easier if it can fit into the printer dimensions. Of all products produced by this approach, the majority are produced at once, hence requiring no further assembly.

3D printing reduces the complexity of the supply chain drastically. The many assembly steps which would have been required during the production of an object are replaced with a single task. In addition, it allows the production to happen based on demand for the product rather than prior to the need for the product by consumers. Therefore, Stock Keeping Units (SKUs) are expected to reduce. Since it will be easier to store electronic files rather than the product itself, 3D printing has created an opportunity for the creation of a 3D model file product portfolio instead of the physical inventory. Physical inventory will mainly be composed of semi-finished product parts [112]. In the case of producing hip implant, it can be manufactured at the location near to the hospital using the patient's specific femur geometric data using Computer Added Design (CAD) software, and inventory space required is minimal as only Titanium Alloy powder will be stored besides the software. Also, no unsold items will be held in reserve as the manufacturing of the parts will be based on demand only.

2.9.4 Life cycle environmental impact of utilizing additive manufacturing

AM printing technologies evolve constantly. Although it holds a great promise for the manufacturing world, it is challenged by quite a number of drawbacks, which is why it is not considered an eco-friendly approach. AM technology uses a lot of energy, considerably more than conventional drilling and milling machines [113]. According to research, some AM printing processes use up to 50-100 times more electricity than injection molding machines [114]. Considering every step of the

supply chain, the additive manufacturing process does not have the lowest carbon output. However, fewer environmental impacts were noted at the material production stage since this is where it performed better. One reason for this is that it tends to use less material and yield fewer waste. However, there are still cases where AM models need support materials. This increases waste materials since the user will still need to discard these at the end of the printing stage [115]. Therefore, AM is only capable of producing low carbon parts at the material production stage but not the energy production stage.

AM still contributes positively on energy and Greenhouse Gas (GHG) emissions reductions for some instances due to its capability to produce lighter parts, single machine required rather than multiple, less waste or scrapped items based on design and product geometry, and distributed and on-demand manufacturing. Resource Efficiency also can be positively impacted as AM processes use the amount of material that is needed as it is based on adding material rather than removing, opportunities for recycling and repairing AM printed parts is also possible, reduction of inventory levels (Powder and Software only) and its associated emissions and reduced need for support materials in manufacturing.

CHAPTER 3: METHODOLOGY

3.1 Introduction

This chapter introduces the details of the procedure followed for designing titanium alloy lightweight femoral stems with cubic porous structures that will be able to reduce stress-shielding, promote stem stability and survive under fatigue loading. These porous structure designs were introduced into the titanium alloy femoral stem as homogeneous and functionally graded porous structures.

First, the cubic cellular structures were simulated under compressive loading to measure the yield and modulus of elasticity for various porosity ranges. Based on the selected porosity range, fifteen different arrangements of radial geometrical functionally graded (FG) designs were developed with average porosities of 30, 50, and 70% respectively. The finite element models developed with physiological loads presenting three different walking speeds (1, 3, and 5 km/hrs.), where the average human body weight was assumed. Stresses at the bone Gruen zones were measured to check the percentage of stress transfer to the bone for each porous stem design and were compared with the bulk / dense stem.

Stresses at the functionally graded stem layers were measured and compared with the yield strength of the relevant porous structure to check the possibility of yielding under the subjected load. The Soderberg approach is utilized to calculate the safety factor ($N_{f)}$ for each design under each loading condition. Several designs were shortlisted as potential candidates for orthopedic implants. figure 3.1 illustrates the interconnected research methodology tasks.

(a)

(b)

(c)
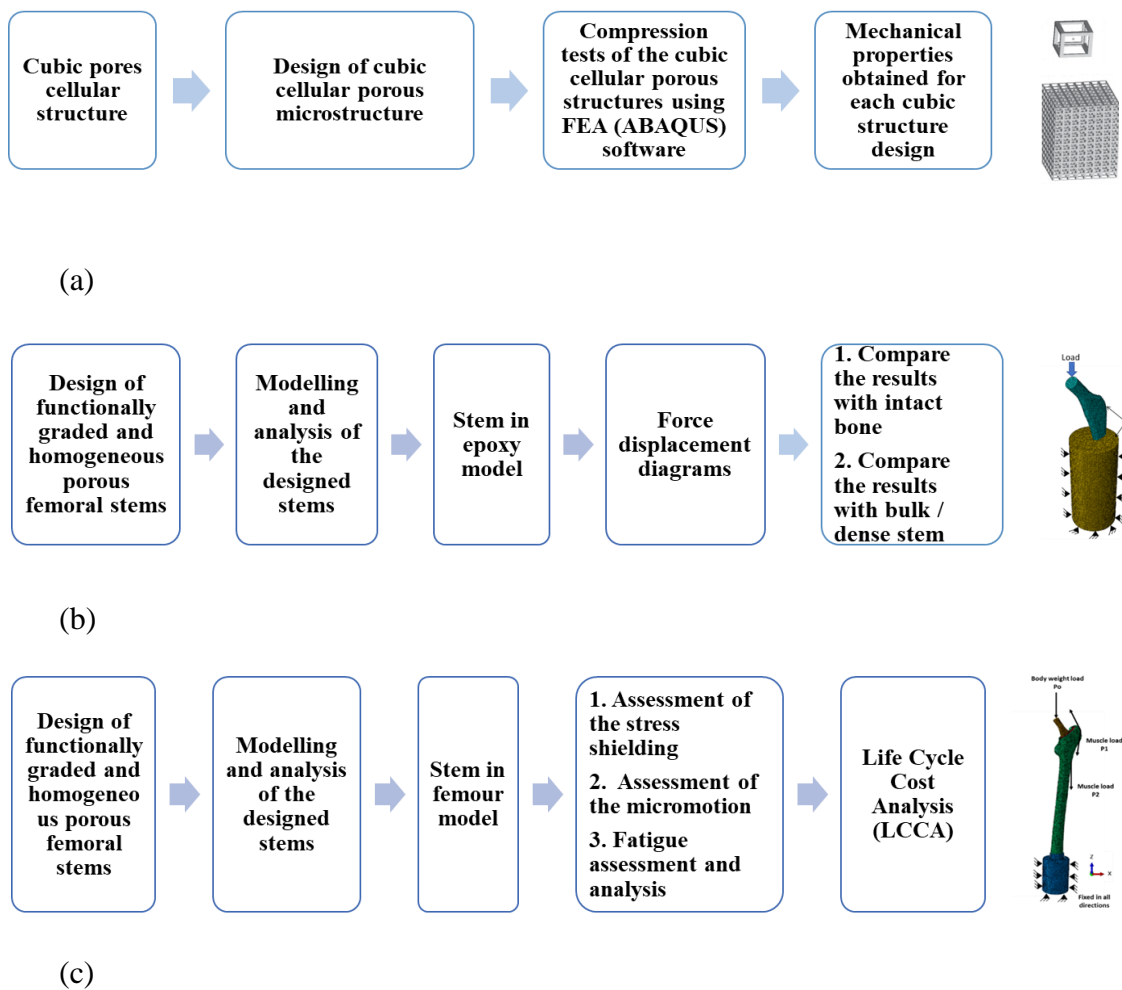
Figure 3.1. Flow chart of interconnectivity of the tasks; (a) Cubic porous cellular structure, (b) Stem in epoxy model, and (c) Stem in bone model

3.2 Finite element models

3.2.1 Cubic pores cellular structure

3.2.1.1 Design of cubic cellular porous microstructure

Square pores microstructure three-dimensional (3D) models with various volumetric porosities ranging from 10% to 90% were designed and simulated under compression loading using ABAQUS 6.17 as illustrated in Figure 3.2 and presented in Table 3.1. Different sizes of square pores with minimum selected strut thicknesses of 3.0mm due to the resolution of the EOS M 280 printing machine [90], these pores were

fitted within 15mm x 15mm x 15mm 3D cubes [73]. The proposed designs were considered with 12-to-23-unit cells enclosed within each dimensional direction of the cubic samples as shown in Figure 3.2. The top and bottom sides of the cubes had been fitted with plates, that were to be utilized for compression loading.

The volumetric porosity for the designed porous cubes was calculated based on equation 3.1, which was derived based on geometric calculations of the designed porous cube. The designed cubes volumetric porosities were compared using the mass properties option in ABAQUS.

$$Vp = L_2^2 N^2 (2Nt + 2t) \qquad (3.1)$$

Where:

V_p: Volumetric porosity

L_2: cubic pore inner dimension

N: Number of pores in a single cube face

x: Full cube dimension

t: Strut thickness

Table 3.1. Designed samples of porous cubes with the relevant volumetric porosities and obtained mechanical properties from the FEA.

Strut Size (t)	Number of pores / Unit cells enclosed within each dimensional direction the cubic	Pore size (L2)	Volumetric Porosity (%)	E (GPa)	Ys (MPa)	Ut (MPa)
(mm)	(N)	(mm)				
0.3	10	1.36	90%	3.5	31.14	33.27
0.3	12	1	85%	7.6	50.17	58.47
0.3	14	0.8	80%	11.68	77.52	90.99
0.32	15	0.72	76%	16.18	105.95	113.50
0.32	17	0.6	70%	19.76	123.28	165.13
0.34	18	0.49	62%	24.09	152.26	177.27
0.34	18	0.47	60%	27.78	168.77	216.30
0.36	20	0.38	50%	35.12	208.31	269.29
0.38	21	0.3	40%	46.33	272.75	355.63
0.4	23	0.23	30%	52.23	307.13	402.87
0.42	24	0.18	20%	60.38	353.5	468.43
0.44	26	0.11	10%	68.52	399.66	533.69

(a)
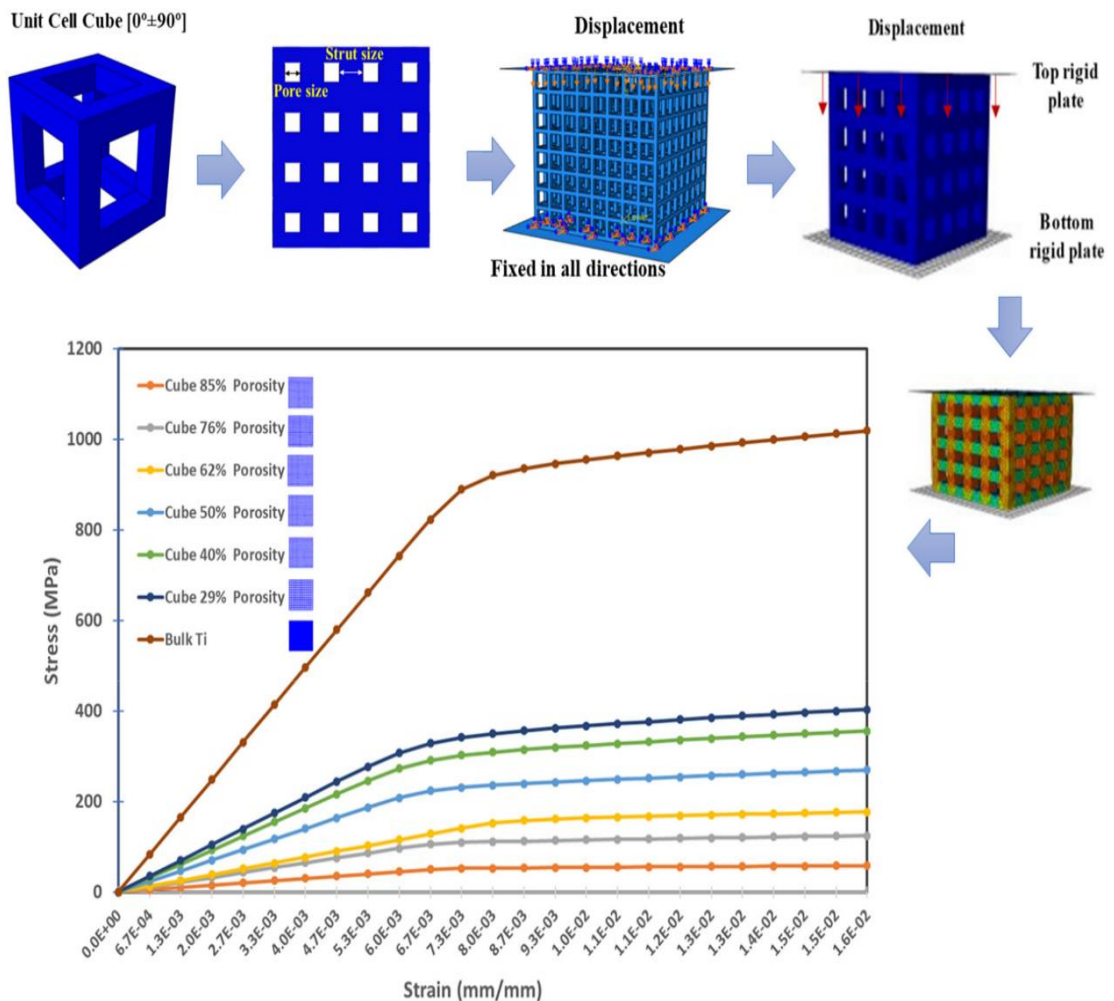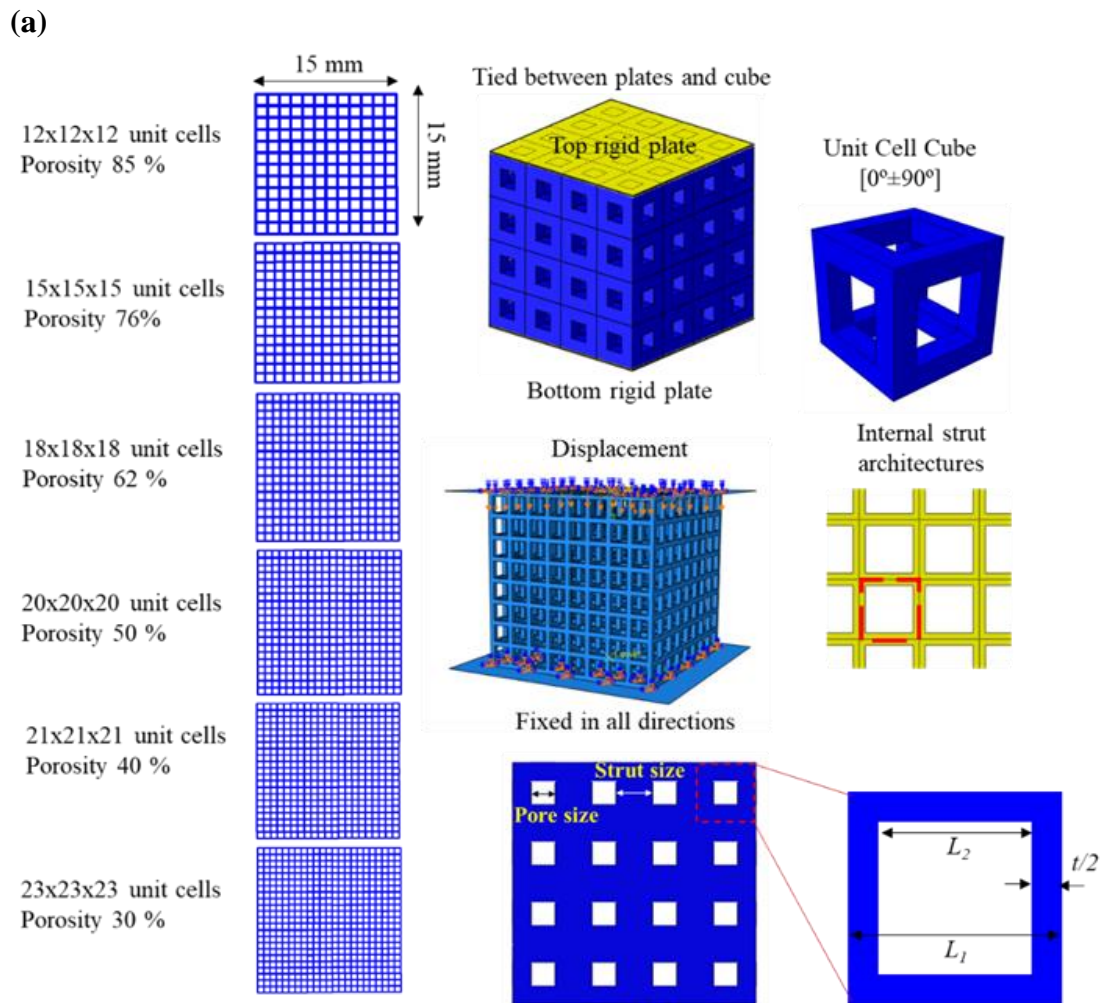
(b)

Figure 3.2. Porous structure designs along with finite element model to study the mechanical properties of (a) different volumetric porosities, (b) study flowchart

3.2.1.2 Compression assessments of the cubic cellular porous structures using FEA (ABAQUS) software

The designed cubic cellular porous structures were assessed using finite element software (ABAQUS) under compression loads. The top side of the cube's fitted plate had been assigned with a displacement boundary condition, and encastre boundary

condition was used to tie up the bottom plate. The designed structures had been assigned with bulk / dense Ti-4Al-6V material properties. C3D10 quadratic tetrahedral meshing elements had been used to mesh the assembly using a mesh size of 0.2 mm based on a sensitivity study determined from stiffness convergence of dense cube as shown in Figure 3.3 [73]. It is obvious from the figure that there were no significant changes in the modulus of elasticity at mesh sizes of 0.4, 0.3, and 0.2 with a change of -0.081% between mesh sizes of 0.2 and 0.3mm. hence, the FEA model depicts the structure's behavior, with less solving time.

Axial displacement on the upper plate was applied to achieve the yield points at least with 0.05 increment size and with twenty increments to generate a more accurate value of the yield points and modulus of elasticity.
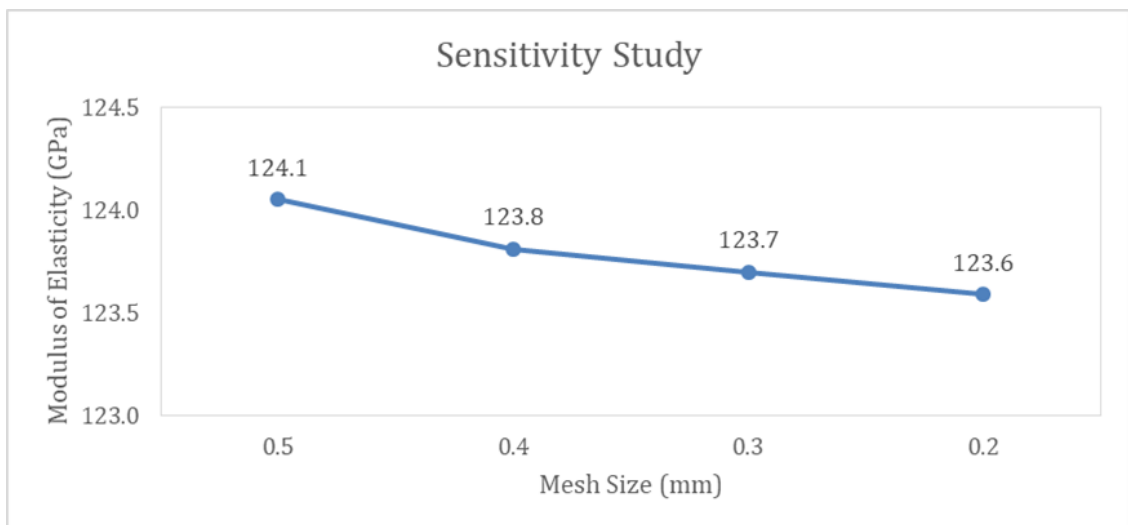
Figure 3.3. Sensitivity study to indicate the mesh size to which the Modulus of Elasticity converges using a solid cube.

3.2.1.3 Mechanical properties obtained for each porous structure design

Stress and strain values were calculated from the finite element analysis results at each increment, strain values were calculated from the displacements values and reaction force values were used to calculate the stress. The calculated results were used to plot the stress-strain diagram for each of the designed porous cubic structures in order to obtain the required mechanical properties that are essential for further femoral stem design and analysis. The mechanical properties of each design are illustrated in table 3.1.

3.2.2 Design of functionally graded and homogeneous porous femoral stems

The mechanical properties of cubic structures (Figure 3.2) were used to design twelve different functionally graded stems, as shown in Table 3.2 and Figure 3.4. The layer's cross-sectional areas are 15.9mm^2, 17.3mm^2, and 23.6mm^2 for the core, layer 1, and layer 2, respectively. The average porosities of the designed stems in radial direction were calculated based on equation 3.2. These designs were grouped into three different sets of 30%, 50%, and 70%, with each set having the same overall average volumetric porosity through the stem's layers in the radial direction. These porosities were selected based on the USA food and drug administration (FDA, 2016), where the approved range of the femoral stem porosities should be between 30–70% that enhance the bone tissue ingrowth [116].

Three more designs, namely designs D5, D10, and D15 were considered to represent the homogeneous volumetric porosities of 30%, 50%, and 70% respectively. A total of fifteen designs were modeled as shown in Figure 3.4.

$$\overline{P} = (V_P)_h + \frac{(\overline{AV}_p)_{fg} - (\overline{AV}_p)_h}{(\overline{AV}_p)_h} \qquad (3.2)$$

Where;

A: Stem's radial Layer cross-sectional Area

V_p: Stems radial Layer Volumetric Porosity

$\overline{(AV_p)_{fg}}$: Average functionally graded Porosity along with the stem's layers

$\overline{(AV_p)_h}$: Average homogeneous Porosity along with the stem's layers

$(V_p)_h$: Stem Homogenous porosity.

Table 3.2. Porous functionally graded (FG) and homogeneous (H) designs introduced to stem redial layers.

Stem's Layers	FG-Design 1 (D1)	FG-Design 2 (D2)	FG-Design 3 (D3)	FG-Design 4 (D4)	H-Design 5 (D5)
30% Overall Volumetric Porosity					
Layer 1 (L1-Core)	40%	20%	59%	10%	
Layer 2 (1mm) (L2)	30%	30%	30%	30%	30%
Layer 3 (1mm) (L3)	23%	37%	10%	43%	

Stem's Layers	FG-Design 6 (D6)	FG-Design 7 (D7)	FG-Design 8 (D8)	FG-Design 9 (D9)	H-Design 10 (D10)
50% Overall Volumetric Porosity					
Layer 1 (L1-Core)	60%	37%	80%	10%	
Layer 2 (1mm) (L2)	55%	50%	77%	60%	50%
Layer 3 (1mm) (L3)	40%	59%	10%	70%	

Stem's Layers	FG-Design 11 (D11)	FG-Design 12 (D12)	FG-Design 13 (D13)	FG-Design 14 (D14)	H-Design 15 (D15)
70% Overall Volumetric Porosity					
Layer 1 (L1-Core)	80%	55%	90%	49%	
Layer 2 (1mm) (L2)	70%	70%	80%	70%	70%
Layer 3 (1mm) (L3)	63%	80%	50%	85%	

(a)

(b)
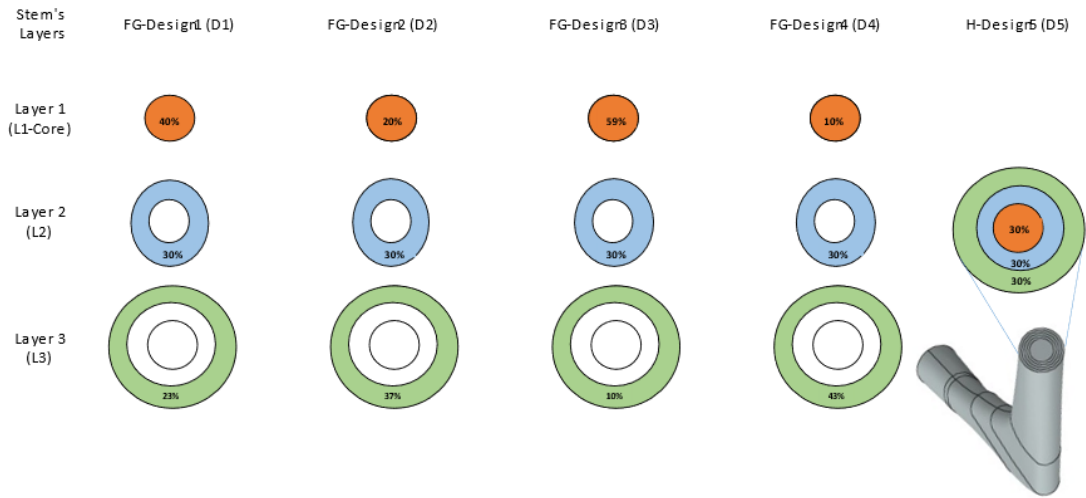
70% Overall Volumetric Porosity
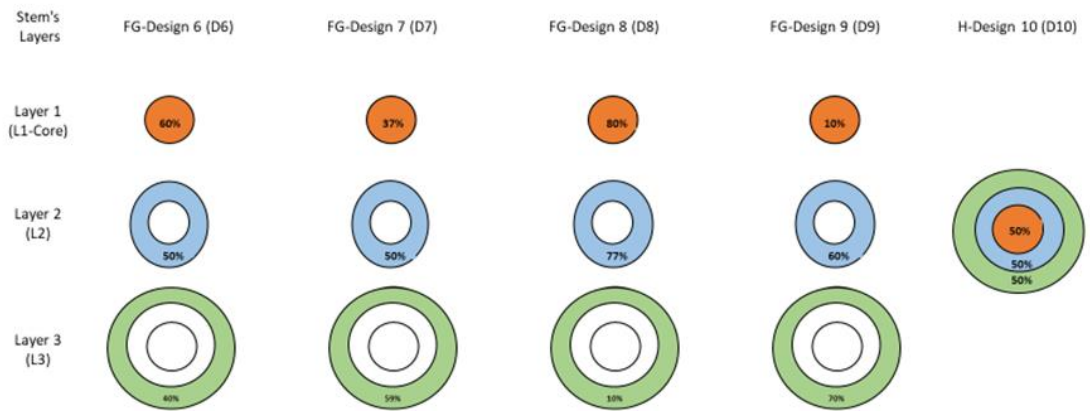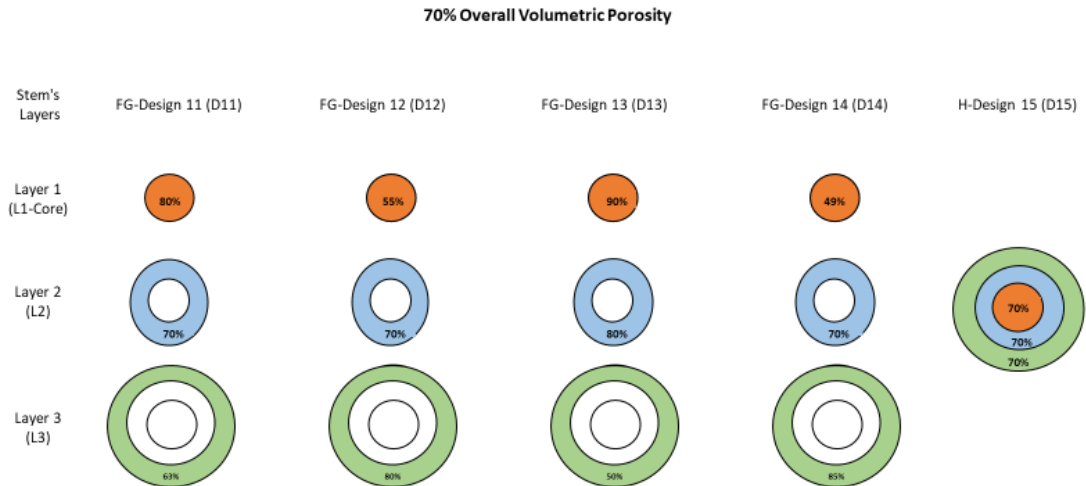
(c)

Figure 3.4. Design groups of porous functionally graded (FG) and homogeneous designs introduced to stem's redial layers: (a) average porosity of 30%, (b) average porosity of 50%, (c) average porosity of 70%.

3.2.2.1 Modelling and analysis of the designed stems

3.2.2.1.1 Stem in epoxy model

All designs were initially integrated into 3D finite element models in ABAQUS 6.17 as shown in Figure 3.5 to study the stiffness performance of the designed stems concerning the intact femur bone. The setup shown in Figure 3.5 is per ISO standard (ISO 7206-4). The stem was positioned inside cylindrical shape epoxy with a specific orientation of 9° in the lateral plane, and 10° in the ventral plane, the dimension between the stem's head and the epoxy surface is 80mm.

Then the stem was tied together with the epoxy, while the epoxy was constrained to move or revolve in any direction. The assembly was meshed with fine meshes and tetrahedral elements were employed. A 2250 N force [41] was applied on

the stem's head using a 0.1 increment size in 10 increments. The material properties of the bulk Ti and designed porous structures (Table 3.2) were assigned to the stems based on the simplified FE model to reduce design time and computation [9], [24], [117]. The proximal part of the stem was assigned with bulk / dense Ti-4Al-6V material properties. The epoxy material was assigned with isotropic property with Young's modulus of 3.7 GPa and Poisson's ratio of 0.3.

Force – displacement diagrams to be plotted for each stem and the results to be compared with the intact bone and bulk / dense Ti-4Al-6V alloy stem.
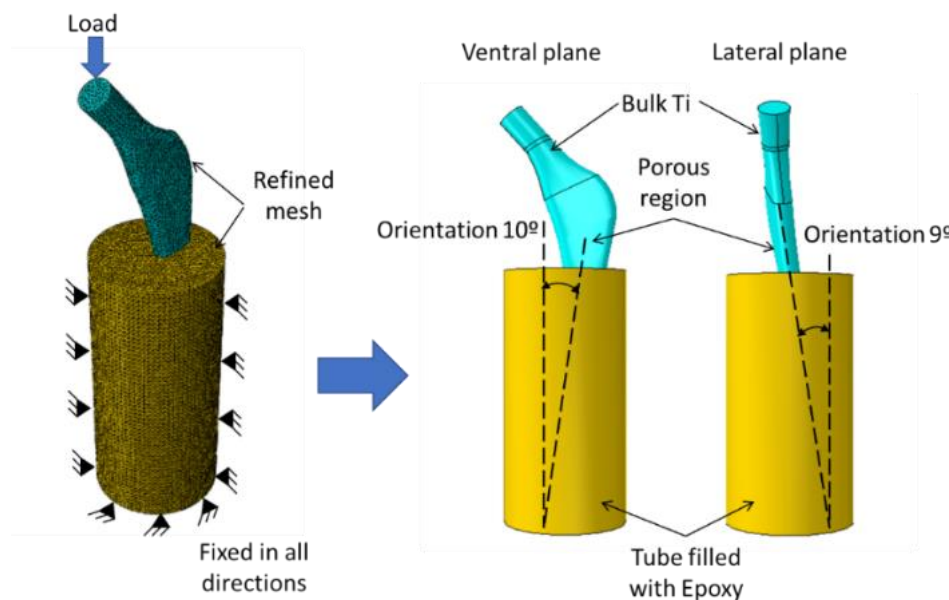
F

Figure 3.5. Finite element analysis of porous Ti-6Al-4V alloy and bulk / dense stems according to the ISO 7206-4 standard

3.2.2.1.2 Porous stem – femur bone model

To study the effect of the designed porous stems on stress reduction and micromotion, it is vital to use a finite element model that incorporates the stem and

femur bone along with proper physiological loads. This finite element model has been adopted in previous studies conducted by authors [7]–[11]. 3D models of homogeneous and functionally graded stems (D1 – D15) were assembled with femur by using surface to surface contact with a coefficient of friction of 0.4, and the assembly was incorporated inside a cylindrical shape epoxy. The bone was tied with the epoxy and constrained to move or revolve in any direction [8]. The 3D model of the femur was constructed using computed tomography (CT) scanned images of a patient femur as explained in previous studies [8], [84]. Cortical and trabecular bone were considered homogeneous and linear elastic isotropic materials respectively with material properties as listed in Table 3.3 [26], [84], [118]. The bone was subjected to three physiological loads namely P_0, P_1, and P_2 where P_0 is the hip contact force, P_1 and P_2 are muscular forces attached to the femur. These forces were calculated based on the loading reflected by the studied physiological loading conditions which are unique and not used before [119]. The assembly is shown in Figure 3.6a. Table 3.4 displays these forces in their components (Fx, Fy, Fz). The directions of these component forces were obtained from previous studies [41], [119]. The simulation was done for three different walking speeds 1km/hr., 3 km/hr., and 5 km/hr. The peak hip contact forces used in percent of body weight (%BW) were 293%, 352%, and 471% for walking speeds of 1km/hr., 3 km/hr., and 5km/hr. respectively [93], [120]. For this study, a human body weight of 900 N was assumed. The assembly was meshed using C3D10 quadratic tetrahedral elements using a mesh of 3 mm size, which was used based on a previous sensitivity study [10]. Bone Gruen zones locations [66] were identified as illustrated in Figure 3.6 - b. These zones will be used for identifying the stress transfer to the bone from the designed stems at the predefined loading conditions.

Table 3.3. Femur material properties utilized for the finite element model [23], [56]

Bone material	Young's Modulus (GPa)	Shear Modulus (GPa)	Poisson's ratio
Spongy Bone (trabecular bone)	0.4	-	0.3
Cortical bone	$E_{xx} = 11.5$	$G_{xy} = 3.6$	$\nu_{xy} = 0.51$
	$E_{yy} = 11.5$	$G_{yz} = 3.3$	$\nu_{yz} = 0.31$
	$E_{zz} = 17$	$G_{yz} = 3.3$	$\nu_{yz} = 0.31$
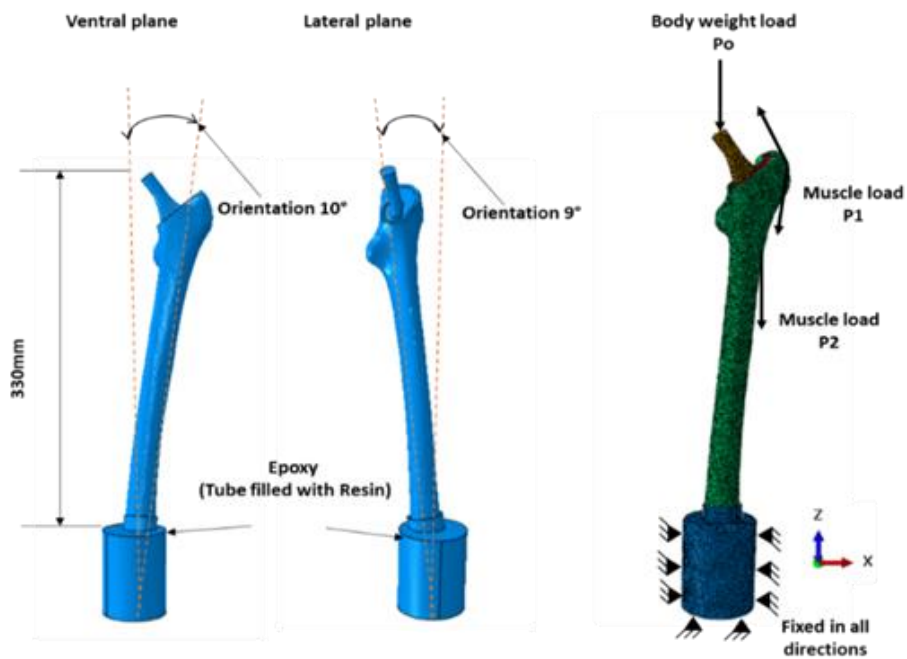
(a)
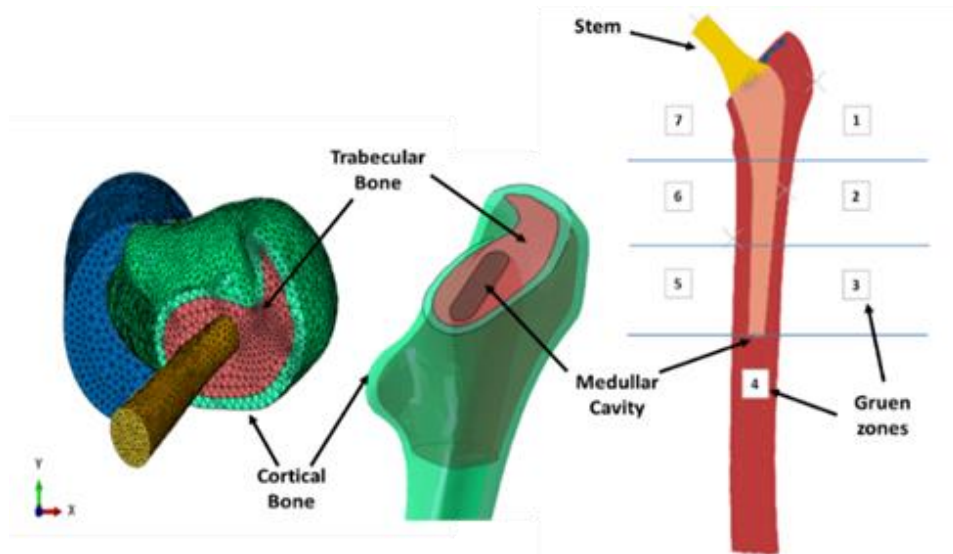
(b)

Figure 3.6. Finite element analysis of stemmed femur; (a) complete finite element model with applied physiological loads, (b) bone Gruen Zones [66].

Table 3.4. Bodyweight and muscular loads for different walking speeds (Calculated with reference to Bergmann et. al; 1993, Heller et. al 2005) [93], [120]

Force (Body weight used BW = 900 N)	%P_o	1 km/hr (P_o = 293% BW)			3 km/hr (P_o = 352% BW)			5 km/hr (P_o = 471% BW)		
		F_x	F_y	F_z	F_x	F_y	F_z	F_x	F_y	F_z
P_o	100	-599	-363	-2542	-719	-437	-3054	-962	-584.	-4086
P_1	44	643	8.0	959	772	57.3	1152	1034	76.7	1542
$P_{1\text{-tensor fascia latae, proximal part}}$	8	79.9	129	146	95.9	154	175	128	206	235.4
$P_{1\text{-tensor fascia latae, distal part}}$	8	-5.5	-7.8	-210	-6.7	-9.3	-253	-8.9	-12.5	-338
P_2	40	-10.0	205	-1030	-12.0	246	-1237	-16.0	329.9	-1656

3.2.3 Fatigue assessment and analysis of the designed porous stems

A fatigue study was performed on the designed stems implanted inside bone by performing finite element analysis based on physiological loading conditions obtained

from the three walking speeds as presented in Table 3.4. Von Mises stress on the stem / stem layers was measured using ABAQUS FEA software as illustrated in Figure 3.7.

The factor of safety was calculated using the Soderberg approach [83] as shown in Equations 3.1 – 3.4:

The minimum stresses and the maximum stresses were measured at the loads associated with stress ratios equal to 0.1 (R=0.1):

$$\sigma_m = \frac{(\sigma_{max.} + \sigma_{min.})}{2} \tag{3.1}$$

$$\sigma_a = \frac{(\sigma_{max.} - \sigma_{min.})}{2} \tag{3.2}$$

Where; (σ_m) and (σ_a) denote mean and alternating stresses created in the porous stems and ($\sigma_{min.}$) and ($\sigma_{max.}$) refer to minimum stresses at 0.1 of the applied physiological load and maximum stresses associated with the full load generated from each walking speed.

$$\left(\frac{\sigma_a}{S_e}\right) + \left(\frac{\sigma_m}{S_{ys}}\right) = \frac{1}{N} \tag{3.3}$$

And hence, the fatigue factor of safety (N_f) is as the following:

$$N_f = \frac{1}{\dfrac{\sigma_a}{S_e} + \dfrac{\sigma_m}{S_{ys}}} \tag{3.4}$$

Where, S_e, S_{ys}, and N_f represent, the porous material endurance limit calculated using equation (3.5) [121], relevant porous material yield strength, and factor of safety, respectively.

$$S_e = K_a \times K_b \times K_c \times K_d \times K_e \times K_f \times S_u \tag{3.5}$$

K_a : Surface quality factor.

K_b: Size factor.

K_c: Reliability factor.

K_d: Temperature factor.

K_e: Stress concentration factor.

K_f: Miscellaneous factor.

For Ti6Al4V [53]: $S_e = 0.54 \times S_u$

S_u: The Ultimate tensile stress of the porous material, (the S_u for the outer stem's porous layer for each design was used where it is associated with the maximum stresses obtained from each walking speed), the reduction percentage in S_u and the calculated endurance limit S_e are shown in Table 3.5 below:
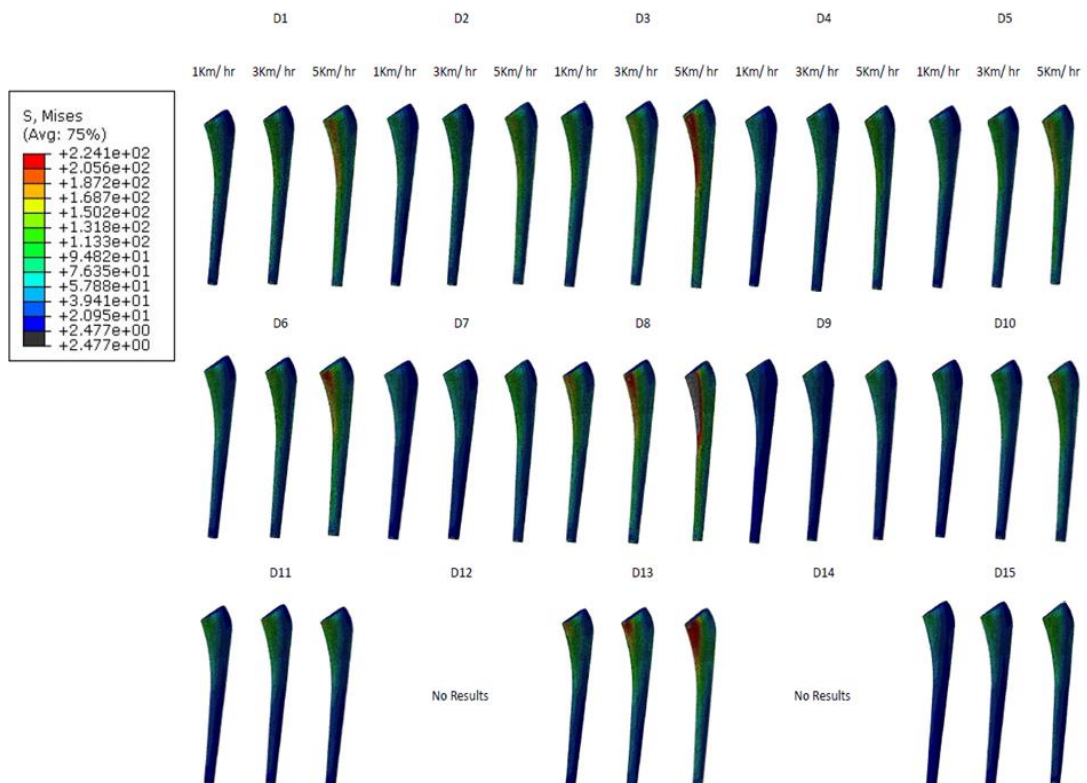
Figure 3.7. von Mises stress achieved from the FEA for the fifteen designed stems planted inside the femur and subjected to the three physiological loads (1Km/hr, 3Km/hr, and 5Km/hr.

57

Table 3.5. The percentage of reduction in S_u due to the introduced porosities and the associated calculated endurance limit S_e values.

Endurance Limit for The Designed Porous Structures			
Volumetric Porosity	S_u (MPa)	Reduction factor	S_e (MPa)
90%	33.27		17.97
85%	58.47		31.58
80%	90.99		49.13
77%	107.46		58.03
76%	113.50		61.29
76%	124.80		67.39
70%	165.13		89.17
63%	243.15		131.30
62%	177.27		95.72
60%	216.30		116.80
59%	219.77	0.54	118.68
55%	239.53		129.34
50%	269.29		145.42
49%	283.16		152.91
43%	323.20		174.53
40%	355.63		192.04
37%	359.83		194.31
30%	402.87		217.55
23%	450.32		243.17
20%	468.43		252.95
10%	533.69		288.20
Bulk Ti	1018.67		550.08

3.2.4 Fatigue life assessment

Stress based approach is used for evaluation of the fatigue life of the designed femoral stems using the Basquin formula [72], [122], [123]. Von Mises stresses obtained from the static analysis were used for fatigue life estimation based on the Soderbergh concept [72] as shown in Equations 3.6 – 3.9:

$$\sigma_{f\prime} = \frac{\sigma_a}{1+\left(\frac{\sigma_m}{\sigma_u}\right)} \qquad (3.6)$$

$$a = \frac{0.9\sigma_u^2}{\sigma_e} \qquad\qquad (3.7)$$

$$b = \frac{-1}{3} log \frac{0.9\sigma_u}{\sigma_e} \qquad\qquad (3.8)$$

$$N = \left(\frac{\sigma_{f\prime}}{a}\right)^{\frac{1}{b}} \qquad\qquad (3.9)$$

Where;

σ_a = Alternating Stress,

$\sigma_{f\prime}$ = Effective alternating Stress,

σ_m = Mean Stress

σ_u = Ultimate Tensile Stress,

σ_e = Effective alternating Stress,

N = Number of cycles to failure,

The daily physiological activities evaluation for the patient is vital for the surgeon for proper decision and selection before total hip arthroplasty (THA). Kinkel et al. (2009) [124] evaluated the patient's level of activities based on age, gender, and other factors as presented in table 3.6. The daily patient's average walking cycle is around 6000 steps, which represents 2.19 million cycles/year [124]. This data provides an idea about the durability of the stems in terms of fatigue life.

Table 3.6. Patient demographics and measured walking cycles according to patient factors [124]

Demographic	Number of patients (n = 105)	Walking cycles/day	Standard deviation (cycles/day)	Walking cycles/year
Age				
< 50 years	22	6598	1825	2,408,170
50–59 years	41	6722	1896	2,453,485
60–69 years	23	5900	2447	2,153,341
70–79 years	19	4669	1808	1,704,300
Gender				
Male	45	6881	2061	2511719
Female	60	5592	1998	2040898

3.3 Sustainability and cost study

Utilizing additive manufacturing to produce the designed stems tends to minimize losses that would occur in the form of wastage of time and materials during the production process. In addition, it provides innovation and workforce opportunity that leads to reduced expenditure on employees. This is because a single employee would be capable of developing a number of parts alone, compared to what would have been achieved without this technology. It is worth stating that the expected savings in materials due to the reduction of the femoral stem's weight as a result of introducing porosity ranges from 30% to around 50 % [62].

A comparison between utilizing additive manufacturing (mainly, Direct Metal Laser Sintering (DMLS)) related parameters versus the traditional manufacturing of femoral stem is illustrated in table 3.7.

Table 3.7 Cost comparison of manufacturing the Titanium Alloy Femoral Stem using AM (DMLS) versus traditional manufacturing (US $)

Parameter	Value		Unit	Reference
	TM	AM		
Hip implant cost	2308		$/Unit	[112]
Build time		12	hrs/ unit	[112]
Transportation cost	35.4 + 0.02a		to be ignored	[112]
Inventory holding cost	25%	2.50%	of inventory value or revenue	[112]
US demand (Hip Implant)	332000		Unit/Year	[112]
lead time	60	14	Days	[112]
Technician cost		18.6	$/Hr	[125]
Maximum energy consumption		135	MJ/Kg	Technical Description EOSINT M 280 [126]
Femoral stem weight	1.4 to 2.3	1.04 to 1.74*	Kg	[127]
Electricity cost		0.028	$/MJ	[125]
Operation cost		41.56	$/Hr	[125]
Powder price (Average)		210	$/Kg	[110]

* 50% volume reduction based on optimum porosity introduced to the femoral stem [62]

An average bulk/density Ti-4Al-6V alloy stem's weight of 1.85 Kg will be considered for the life cycle cost analysis (LCCA). Hence, the average weight of the porous stem is 0.92 Kg referring to stems with volumetric porosity of 50%. The porous portion of the stem represents 74.2 % hence, the porous stem's total weight was calculated as follows:

Porous stem weight = Weight of the porous portion + Weight of the dense portion

Hence, Porous stem weight (50% porosity) = 0.68 + 0.478 = 1.16 Kg.

Life cycle cost analysis (LCCA) is calculated using the following formulas [108], [109]:

Nominal rate with inflation adjustment:

$$D_{real} = \frac{1+D}{1+i} - 1 \tag{3.6}$$

Where, D_{real}, D, and i donate, real discount rate, nominal discount rate, inflation rate, respectively.

$$S_0 = \sum_{t=0}^{t=t} \frac{S_t}{(1+D_{real})^t} \tag{3.7}$$

Where, $S_0, S_t,$ and t, denote Present value, future value, and number of years, respectively.

$$\frac{S_0}{S_t} = \frac{1}{(1+D_{real})^t} \tag{3.8}$$

Where, $\frac{S_0}{S_t}$ is the discount rate

The nominal discount rate and the inflation rate are assumed to have values of 7.5% and 3.5% respectively [128].

It has been reported that the rate of revision surgeries is 6.5 % after 5 years and 12.9 % after 10 years of the primary surgery [12], [129]. Proposed porous stems are expected to last for more than 20 years without revision surgeries, however, for comparison purposes, the same percentages will be considered for both stems.

All costs associated with inventory, transportation, lead-time to produce, and other related costs which are normally associated with traditional manufacturing were not taken into consideration in this study.

CHAPTER 4 : RESULTS AND DISCUSSION

This chapter explains the research justification, data presentation, findings, and analyses. The mechanical performance assessment and fatigue analysis of the designed porous cubes with cubic cellular structure and the fifteen designed fully porous homogeneous and functionally graded stems are described and discussed.

The main results achieved from the finite element models (ABAQUS) simulation of the stems implanted inside the femur are systematically detailed and presented. Load transfer from the implanted stems to the intact bone was investigated to estimate the stress shielding. The magnitude of the displacements that occurred between the implanted stems and the intact bone surfaces were measured to evaluate the micromotion. A fatigue study based on the measured yield strength and the Soderberg approach to calculate the factor of safety for each design are presented and detailed.

Bulk / dense Ti-4Al-6V alloy stem was utilized as a comparison point of reference concerning the porous femoral stems.

Figure 4.1 illustrates the results and discussion of interconnective tasks.
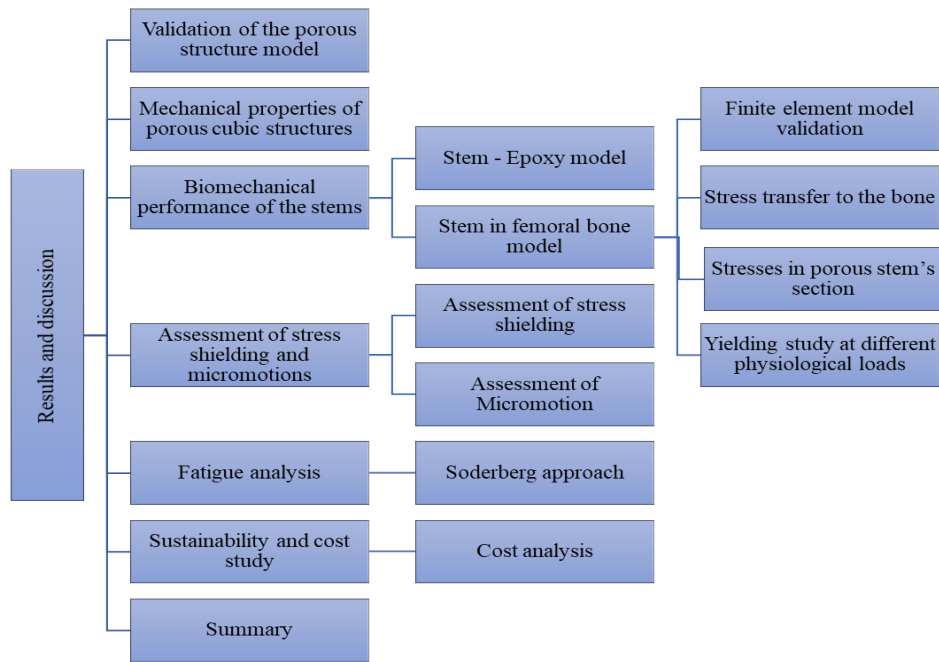
Figure 4.1. Flow Chart of Interconnectivity of the Results and Discussions Tasks

4.1 Validation of the porous structure model

For validation of the work out, the finite element model of the cubic porous structure utilized in this study (Section 3.1.2.1) was validated with Kiven et al. study [130] in which cobalt-chromium-molybdenum (CoCrMo) material was used. Kiven et al. model was reconstructed in ABAQUS software and the same boundary conditions used in the model were applied for the purpose of this validation, the material properties of CoCrMo were reflected in the model as the only change made to the existing one. Cobalt-chrome alloy was selected in order to compare with existing work in literature. Displacement – reaction force results of the finite element model for selected volumetric porosities of 20%, 40%, 60%, 80%, and 95% were obtained and used to generate the stress–strain diagrams. Then, the effective elastic modulus values for the porous structures were determined from these stress–strain graphs. The stiffness obtained from the finite element model utilized in this study generates a strong agreement with the finite element analysis published work (Kevin et. al 2013) [130] as

shown in Figure 4.2.
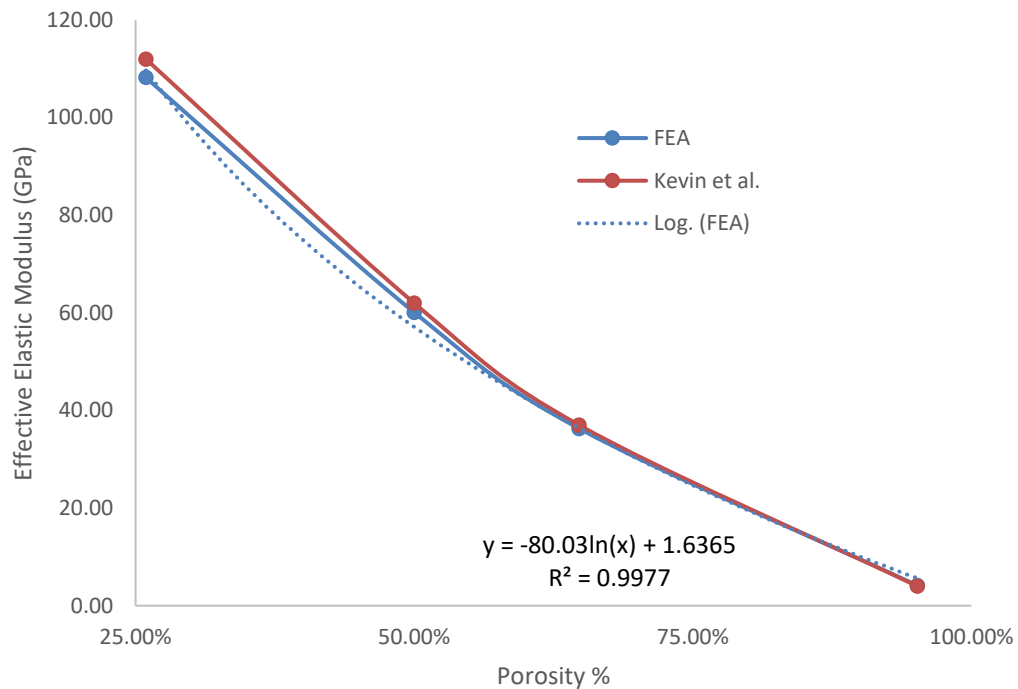
Figure 4.2. Validation of porous structures against FEA results of Kevin et al [130]

The response of the stress-strain of the bulk/dense Ti-6Al-4V alloy with similar cube dimensions of 15 x 15 x 15 mm was also verified for validation when exposed to displacement boundary condition to attain yield point as a minimum. The effective Young's Modulus of the bulk/dense Ti-6Al-4V alloy block was measured from the obtained stress – strain diagram and found to be 123.6 GPa which strongly agrees with the result reported by Hedayat et al. [56], in which the reported Young's modulus was found to be 122.3 GPa.

4.2. Mechanical properties of porous cubic structures

The validated computational model of the cubic porous structure was used to investigate the stress-strain behavior of the structure with different volumetric porosities used in this study. The stress-strain responses obtained for the designed structures with different volumetric porosities are shown in Figure 4.3. The calculated effective Young's modulus and the effective Yield strength of volumetric porosities in the range of 30% to 85% were 52.23 GPa to 7.6 GPa and 307.13 N/mm^2 to 50.17 N/mm^2, respectively. It was observed that the yield strength and Young's modulus are linearly increased with decreasing the structure volumetric porosity, as illustrated in Figure 4.4, which agrees with the findings of the previous study [64].

The Young's modulus and Yield strength of the porous structures having volumetric porosities ranging from 85 % to 70 % were 7.6 GPa to 19.8 GPa and 50.17 N/mm^2 to 123.28 N/mm^2, respectively, which match with the properties of the cortical bone material (Young's modulus 8 – 20 GPa and Yield strength 85 – 109 N/mm^2) [9], [131], [132]. However, based on the USA Food and Drug Administration regulations (FDA, 2016), the approved range of the femoral stem porosities should be between 30–70% to enhance the bone tissue ingrowth [116].

The proposed porosity range was extended to 10% - 90% to design the femoral stems with functionally graded porous structure in the radial direction. The obtained stress-strain mechanical results from the finite element analysis were used to design the stems (the effective Young's modulus and the effective yield strength). Several functionally graded porous designs in the radial direction were developed to achieve the consistent average volumetric porosities of 30%, 50%, and 70%, as listed in Table 3.2 and illustrated in Figure 3.4.
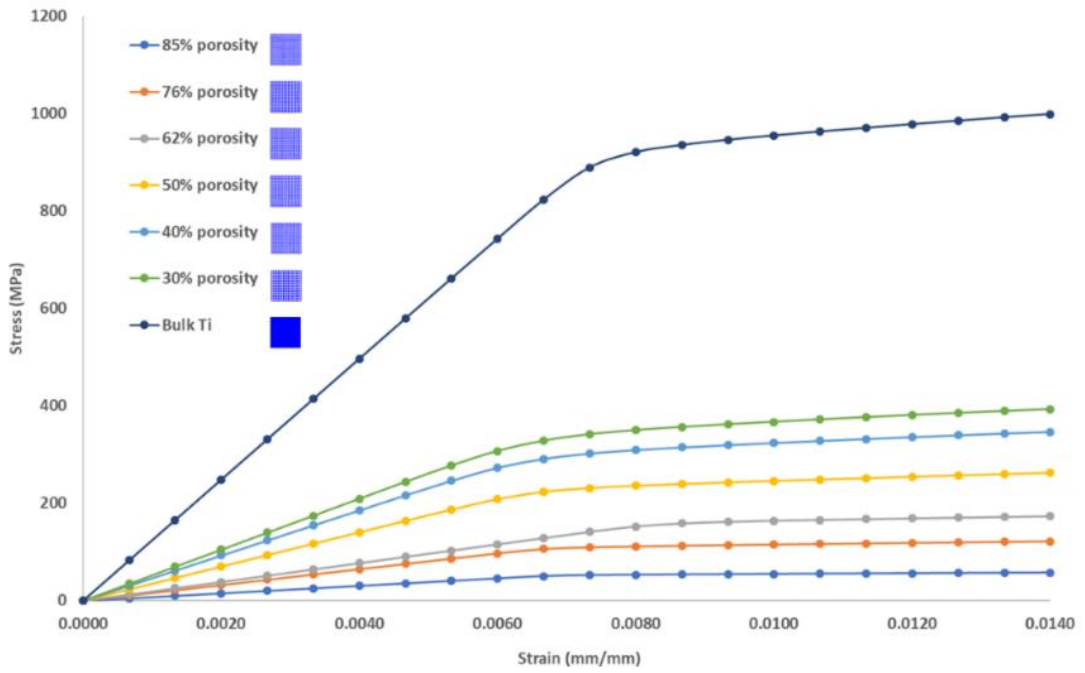
Figure 4.3. Stress-Strain diagram for the designed porous cubes with relevant volumetric porosities.
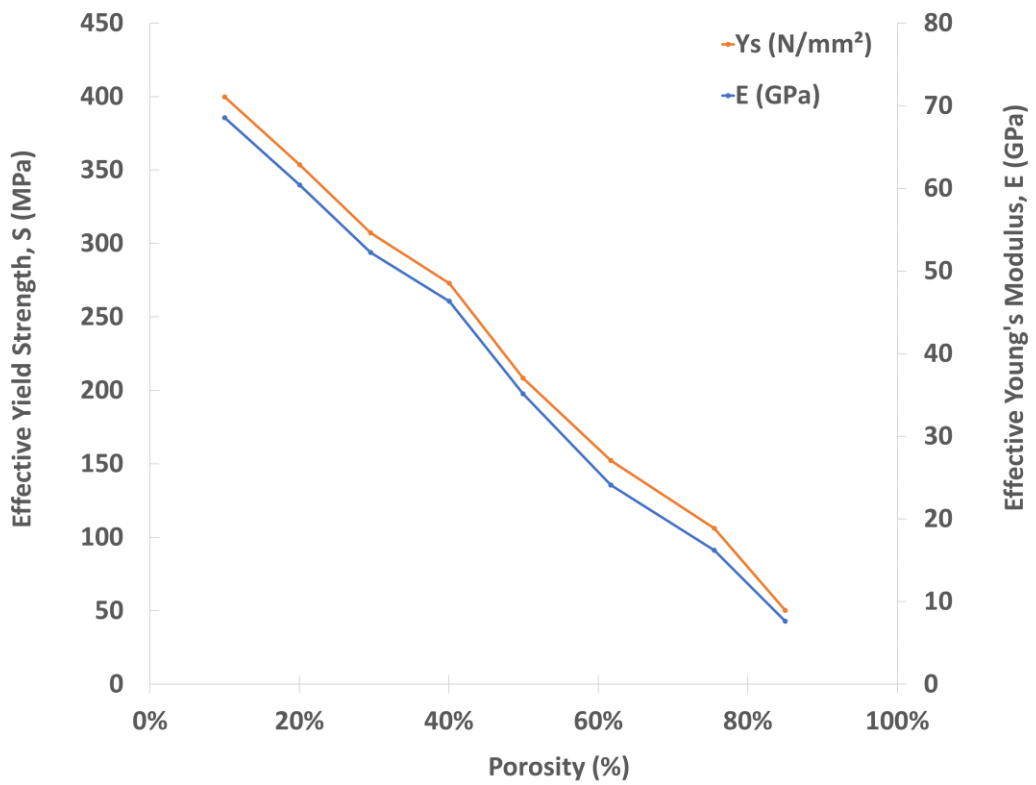
Figure 4.4. Effective Young's modulus and effective yield strength with varying porosity obtained from the finite element simulation

4.3 Biomechanical performance of stems

4.3.1 Stem in epoxy model

The total displacement was measured at the femoral stem head for all porous stem designs and bulk/dense Ti-4Al-6V alloy stem at each loading increment/step. Force–displacement diagrams were plotted for the bulk / dense Ti-4Al-6V alloy and the porous stem structures of the stem in the epoxy model as illustrated in Figure 3.5 and the results were compared with the intact bone [130] force-displacement response as illustrated in Figure 4.5. It is evident from the force-displacement curves that the stiffness of the porous stems were increased as the volumetric porosity decreased. It is also obvious that the stems designed with 70% volumetric porosity (functionally graded and homogeneous porous structures) were found to offer the best match with the force-displacement diagram of the intact bone. Designs D12 and D14 presented the stiffness of 361N/mm and 417N/mm, respectively, and these values are comparable with the intact bone stiffness (375N/mm). There was considerable reduction in the stiffness of around 80 % to 83 % with relevance to the bulk / dense Ti-6Al-4V alloy stem (2149N/mm). However, yielding for all stems with average volumetric porosity of 70% at an applied force of more than 1500N is observed, which agrees with previous studies' findings [7], [87]. This yielding status is attributed to the stresses applied at 2250N which exceed the yield stresses of the equivalent porous material.
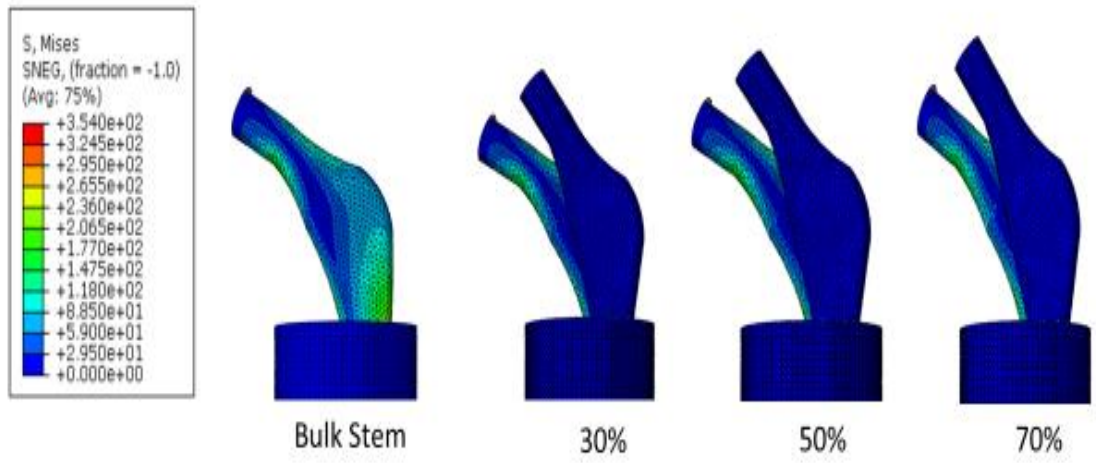
(a)
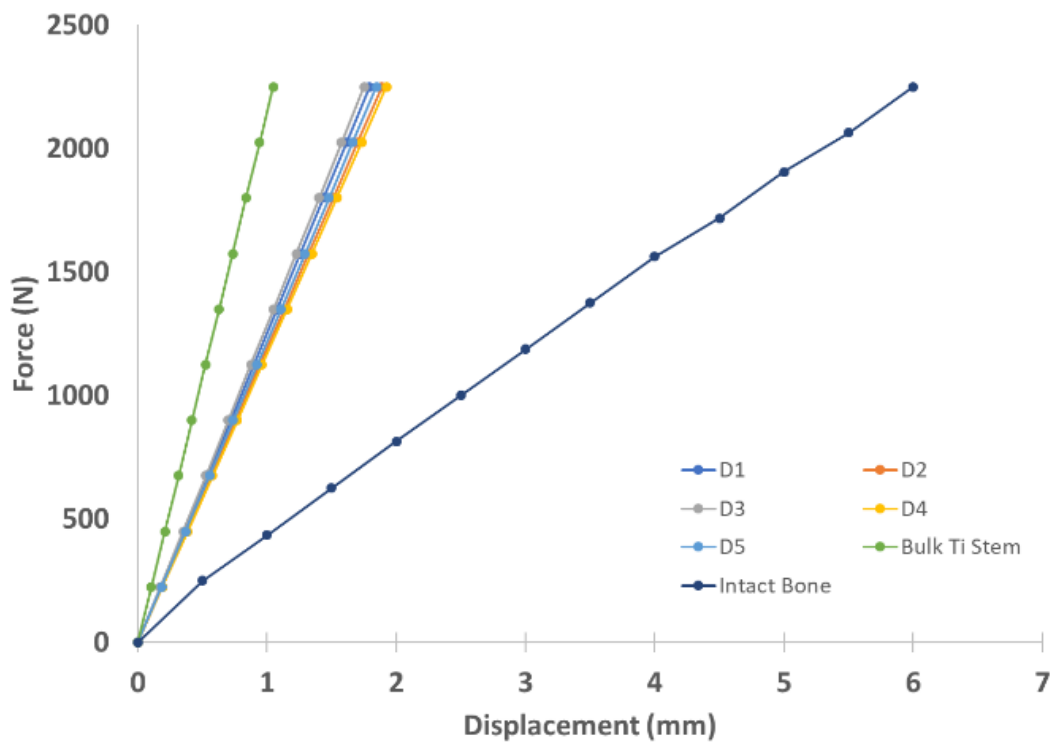
(b)
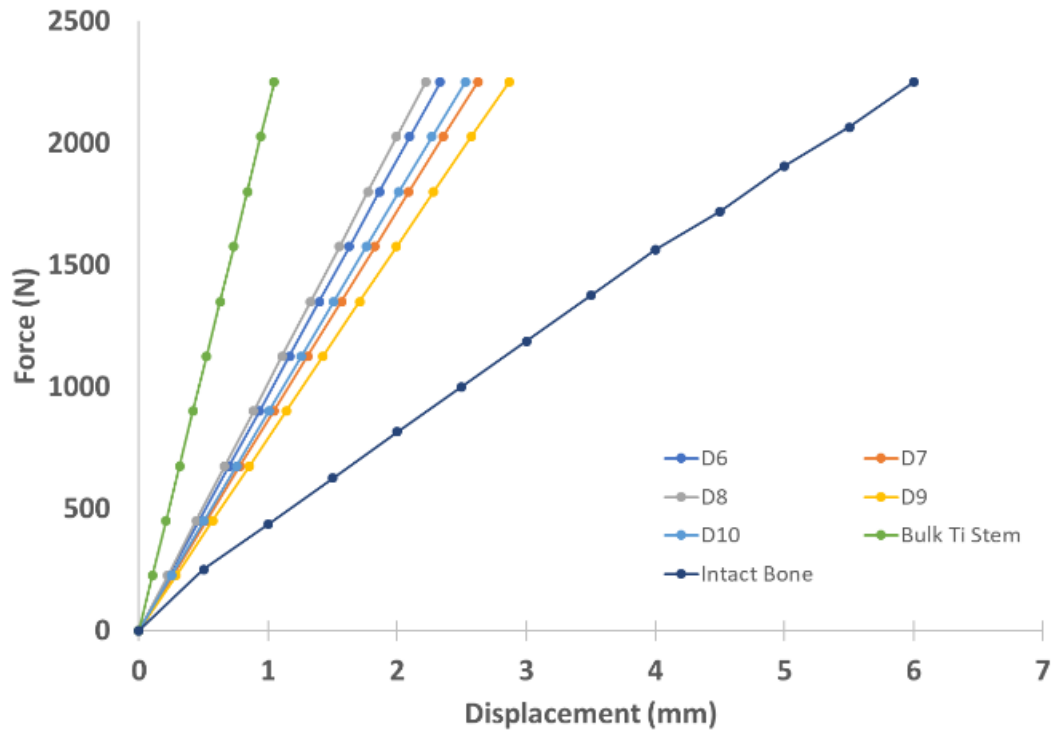
(c)
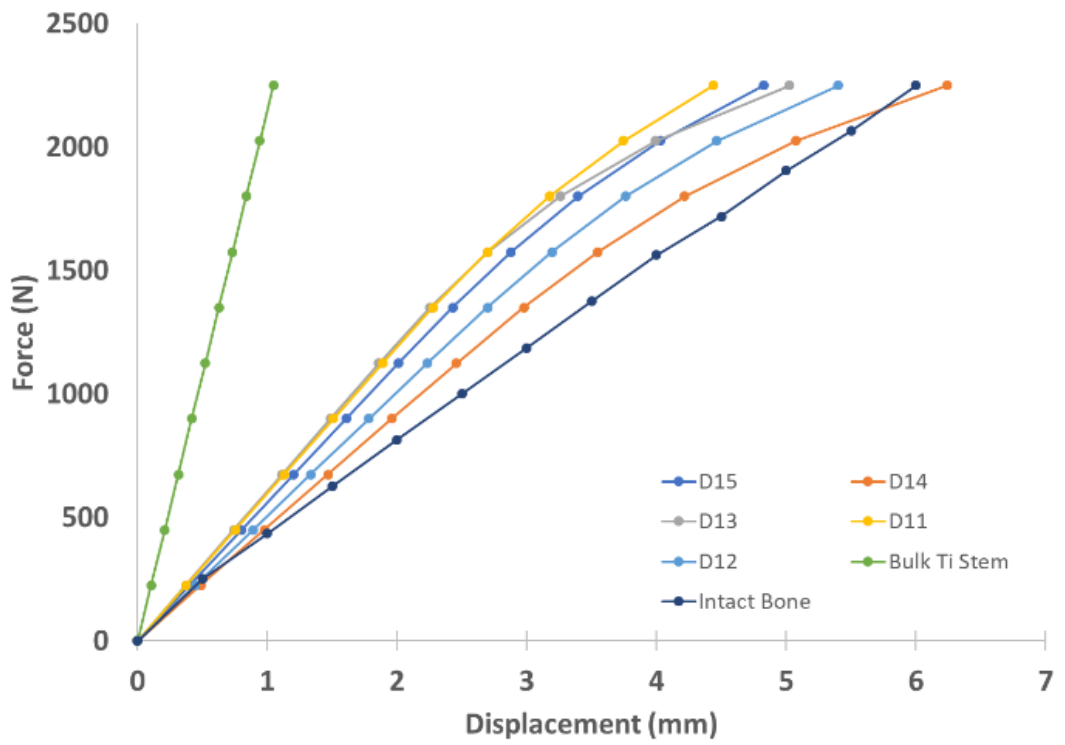
(d)

Figure 4.5 Force displacement diagram for stem designs; (a) 30%, (b) 50%, and (c) 70% volumetric porosities respectively, along with Intact bone and Bulk / dense Ti-6Al-4V alloy stem

In addition to the above, and in reference to the results obtained from the force – displacement calculations and figure 4.5, the average percentages of stiffness reductions of the femoral stems as a result of introducing porosities of an average of 30%, 50%, and 70 % to the femoral stems in comparison with the bulk / dense femoral stem are 43%, 58%, and 83%, respectively. This finding strongly agrees with the results obtained in the literature [88], [133], [134]. Hence, the proposed designs achieved the target of reducing the stiffness of the femoral stems significantly in order to be as close as possible to the intact femoral bone properties, leading to an expected significant reduction of the stress shielding in comparison with the bulk /dense Ti-4Al-6V alloy stem. Table 4.1 summarizes the stiffness obtained from the force–displacement diagrams with the percent reduction in stiffness with reference to the bulk /dense Ti-4Al-6V alloy stem.

Table 4.1 Percentage of stiffness reduction achieved from introducing porosities to the femoral stem in comparison with bulk / dense Ti-4Al-6V alloy stem [10], [64], [66], [117], [121], [130]

Stem Design	Stiffness (N/mm)	Average Stiffness (N/mm)	% Reduction in stiffness
D1	1254.18		
D2	1191.11		
D3	1284.98	1223.58	43%
D4	1169.44		
D5	1218.19		
D6	964.01		
D7	857.14		
D8	1013.06	901.68	58%
D9	784.52		
D10	889.68		
D11	507.10		
D12	416.67		
D13	447.67	439.70	80%
D14	360.75		
D15	466.32		
Bulk stem	2149.00		

4.3.2 Stem in femoral bone model

4.3.2.1 Validation of the finite element model

Finite element models of stem implanted in the bone were validated with the model of Jette et al. [87] using ABAQUS finite element analysis software. A bulk /

dense Ti-4Al-6V alloy stem was implanted inside the bone, as illustrated in Figure 4.6, and subjected to a concentrated load of 3000 N at the stem's head, with the load applied in ten increments. The displacement was tracked at a selected point on the bone head. Force–Displacement data were plotted and compared with Jette et al. experimental results [87]; a strong agreement was noticed between the two models, as shown in Figure 4.6. It can be concluded from this validation result that the difference in implant geometry between Jette et al. and the model has less impact on the results. The slight difference in the curves can be attributed to the difference in the exact position of the selected point on the bone head.
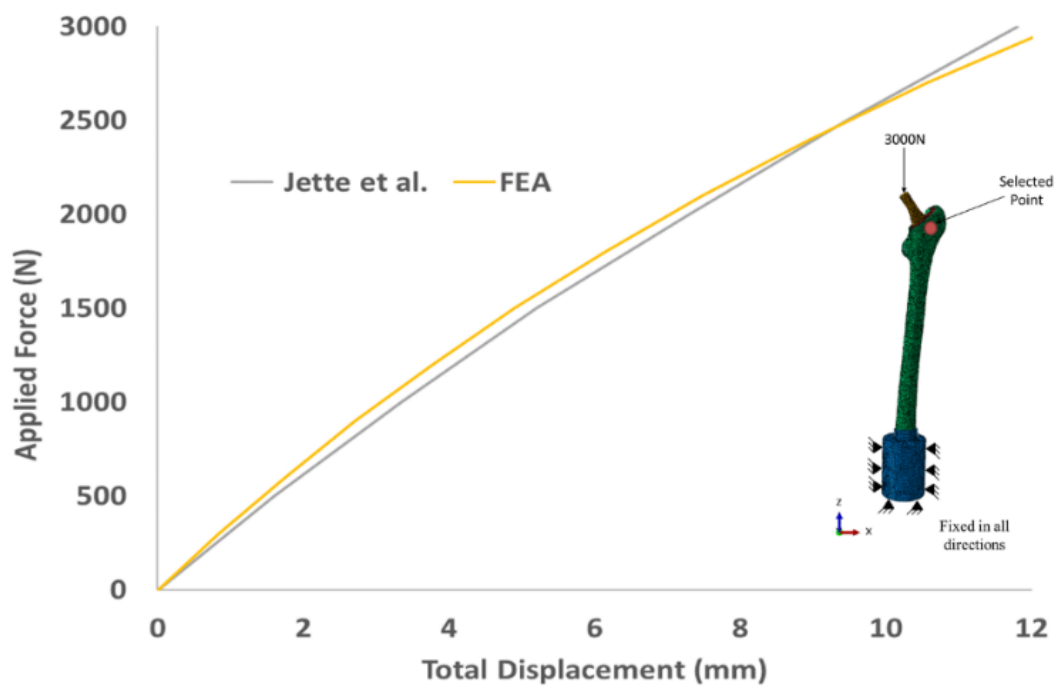
Figure 4.6. Stem–Bone assembly validation.

4.3.2.2 Stress transfer to the bone

The distributions of von Mises stress in the femur bone implanted with bulk / dense and porous Ti-4Al-6V alloy stems with homogeneous volumetric porosities of

30%, 50%, and 70% which occurred due to applying the three physiological loads resulting from the walking speed at 1km/hr., 3km/hr., and 5km/hr., are shown in figure 4.7. It is obvious from the figure that the femur implanted with a bulk/dense Ti-4Al-6V alloy stem displays a lower amount of stress transferred at all loading conditions. In addition, the amount of stresses transferred from the stem to the bone increased as the volumetric porosity increased. This can be attributed to the stem's stiffness reduction by introducing a porous structure that provides extra load stress transfer to the femur. This finding is in agreement with other published works [10], [130], [133]–[135]. The stresses transfer percentages of the functionally graded and homogeneous porous stems in comparison to the Bulk / dense Ti-4Al-6V stem are illustrated in table 4.1. Further discussion on the stress transfer results will be elaborated in section 4.4.
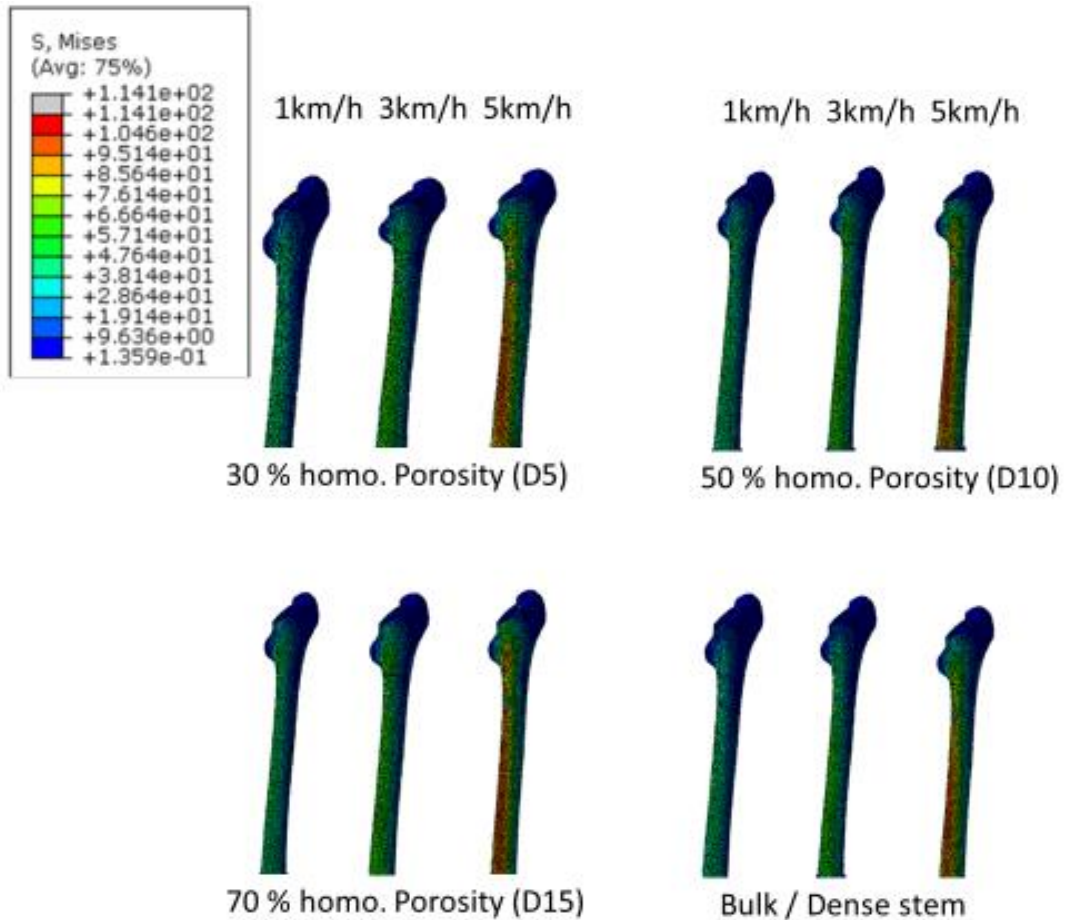
Figure 4.7 The distribution of von Mises stress in the femur as a result of physiological loading conditions associated with the three walking speeds

4.3.2.3 Stresses in porous stem's section

The stresses within each stem's porous layer were computed through the finite element analysis (FEA) results for the fifteen functionally graded and homogeneous stem designs and for each of the three walking speeds (1 km/hr, 3 km/hr, and 5 km/hr) as illustrated in Figure 4.8. Stresses in the porous stems were found to be less than bulk / dense stem one, which indicates that, part of the applied loads/stresses are distributed between the femur bone and the stem as explained in section 4.4 in detail. This is attributed to the difference in the stiffness value associated with each stem's design in

comparison with the bulk / dense stem stiffness (114 GPa). Hence, the stress level on the stem is affected by two factors, firstly, the applied loads associated with the different walking speeds and secondly, the stiffness of the designed stems. Though the stress distributions along the functionally graded stem's layers were varied with the maximum values reported at the outer stem's layer for all designs and all walking speeds, this is attributed to the variance in Young's modulus of each porous layer and the stem's outer layer is in direct surface to surface contact with the femur bone canal.
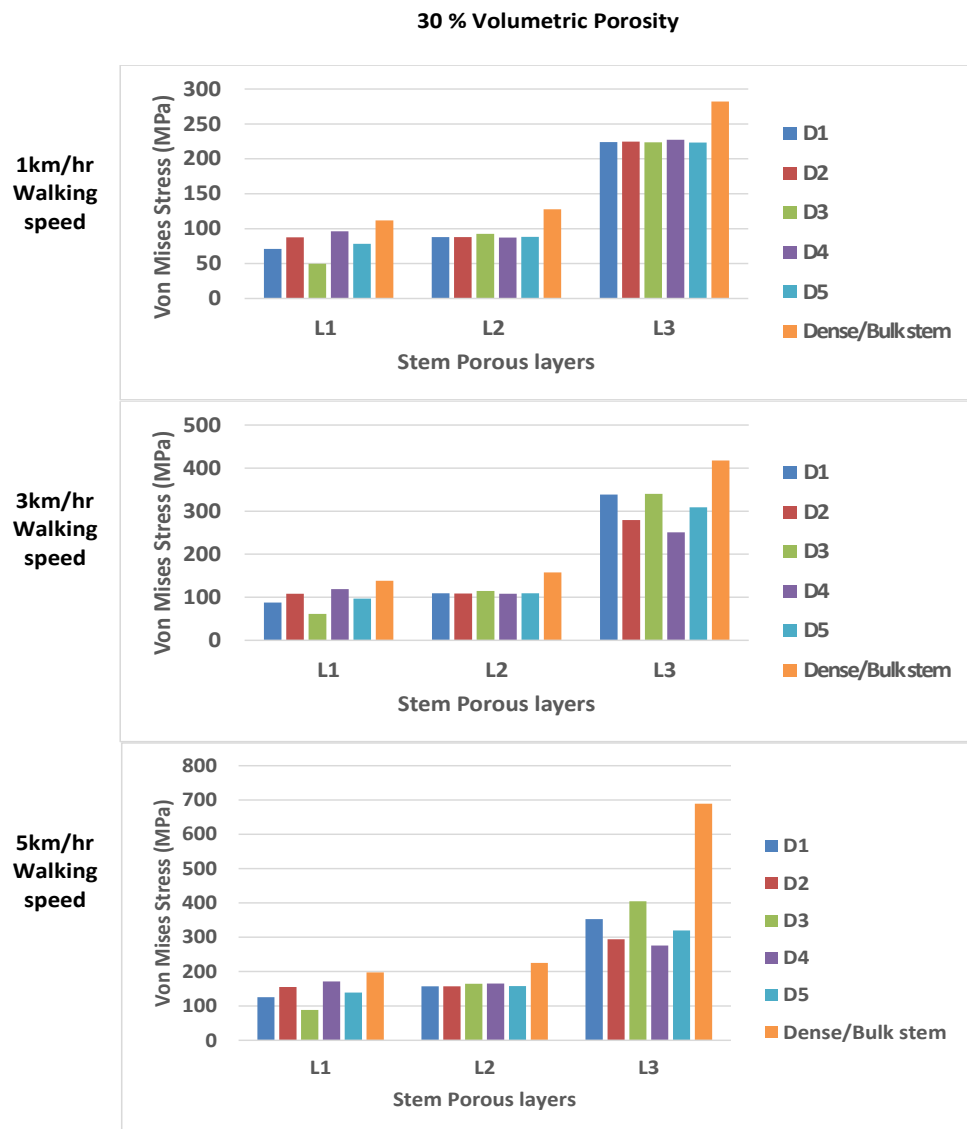
(a)

50 % Volumetric Porosity

(b)

70 % Volumetric Porosity
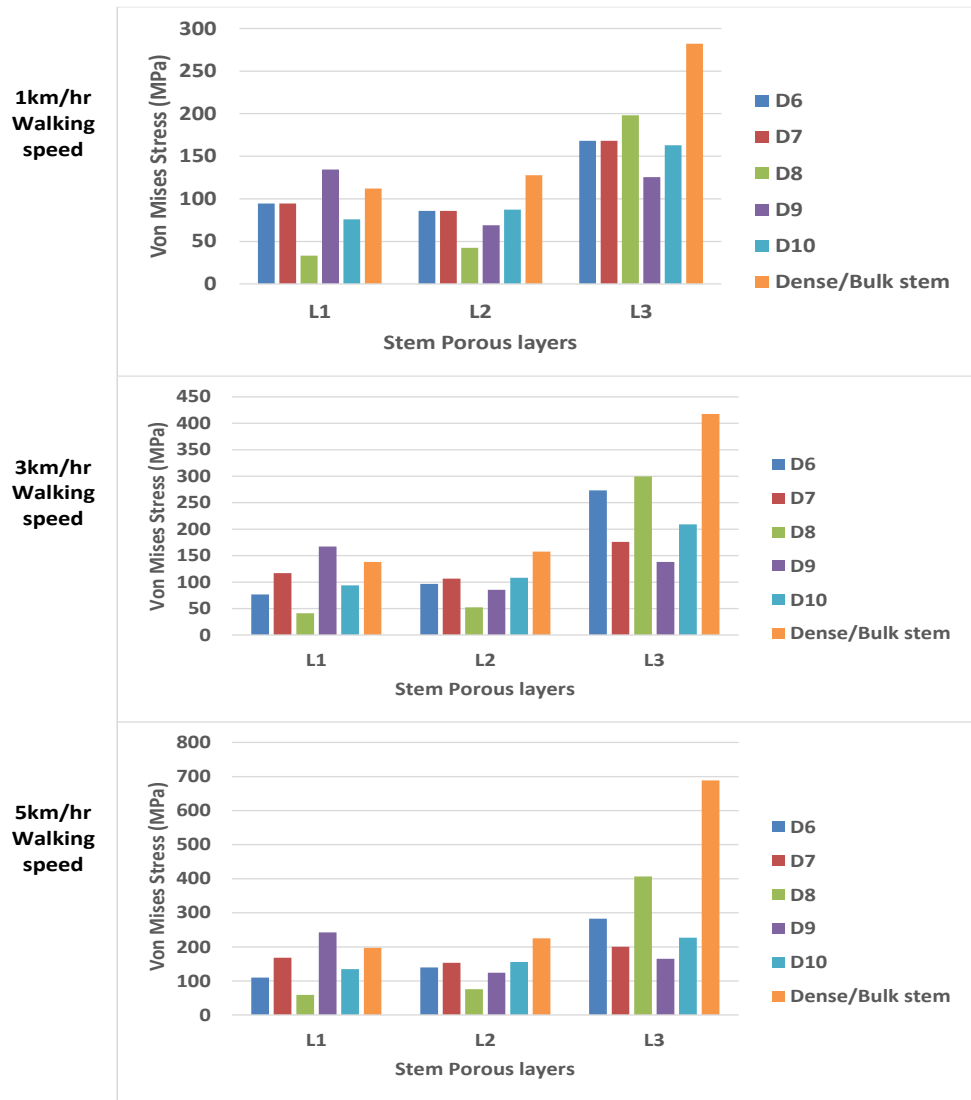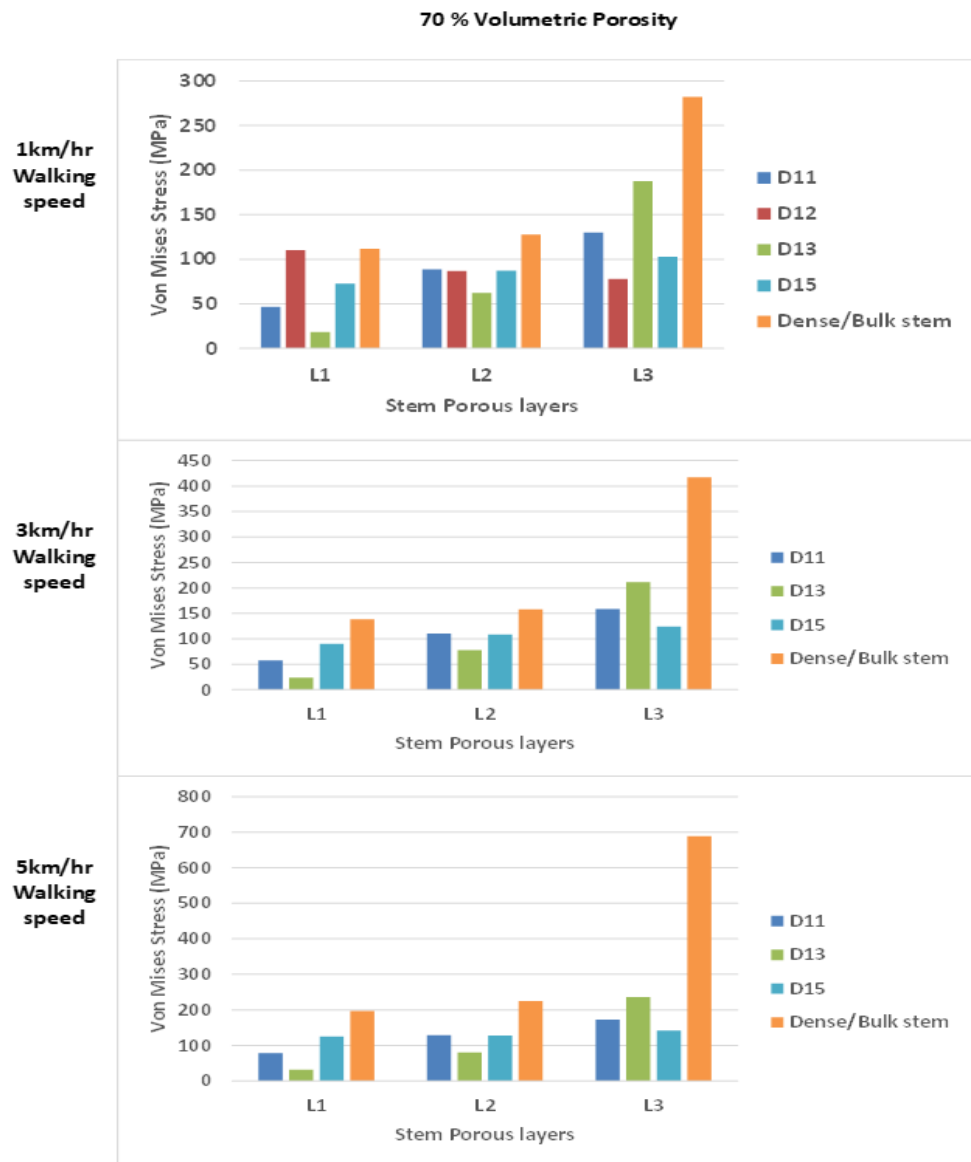
(c)

Figure 4.8. Stresses within each porous layer computed through the FEA results for the fifteen homogeneous and FG designs and each of the three walking speeds: (a) 30% volumetric porosity, (b) 50% volumetric porosity, and (c) 70% volumetric porosity

79

4.3.2.4 Yielding study at different physiological loads

The yield strength was studied for each stem's porous layer associated with the relevant cellular structure volumetric porosity and compared with the stress values computed via the finite element analysis of the stem – bone models. The obtained results show that all designs are not yielding at a walking speed of 1 Km/hr except designs D9 and D12 which hold a stress value at the stem's outer layer equal to the yield strength value related to 70% and 80% porosity, respectively, and design D14 which has a porosity value at the stem's outer layer of 85% and that gave no results in ABAQUS finite element analysis (no convergence reached). At 3 Km/hr walking speed only designs D1, D3 and D8 were observed to be not yielding and safe. All designs were found to be yielding at a walking speed of 5 Km/hr as the stresses encountered are higher than the yield strength associated with the relevant porous structure of each design. Stem failure (SF) is calculated based on the stress ratio between the relevant stem layer yield strength (Y_{sl}) and the maximum stress value of that layer (σ_{Lm})as per equation 4.1.

$$SF = \frac{Y_{sl}}{\sigma_{Lm}} \qquad\qquad (4.1)$$

The design will not fail / yield if *SF* value > 1.0, the results are illustrated in Figure 4.9.

(a)

(b)
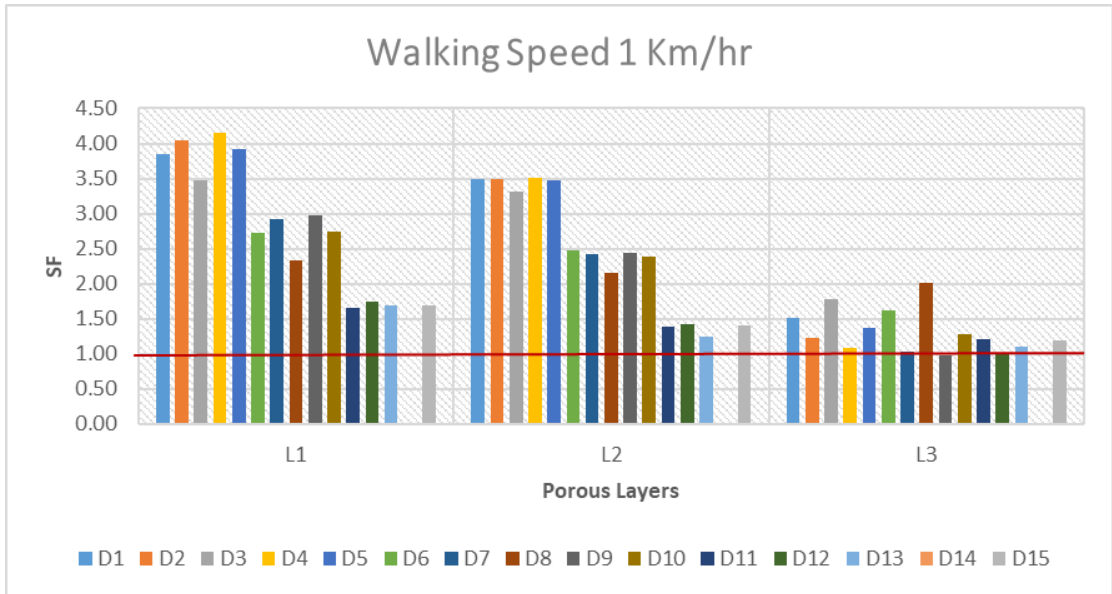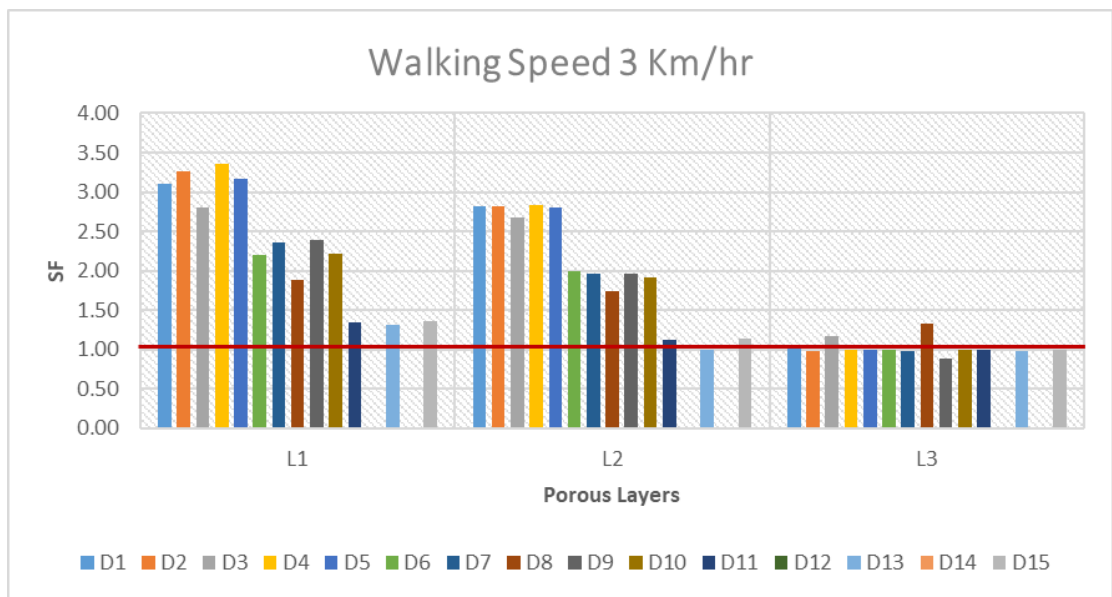
Walking Speed 5 Km/hr
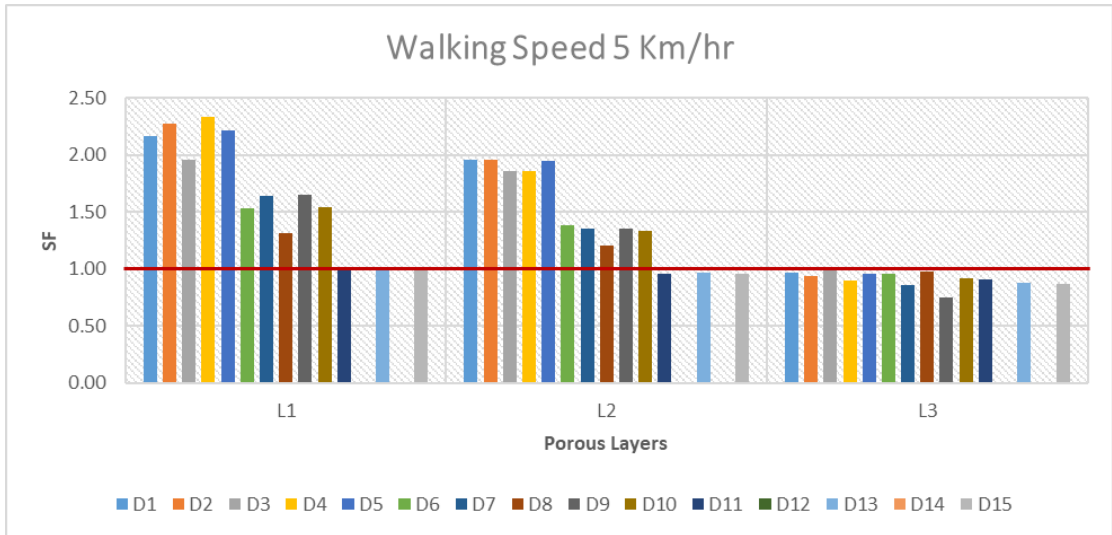
(c)

Figure 4.9 Stress ratio between the relevant stem layer yield strength (Y_{sl}) and the maximum stress value of that layer (σ_{Lm}); a: at 1 km/hr walking speed, b: at 3 km/hr walking speed and c: at 5 km/hr walking speed

It is evident from figure 4.9 that as the volumetric porosity increased the SF value decreased, which is attributed to the reduction of the stiffness and yield strength with the increasing the volumetric porosity percentage.

A previous experimental study by Yavari et al. [81] shows the superiority of the cubic porous structures over the other structures such as diamond shape structures. None of their cubic structure tested samples failed under cyclic loading at a maximum load of 80% of the relevant porous structure yield strength ($0.8\sigma_{Ys}$) [81]. This finding is comparable with the computational analysis findings up to certain loading conditions as illustrated in figure 4.9.

4.4 Assessment of stress shielding and micromotions

4.4.1 Assessment of stress shielding

The stress shielding assessment was done to evaluate the femoral stems performance based on stress distribution along the Gruen Zones resulting from transferring the loads / stresses from the implanted stem to the femur bone. The region of interface between the femur bone and the implanted stem is split into seven zones (Gruen zones) as shown in figure 3.6 -b [65], [66]. The highest von Mises stress values for the cortical bone (1-7 Gruen zones) and trabecular bone (1, 2, 6, and 7 Gruen zones) which have direct contact with the stem were specified and recorded. In general, to reduce stress shielding, an implant should transfer some of the stresses to the bone Gruen zones. The von Mises stresses obtained for the fifteen homogeneous and functionally graded (FG) designed stems and bulk / dense Ti-6Al-4V alloy stem implanted in the femur for the three different walking speeds (1 km/hr, 3 km/hr, and 5km/hr) are shown in (Figure 4.10). From these plots, it is seen that porous Ti-6Al-4V alloy stems show better performance than bulk / dense Ti-6Al-4V alloy stem in terms of reducing stress shielding (higher stress values reported in the bone due to stress transfer from femoral stems to the femur bone). There was almost no obvious difference between the FG designs for each used average porosity (30%, 50%, and 70%) regardless of the walking speed for both areas of the cortical and trabecular bone. The maximum stress values are reported at stems distal zones of the femur and the values are decreased gradually as moving to the proximal zones, which is in agreement with the other published works [24], [136]. However, the most critical zone 7 which is near the femur calcar area shows higher stress values compared to zone 6. This is required as zone 7 is the critical area where the implant failures due to the stress shielding occurred at this zone [65], [117]. It is worth mentioning that, comparing the stress values in the femur with other studies is difficult because of the differences in porous

structures geometries, loading conditions, boundary conditions, and assigned material properties in femur bone and femoral stems.

The stress transfer to the bone and percent of the stress shielding reduction is obvious, as shown in Figure 4.10 and illustrated in Table 4.2. It is evident that the highest percentages of stresses transfer in comparison with the bulk / dense Ti-4Al-6V alloy stem have occurred at the proximal area of the femur at Gruen zones G7, G1, G6, and G2, and the lowest values have occurred at the distal zones (G4, G3, and G5). The minimum values were reported at Gruen zone 4 (G4), and the maximum values occurred at Gruen zone 7 (G7) with approximate percentages of 36 %, 48 %, and 63 % for volumetric porosities of 30%, 50%, and 70%, respectively. It has been noted that the stress transfer percentage values at Gruen zone 7 (G7) are not significantly affected by increasing or decreasing the walking speed.

The stress shielding was evaluated based on the percent of stress transfer to the femur bone from the designed FG stems compared with the bulk / dense stem. The transfer of the stresses at the trabecular bone from the designed FG and homogeneous porous stems is higher (20% to 65%) than that from the bulk / dense stem, indicating sufficient reduction in stress shielding.

30% Porosity
1Km/hr Walking Speed

50% Porosity
1Km/hr Walking Speed

70% Porosity
1Km/hr Walking Speed
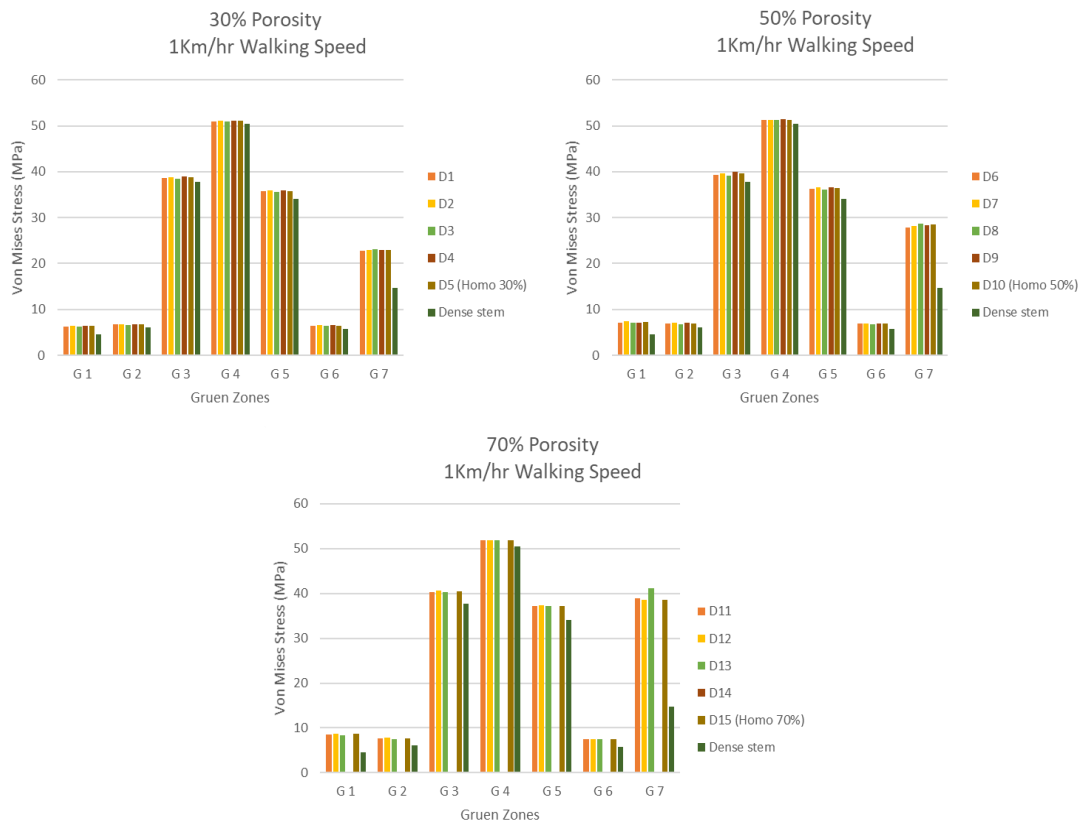
(a)
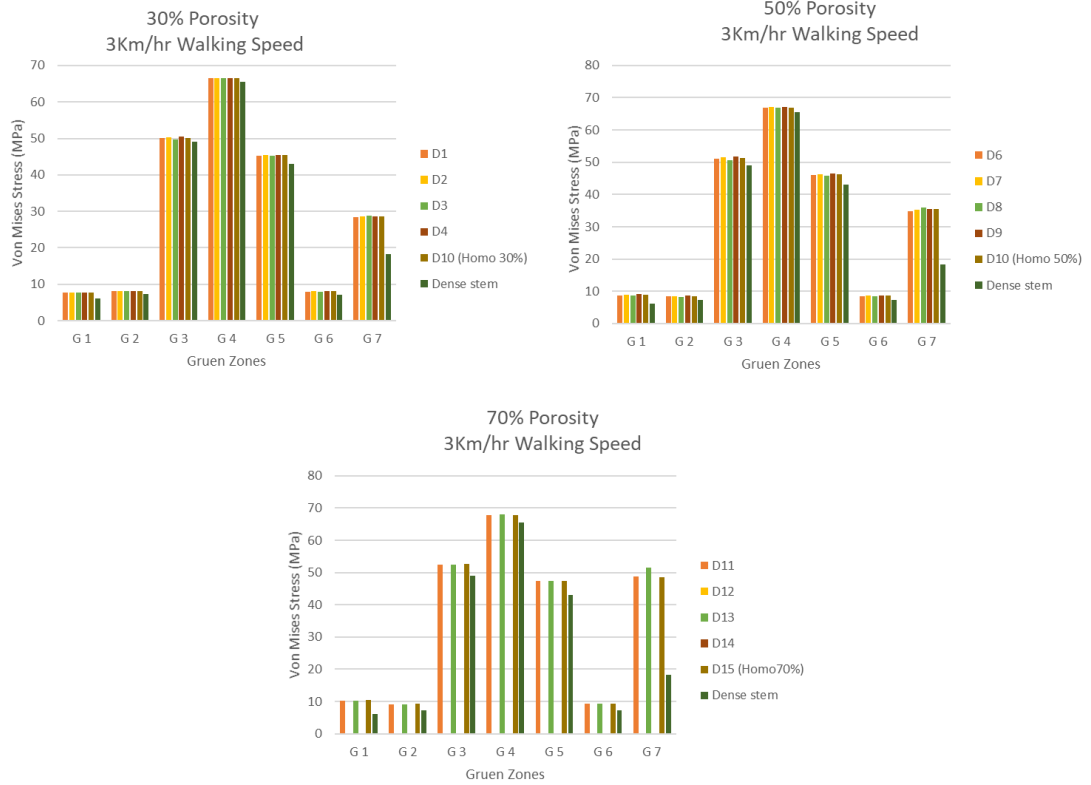
(b)
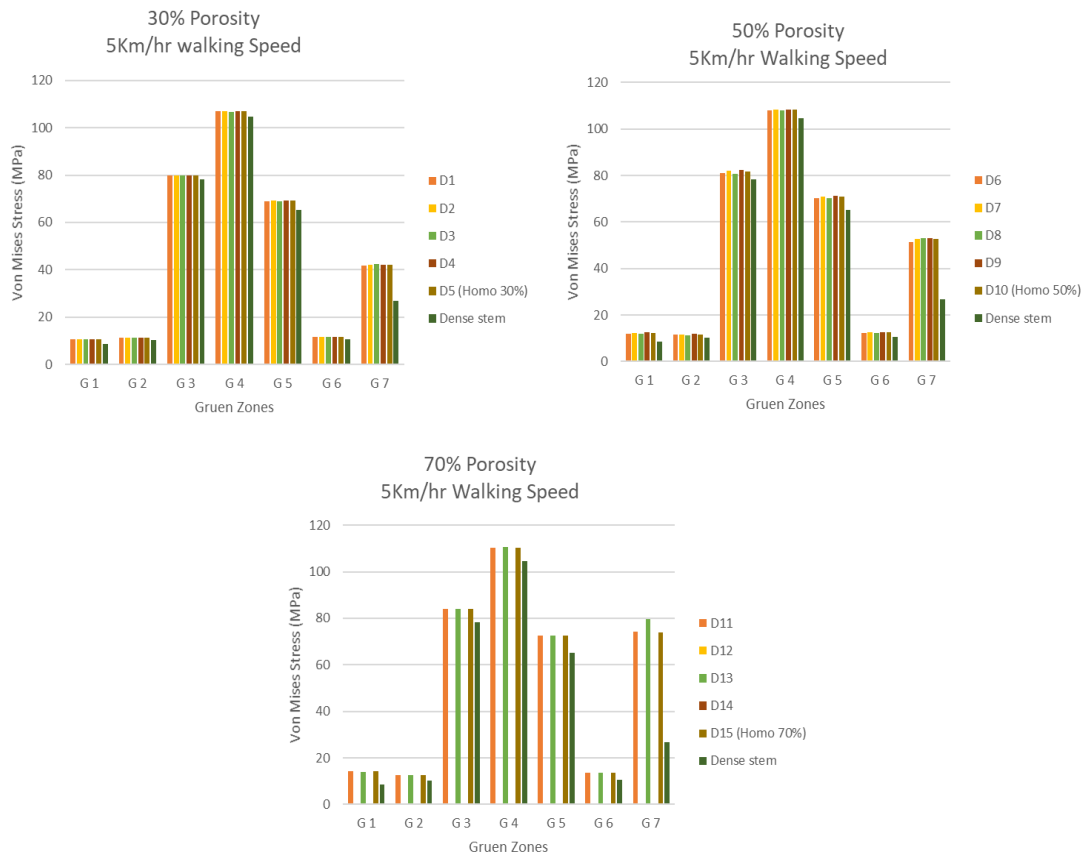
(c)

Figure 4.10 Stresses at Gruen Zones of the functionally graded porous stems and the Bulk / dense Ti-6Al-4V alloy stem for proposed designs for different walking speeds: (a) 1 km/ hr., (b) 3 km/ hr., (a) 5 km/ hr.

It can be concluded from Figure 4.10 and Table 4.2 that the stress transfer from the stem to the bone at Gruen zone 7 increases as the porosity increases, which is associated with lower stiffness at a higher volumetric porosity percentage, and these findings agree with the previous studies [10], [87], [117]. It is also obvious that the highest stress transfer to the bone at proximal area is depicted at Gruen zone 7 for all porous stem designs, which is required to avoid the hip stem failures due to the stress shielding [29], [137] as this zone is susceptible to bone resorption [138]. The distal part of the stems has more stress values than the proximal part with a minimum value of the stress transfer to the bone for all porous stem designs found in Gruen zone 4, which agrees with the results stated in the literature [24], [26], [29], [137], [139]. The inadequate stress transfer to the bone for all porous stem designs in zones 3, 4, and 5 is attributed to the proximal load transfer to the bone, and torsional stress induced by the applied load in these areas [29], [117].

The stress values at Gruen zones G3, G4 and G5 are almost identical for all volumetric porosities stems at each same walking speed, and the values are increased as the walking speed increases. Hence, it can be concluded that, there is no significant effect of introducing porous structure at any value at the distal area of the stems as most of the loads are being transferred to the proximal area of the femur.

In summary, the proposed designs achieved the target to reduce the stress shielding of the femoral stems significantly with reference to the bulk / dense Ti-4Al-6V alloy stem. However, as the volumetric porosity of the femoral stem increased, the

stiffness decreased which can be risky and can lead to implant failure under certain loading conditions due to excessive micromotion and fatigue failure.

Table 4.2 Stress transfer percentages of the homogeneous and functionally graded porous stems when compared to the Bulk / dense Ti-6Al-4V alloy (reduction in stress shielding)

	1km/hr Walking Speed						
Design	**G 1**	**G 2**	**G 3**	**G 4**	**G 5**	**G 6**	**G 7**
30% Porosity	27.1%	9.4%	2.5%	1.2%	7.4%	10.4%	35.9%
50% Porosity	35.8%	12.2%	4.5%	1.8%	9.6%	16.1%	48.1%
70% Porosity	46.1%	20.3%	6.6%	2.8%	12.3%	22.3%	62.6%

	3km/hr Walking Speed						
Design	**G 1**	**G 2**	**G 3**	**G 4**	**G 5**	**G 6**	**G 7**
30% Porosity	21.8%	9.5%	2.2%	1.5%	7.8%	10.2%	36.1%
50% Porosity	31.8%	12.3%	4.3%	2.2%	10.1%	16.0%	48.4%
70% Porosity	41.4%	19.8%	6.6%	3.5%	12.7%	22.1%	63.1%

	5km/hr Walking Speed						
Design	**G 1**	**G 2**	**G 3**	**G 4**	**G 5**	**G 6**	**G 7**
30% Porosity	20.3%	10.5%	2.2%	2.2%	-70.9%	9.9%	36.6%
50% Porosity	30.5%	12.9%	4.1%	3.3%	-66.1%	15.9%	49.2%
70% Porosity	40.0%	19.2%	6.8%	5.2%	-60.8%	22.4%	64.9%

4.4.2 Assessment of micromotion

Micromotion at the stem–femur interface was studied for the proposed designs, which are vital to evaluating stem stability by enhancing bone tissue ingrowth.

Debonding at the bone–stem interface can lead to premature implant failure. A micromotion value of more than 150 µm is considered excessive and causes instability of the implant [9], [11], [140]. The average micromotion of the proposed designs is illustrated in Figure 4.11. Stem designs with an average porosity of 70% showed the maximum micromotion values of more than 150 µm at 3 km/hr and 5 km/hr walking speed beside the design with 50% porosity at 5 km/hr, which is attributed to low stiffness values of the higher porosity stems, and the loading conditions associated with the walking speed. These designs are susceptible to aseptic loosening and the instability of the implants which may lead to premature failure of the stem. Adding a thin bulk / dense Ti-4Al-6V alloy as an outer skin to the designed stems may reduce the micromotion value and the porosity can be replaced by porous coating to enhance the bone tissue ingrowth which will be part of a future study.

The lowest stem – femur micromotions of the porous stem structures were observed for the 30 % volumetric porosity stems and the overall lowest stem – femur micromotions are observed for the highest stiffness of the bulk / dense Ti-4Al-6V alloy stem for all loading conditions associated with all applied walking speeds. These findings agree with the previous studies [26], [117].

Even though many potential stem candidates that provide enhanced resistance to micromotion have been identified, there are some limitations associated with bone quality, body weight, age, gender and further loading conditions and daily activities scenarios, which will be part of a future study.
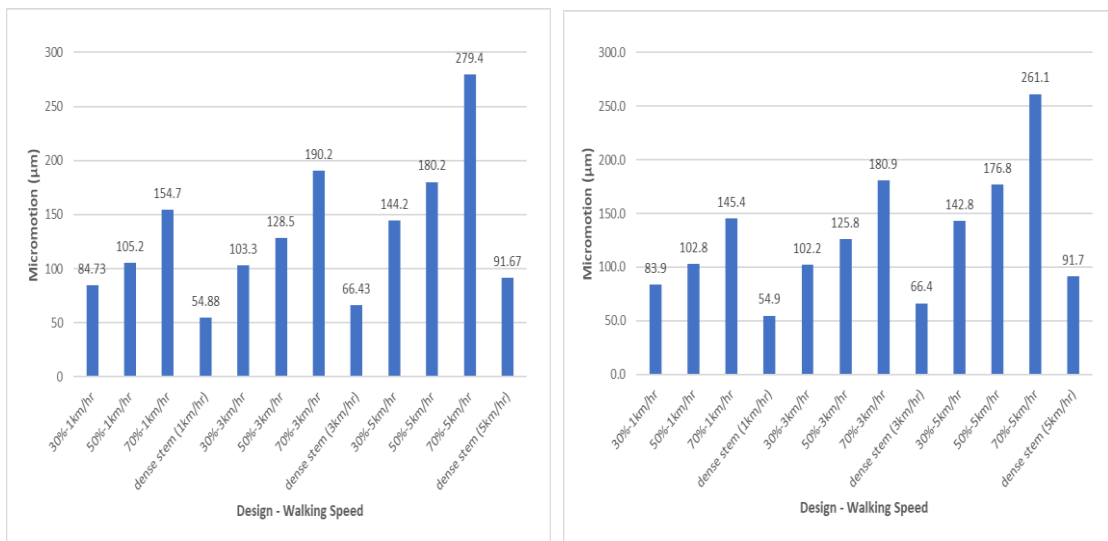
(a)

(b)
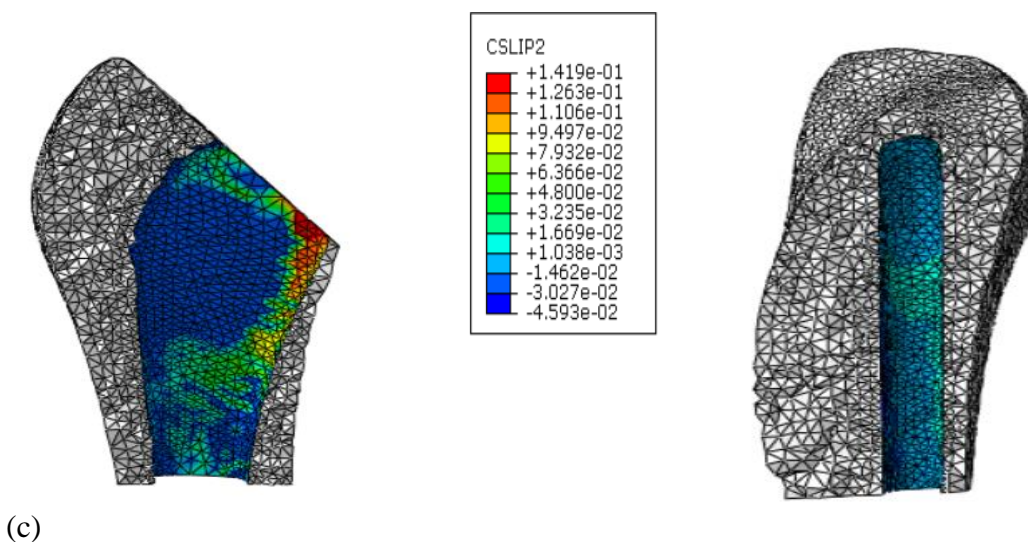
(c)

Figure 4.11 Micromotions (a) maximum micromotion, (b) average micromotion of the designed FG stems vs. bulk / dense stem at 1, 3, and 5 km/hr. walking speed. (c) graphical representation of micromotion in the bone (typical example)

4.5 Fatigue factor of safety (Soderberg approach)

Fatigue factor of safety is one of the important factors used for the evaluation of the femoral stem's durability [54]. Taking into consideration the other factors that need to be included in the porous femoral stem design such as stress shielding, and micromotion for enhancing the implant's stability through improving bone tissue ingrowth in order to avoid premature implant failures. Stresses encountered within the stem during the daily activities shall be computed and compared with the yield strength of the used porous structure [79], [141]. Most of the previous studies predicted the fatigue limit using FEA for solid stems and under concentrated compression load, but very few studies were found performed for porous stem [51], [83], and no literature was discovered on computing the fatigue life for porous stems using different physiological loads. Hence, in this study, the factor of safety was calculated for each design using Soderberg Approach. This approach is efficiently capable to estimate the fatigue limit of the femoral stem under high cyclic loading condition [83] and this approach provides the worst-case scenario among the other approaches, namely, Goodman and Gerber [83].

The maximum and the minimum stresses were identified based on increments 1 and 10 of the FEA (ABAQUS) results, i.e., cyclic stress ratios R=0.1 for calculating the minimum and maximum stresses as shown in equations 3.1 – 3.4. The factors of safety (N_f) were calculated and the results for all designs in relation to the three walking speeds are shown in Figure 4.12. The designs that have a factor of safety > 1 are considered safe under cyclic fatigue loading. None of the fifteen designs was found to be safe under a walking speed of 5 Km/hr. Only design 8 (D8) is safe to be used up to a walking speed of 3 km/hr and the von Mises stress is less than the associated yield strength at 1 km/hr and 3 km/hr. Designs D1, D2, D3, D5, D6, D8, D10, D11, and D15

are safe under a walking speed of 1 km/hr. All of these designs also had von Mises stresses less than their associated yield strength at 1 km/hr walking speed. Most the THA patients normally have a maximum normal walking speed of 1.54 km/hr, however, the speed level is expected to be less than that for the elderly patients [142], [143]. Hence, the target to have sustainable porous stems at high cyclic loading is attained at certain loading conditions which are suitable mostly for elderly patients.

The proposed femoral stem designs can be improved to enhance the fatigue factor of safety by adding an outer dense shell to the porous stem structure with different thicknesses [9] which will be part of a future study.
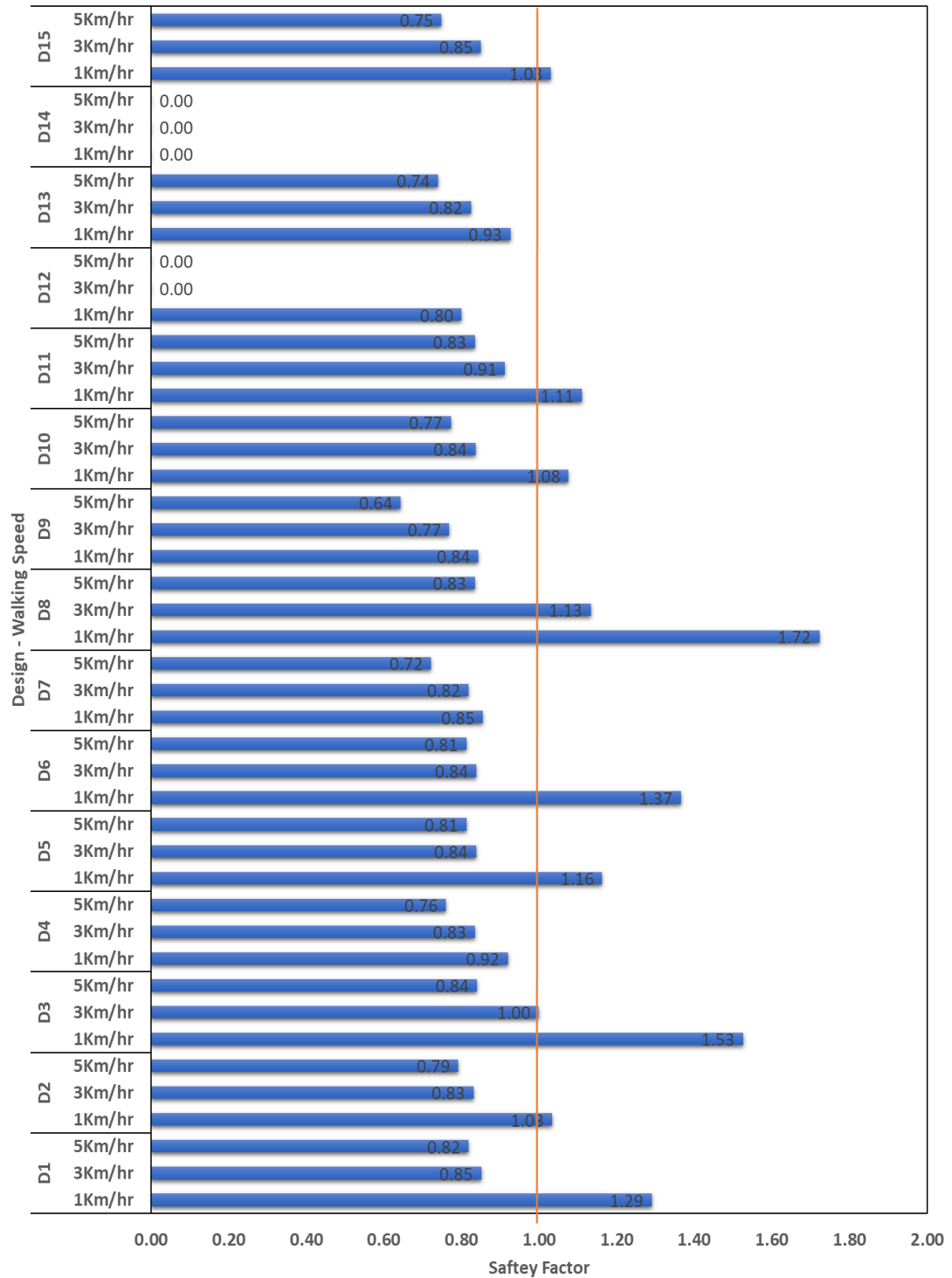
Figure 4.12 Soderberg Factors of safety obtained for the designed stems under the three loading conditions. (0.0 values shown for D12 and D14 denotes that no results are obtained as the FEA simulation does not converge due to the high volumetric porosity at the outer layer of the stem).

4.6 Fatigue life estimation

The applied forces to the stem create dynamic stresses which lead to fatigue failure of the stem after a certain period. The estimated fatigue life which is represented by the number of cycles to failure was calculated for all femoral stem designs having a factor of safety > 1.0 at the relevant loading conditions based on the equations presented in section 3.2.4 as shown in table 4.3. The results illustrated in figure 4.9 provide an idea pertaining to the critical area of the stem associated with the maximum von Misses stress which is the outer layer of the stem in comparison with the other layers. The maximum von Misses stress and the minimum ultimate tensile strength associated with stems porous layers were used for fatigue calculations. This is important to provide the optimal designs in terms of durability and safety life span.

Table 4.3 Fatigue life / number of cycles to failure corresponding to an acceptable factor of safety designs

Design	Walking speed	Fatigue life (Nc)
D1	1Km/hr	9.07E+09
D2	1Km/hr	1.02E+08
D3	1Km/hr	2.10E+11
D5	1Km/hr	1.15E+09
D6	1Km/hr	2.67E+10
D8	1Km/hr	1.77E+12
	3Km/hr	7.14E+08
D10	1Km/hr	2.33E+08
D11	1Km/hr	2.66E+09
D15	1Km/hr	1.48E+08

Since the stem material is Ti-4Al-6V and the applied load is relatively small, the fatigue life for the proposed stems shown in table 4.3 is long. But practically, the hip is replaced due to stress shielding and other biological related matters. With these innovative designs we succeeded in reducing the stress shielding and delaying the bone wracking which will reduce the implant loosening.

4.7 Sustainability and cost study

The manufacturing of femoral stems using an additive manufacturing technology offers an innovative sustainable development strategy in terms of reducing lead time, manpower costs, inventory risks (only software and powder are stored), transportation costs, tools, consumables, energy consumption, carbon footprint, and manufacturing waste as it provides a tool to manufacture a customized product which meets the patient's specific bone geometry. It provides Just-In-Time (JIT) at an efficient manufacturing speed and a low price with precise accuracy at the customer's location; and it has the ability to join different operations that were typically done through different processes. Therefore, it has a significant impact on ecological, institutional, economic, and financial sustainability.

Additive manufacturing with the use of titanium alloy is predicted to be a sustainable approach for manufacturing in the future. This is after several improvements have been made to the process to improve its outcomes. It is evident that additive manufacturing leads to lower costs compared to traditional approaches, however, the cost for specific materials varies significantly from one to the other. This is due to the reduced waste produced and time taken to produce the materials. In addition, the inventory is more manageable as it shifts to a digital inventory. This is where the product is stored in the form of blueprint files rather than physical final

products. Its contributions to the social aspects of life are also noticeable as additive manufacturing has improved medical procedures as well as productive activities in the manufacturing sector.

4.7.1 Cost analysis

The cost associated with each manufacturing process were calculated and analyzed, and it is evident from the results that the superiority of introducing the porous structures to the design of the stem that can be manufactured using the additive manufacturing method over the traditional manufacturing techniques of the bulk /dense Ti-4Al-6V alloy femoral stems. Table 4.4 shows the cost input comparison data between both stems with relevant manufacturing methods. The costs presented are present values of both porous AM stem and bulk / dense TM stem, these costs represent the femoral stem cost for a single patient excluding all other costs such as the cost of surgery operations. The percentage of saving for the porous stem manufactured using AM method and the bulk /dense stem manufactured using TM methods is around 58% for primary surgery and this percentage decreases with time for revision surgeries at each lifecycle and is expected to reach 8 % after 20 years. This can be considered as a significant reduction in cost for the first 15 years of the lifecycle besides the other mechanical properties enhanced relevant to the bone's properties.

It is obvious from figure 4.13 that there are significant savings considering the revision surgeries are done typically after every 5 years. However, the proposed designed porous stem is expected to last for more than 20 years without replacement, depending on the patient's age, sex, bone status, and active or inactive lifestyle, while for the bulk / dense stem around 80 % can survive up to 20 years [12], [129].

Table 4.4 The cost input between Porous AM stem and bulk / dense TM stem

Year	AM stem		TM Stem	
	Primary	Revision	Primary	Revision
0	970		2308	
5		970		2308
10		970		2308
15		970		2308
20		970		2308
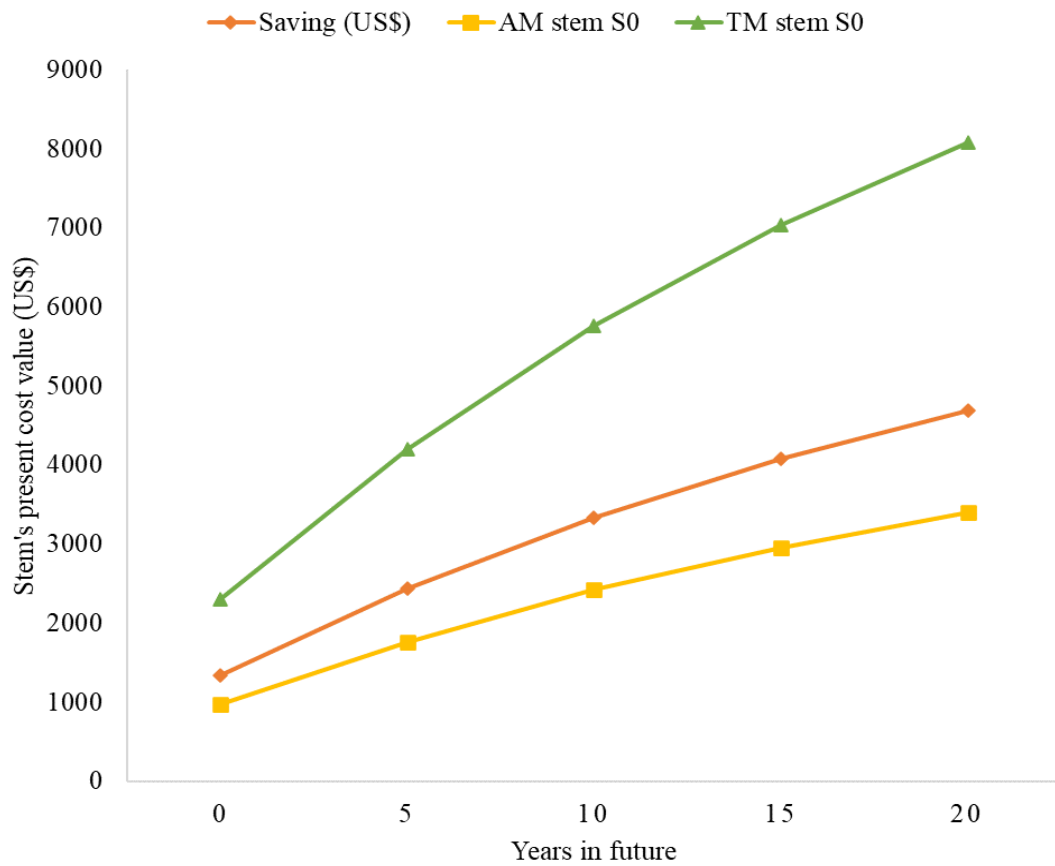
Figure 4.13 Effect of implementing AM method for fabrication of porous stems on cost saving with relevant to bulk /dense stem traditionally manufactured counterpart

The overall saving in the USA alone is significant when utilizing porous stems manufactured via additive manufacturing method as illustrated in figure 4.14 considering the total population that undergoing total hip arthroplasty (THA) in the USA is 930,575 according to year 2020 records, and this number is expected to increase to 1,537,422 in 2050 with an annual growth rate of 1.7% [4].
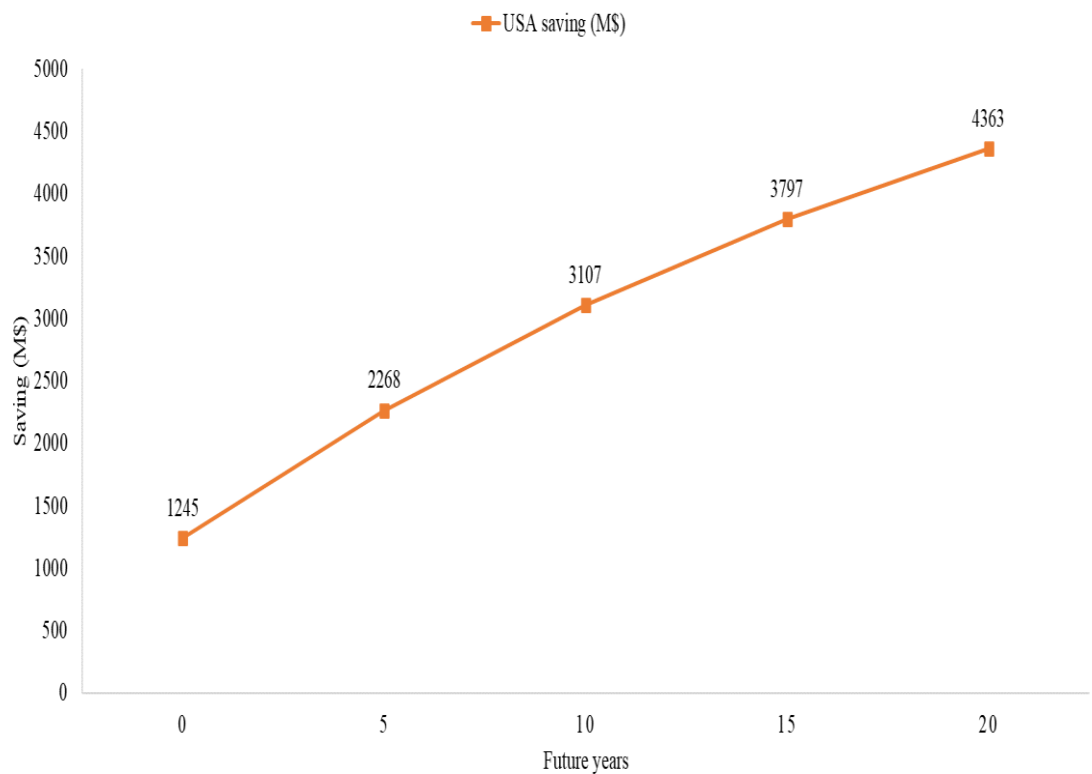
Figure 4.14 The USA's expected saving of Million dollars over the lifecycle considering AM porous stems with relevant to bulk / dense TM stem

The initial saving is expected to reach 1245 Million dollars if the proposed stem manufactured using additive manufacturing method as per year 2020 demand, and the savings are expected to reach 147.4 Million dollars for revision surgeries after 5 years, and 400.8 Million dollars if the revisions were done after 10 years of the primary

operation considering that the rate of revision surgeries is 6.5 % after 5 years and 12.9 % after 10 years of the primary surgery, respectively [12], [129].

4.8 Summary

Finite element analysis method was used successfully to design and study the Ti-4Al-6V alloy porous cubic structures, porous femoral stems, femoral stems performance under physiological load related to walking speeds at 1km/hr, 3km/hr and 5km/hr, stress shielding, micromotion and fatigue analysis aiming to design a lightweight Ti-4Al-6V alloy femoral stem that can survive under certain daily activities with a long lifespan. Table 4.5 illustrates a summary of all investigations and studied tasks conducted with the acceptance and rejection of the stem design to achieve the study objectives.

Significant savings are expected globally when utilizing the proposed porous stems which are safe in terms of stress shielding, micromotions, and having acceptable fatigue performance when manufactured using additive manufacturing method, i.e., Direct Metal Laser Sintering (DMLS), with reference to the traditional bulk / dense stem which is currently manufactured using the traditional methods.

Table 4.5 Summary of acceptance and rejection of the femoral stem design based on the studied tasks

Design	Loading condition (Walking speed)	Micromotion	Stress Shielding	SF= Y_sl/σ_Lm	Fatigue Factor of Safety - Soderberg approach	conclusion
D1	1km/hr	√	√	√	√	√
	3Km/Hr	√	√	√	X	X
	5Km/Hr	√	√	X	X	X
D2	1Km/Hr	√	√	√	√	√
	3Km/Hr	√	√	X	X	X
	5Km/Hr	√	√	X	X	X
D3	1Km/Hr	√	√	√	√	√
	3Km/Hr	√	√	√	X	X
	5Km/Hr	√	√	X	X	X
D4	1Km/Hr	√	√	√	X	X
	3Km/Hr	√	√	X	X	X
	5Km/Hr	√	√	X	X	X
D5	1Km/Hr	√	√	√	√	√
	3Km/Hr	√	√	X	X	X
	5Km/Hr	√	√	X	X	X
D6	1Km/Hr	√	√	√	√	√
	3Km/Hr	√	√	X	X	X
	5Km/Hr	X	√	X	X	X
D7	1Km/Hr	√	√	√	X	X
	3Km/Hr	√	√	X	X	X
	5Km/Hr	X	√	X	X	X
D8	1Km/Hr	√	√	√	√	√
	3Km/Hr	√	√	√	√	√
	5Km/Hr	X	√	X	X	X
D9	1Km/Hr	√	√	X	X	X
	3Km/Hr	√	√	X	X	X
	5Km/Hr	X	√	X	X	X
D10	1Km/Hr	√	√	√	√	√
	3Km/Hr	√	√	X	X	X
	5Km/Hr	X	√	X	X	X
D11	1Km/Hr	√	√	√	√	√
	3Km/Hr	X	√	X	X	X
	5Km/Hr	X	√	X	X	X
D12	1Km/Hr	√	√	X	X	X
	3Km/Hr	X	X	X	X	X
	5Km/Hr	X	X	X	X	X
D13	1Km/Hr	X	√	√	X	X
	3Km/Hr	X	√	X	X	X
	5Km/Hr	X	√	X	X	X
D14	1Km/Hr	X	X	X	X	X
	3Km/Hr	X	X	X	X	X
	5Km/Hr	X	X	X	X	X
D15	1Km/Hr	√	√	√	√	√
	3Km/Hr	X	√	X	X	X
	5Km/Hr	X	√	X	X	X

√ : Ok

X : Not ok

CHAPTER 5: CONCLUSIONS AND FUTURE WORK

The cubic porous cellular structure three- dimensions (3D) finite element models were built with porosity values of 10 – 90% to construct fifteen different femoral stem designs using different arrangements of volumetric porosities within the stem's layers in radial direction. The hypothesis in this study is that such radial functionally graded porous structure will provide optimum designs that can reduce the stress-shielding, promote stem stability, and survive under high cyclic loading focusing on the level of porosity in the stems required to achieve good biomechanical performance.

The stems were subjected to physiological loads corresponding to three walking speeds (1 km/hr, 3 km/hr, and 5 km/hr). The von Mises stresses at femur Gruen zones and stem layers, and the stem micromotions and fatigue performance of each designed stem were calculated.

5.1 Conclusions

Three-dimensional finite element models of cubic porous cellular structures were built with porosity values of 30–70% representing fifteen different designs using different arrangements of volumetric porosities within the stems' layers. The stems were subjected to physiological loads corresponding to three walking speeds (1 km/h, 3 km/h, and 5 km/h). The von Mises stresses at femur Gruen zones and stem layers and the stems' micromotions were calculated. Fatigue factors of safety were computed for each design under the three loading conditions using Soderberg approach. The optimal design was used for calculating the LCCA. The conclusions obtained from this study can be summarized as follows:

- A significant reduction in stress shielding is successfully achieved which leads to promote the stem's stability and reduce the chance of aseptic loosening and early revision surgery.

- Functionally graded porous stems tend to transfer higher stress values to the bone compared to bulk / dense stem for all physiological loads associated with three studied walking speeds.

- The micromotions values are increased as the porosity and physiological loads / walking speed increase. Hence, the patient is to be advised to walk at a low speed to prevent stem's micromotion that affects the bone tissue ingrowth leading to failure of the implant.

- Designs associated with stems average volumetric porosity of 50% at 5 km/hr. walking speed and 70% at all walking speeds are considered failed in terms of micromotion.

- The stems with 70% average porosity were found to have the best match with the intact bone mechanical properties for the stem inside the epoxy model.

- Porous structure's mechanical properties varied as the volumetric porosities changed and this is affecting the stems performance and fatigue endurance under daily human physical activities.

- FG stems of Designs D1 and D3 with 30% average porosity and Design D8 with 50% average porosity generate enough stress transfer to the bone without yielding and moderate micromotions between the stem and the bone interface surfaces.

- Changing the porosities arrangement within the stem's layers affects the stems durability and the fatigue performance.

- Designs D1, D2, D3, D5, D6, D8, D10, D11 and D15 were found to be safe at a walking speed 1 Km/hr. in terms of micromotion, stress shielding, von Mises stress values compared with the associated yield strength and factor of safety based on Soderberg approach.

- Design D8 is the best candidate that was found not to fail up to a walking speed of 3 Km/hr. in terms of micromotion, stress shielding, and fatigue performance.

- The performance of the proposed designs can be enhanced by adding outer dense shell to the porous stem structures with different thicknesses which will be part of a future study.

- Significant savings are expected globally when utilizing the proposed porous stems when manufactured using additive manufacturing method, i.e., Direct Metal Laser Sintering (DMLS), with reference to the traditional bulk / dense stem counterpart which is currently manufactured using the traditional methods.

5.2 Research implications

Fully dense Ti-4Al-6V alloy stems have an elastic modulus of 115 GPa, such traditionally made femoral stems show stress shielding phenomenon that is not desired for stems stability and stems loosening after a short time of implantation.

This study has proposed a cubic cellular porous structure that can be introduced to the femoral stem in several geometrical functionally graded and homogeneous arrangements of volumetric porosities in stem's radial direction, which was done mainly to reduce the stress shielding effects without compromising on the other risks, namely, micromotions and fatigue performance.

Many porous functionally graded and homogeneous designs can be suggested for the surgeons which are lightweight by 30%, 50% or 70% and less stiffness by 55%

to 82% than the bulk /dense Ti-4Al-6V alloy stem. These proposed designs are able to reduce the stress shielding as shown in table 4.1, promote stability and safe under cyclic loading.

5.3 Future work

a) The proposed designs with functionally graded, homogeneous, and bulk / dense stems are to be manufactured using additive manufacturing technology and to subject these designs for physical mechanical testing.

b) Adding a thin bulk / dense Ti-4Al-6V alloy as an outer skin to the designed stems for further improvement investigations.

c) Additional loading conditions such as jogging, walking upstairs and downstairs are to be studied.

REFERENCES

[1]   D. Garrison, "Osteoarthritis, Osteoporosis, and Exercise," *Workplace Health Saf*, vol. 60, no. 9, pp. 381–383, Sep. 2012, doi: 10.1177/216507991206000902.

[2]   U. G. De Bellis, C. Legnani, and G. M. Calori, "Acute total hip replacement for acetabular fractures: A systematic review of the literature," *Injury*, vol. 45, no. 2, pp. 356–361, Feb. 2014, doi: 10.1016/j.injury.2013.09.018.

[3]   P. Kannus, J. Parkkari, H. Sievänen, A. Heinonen, I. Vuori, and M. Järvinen, "Epidemiology of hip fractures," *Bone*, vol. 18, no. 1, Supplement 1, pp. S57–S63, Jan. 1996, doi: 10.1016/8756-3282(95)00381-9.

[4]   C. Pabinger, H. Lothaller, N. Portner, and A. Geissler, "Projections of hip arthroplasty in OECD countries up to 2050," *HIP International*, vol. 28, no. 5, pp. 498–506, Sep. 2018, doi: 10.1177/1120700018757940.

[5]   "AAOS_AJRR_2020_Annual_Report_FINAL_150DPI.pdf." Accessed: Sep. 21, 2021. [Online]. Available: https://connect.ajrr.net/hubfs/PDFs%20and%20PPTs/AAOS_AJRR_2020_Annual_Report_FINAL_150DPI.pdf?hsCtaTracking=a27254df-dcd3-4fc7-a4c5-0612674cf0af%7C6b1e565d-986f-40bc-8ec1-9b78166f05c5

[6]   E. Eisenbarth, D. Velten, M. Müller, R. Thull, and J. Breme, "Biocompatibility of β-stabilizing elements of titanium alloys," *Biomaterials*, vol. 25, no. 26, pp. 5705–5713, Nov. 2004, doi: 10.1016/j.biomaterials.2004.01.021.

[7]   H. Mehboob, F. Tarlochan, A. Mehboob, and S.-H. Chang, "Finite element modelling and characterization of 3D cellular microstructures for the design of a cementless biomimetic porous hip stem," *Materials & Design*, vol. 149, pp. 101–112, Jul. 2018, doi: 10.1016/j.matdes.2018.04.002.

[8]   H. Mehboob, F. Ahmad, F. Tarlochan, A. Mehboob, and S. H. Chang, "A comprehensive analysis of bio-inspired design of femoral stem on primary and secondary stabilities using mechanoregulatory algorithm," *Biomech Model Mechanobiol*, vol. 19, no. 6, pp. 2213–2226, Dec. 2020, doi: 10.1007/s10237-020-01334-3.

[9]   H. Mehboob *et al.*, "A novel design, analysis and 3D printing of Ti-6Al-4V alloy bio-inspired porous femoral stem," *J Mater Sci: Mater Med*, vol. 31, no. 9, p. 78, Sep. 2020, doi: 10.1007/s10856-020-06420-7.

[10]   S. E. Alkhatib, H. Mehboob, and F. Tarlochan, "Finite Element Analysis of Porous Titanium Alloy Hip Stem to Evaluate the Biomechanical Performance During Walking and Stair Climbing," *J Bionic Eng*, vol. 16, no. 6, pp. 1103–1115, Nov. 2019, doi: 10.1007/s42235-019-0122-4.

[11]   F. Tarlochan, H. Mehboob, A. Mehboob, and S.-H. Chang, "Influence of functionally graded pores on bone ingrowth in cementless hip prosthesis: a finite element study using mechano-regulatory algorithm," *Biomech Model Mechanobiol*, vol. 17, no. 3, pp. 701–716, Jun. 2018, doi: 10.1007/s10237-017-0987-2.

[12]   G. Labek, M. Thaler, W. Janda, M. Agreiter, and B. Stöckl, "Revision rates after total joint replacement: CUMULATIVE RESULTS FROM WORLDWIDE JOINT REGISTER DATASETS," *The Journal of Bone and Joint Surgery. British volume*, vol. 93-B, no. 3, pp. 293–297, Mar. 2011, doi: 10.1302/0301-620X.93B3.25467.

[13]   J. D. Stimac, J. Boles, N. Parkes, A. Gonzalez Della Valle, F. Boettner, and G. H. Westrich, "Revision Total Hip Arthroplasty With Modular Femoral Stems," *The Journal of Arthroplasty*, vol. 29, no. 11, pp. 2167–2170, Nov. 2014, doi: 10.1016/j.arth.2014.06.015.

[14]   M. Khatod, G. Cafri, R. S. Namba, M. C. S. Inacio, and E. W. Paxton, "Risk

Factors for Total Hip Arthroplasty Aseptic Revision," *The Journal of Arthroplasty*, vol. 29, no. 7, pp. 1412–1417, Jul. 2014, doi: 10.1016/j.arth.2014.01.023.

[15]   S. G. Memtsoudis, M. C. Besculides, L. Gaber, S. Liu, and A. González Della Valle, "Risk factors for pulmonary embolism after hip and knee arthroplasty: a population-based study," *International Orthopaedics (SICOT)*, vol. 33, no. 6, pp. 1739–1745, Dec. 2009, doi: 10.1007/s00264-008-0659-z.

[16]   L. E. Bayliss *et al.*, "The effect of patient age at intervention on risk of implant revision after total replacement of the hip or knee: a population-based cohort study," *The Lancet*, vol. 389, no. 10077, pp. 1424–1430, Apr. 2017, doi: 10.1016/S0140-6736(17)30059-4.

[17]   L. Gil, S. Brühl, L. Jiménez, O. Leon, R. Guevara, and M. H. Staia, "Corrosion performance of the plasma nitrided 316L stainless steel," *Surface and Coatings Technology*, vol. 201, no. 7, pp. 4424–4429, Dec. 2006, doi: 10.1016/j.surfcoat.2006.08.081.

[18]   W. L. Healy, J. F. Tilzey, R. Iorio, L. M. Specht, and S. Sharma, "Prospective, Randomized Comparison of Cobalt-Chrome and Titanium Trilock Femoral Stems," *The Journal of Arthroplasty*, vol. 24, no. 6, pp. 831–836, Sep. 2009, doi: 10.1016/j.arth.2008.06.035.

[19]   M. Niinomi, "Mechanical biocompatibilities of titanium alloys for biomedical applications," *Journal of the Mechanical Behavior of Biomedical Materials*, vol. 1, no. 1, pp. 30–42, Jan. 2008, doi: 10.1016/j.jmbbm.2007.07.001.

[20]   M. Niinomi, "Recent metallic materials for biomedical applications," *Metall and Mat Trans A*, vol. 33, no. 3, pp. 477–486, Mar. 2002, doi: 10.1007/s11661-002-0109-2.

[21]   A. M. Schwartz, K. X. Farley, G. N. Guild, and T. L. Bradbury, "Projections

and Epidemiology of Revision Hip and Knee Arthroplasty in the United States to 2030," *The Journal of Arthroplasty*, vol. 35, no. 6, pp. S79–S85, Jun. 2020, doi: 10.1016/j.arth.2020.02.030.

[22]   J.-H. Chen, C. Liu, L. You, and C. A. Simmons, "Boning up on Wolff's Law: Mechanical regulation of the cells that make and maintain bone," *Journal of Biomechanics*, vol. 43, no. 1, pp. 108–118, Jan. 2010, doi: 10.1016/j.jbiomech.2009.09.016.

[23]   A. A. Oshkour, N. A. A. Osman, M. Bayat, R. Afshar, and F. Berto, "Three-dimensional finite element analyses of functionally graded femoral prostheses with different geometrical configurations," *Materials & Design (1980-2015)*, vol. 56, pp. 998–1008, Apr. 2014, doi: 10.1016/j.matdes.2013.12.054.

[24]   K. B. Hazlehurst, C. J. Wang, and M. Stanford, "A numerical investigation into the influence of the properties of cobalt chrome cellular structures on the load transfer to the periprosthetic femur following total hip arthroplasty," *Medical Engineering & Physics*, vol. 36, no. 4, pp. 458–466, Apr. 2014, doi: 10.1016/j.medengphy.2014.02.008.

[25]   F. Schmidutz, Y. Agarwal, P. E. Müller, B. Gueorguiev, R. G. Richards, and C. M. Sprecher, "Stress-shielding induced bone remodeling in cementless shoulder resurfacing arthroplasty: a finite element analysis and in vivo results," *Journal of Biomechanics*, vol. 47, no. 14, pp. 3509–3516, Nov. 2014, doi: 10.1016/j.jbiomech.2014.08.029.

[26]   S. Limmahakhun, A. Oloyede, K. Sitthiseripratip, Y. Xiao, and C. Yan, "Stiffness and strength tailoring of cobalt chromium graded cellular structures for stress-shielding reduction," *Materials & Design*, vol. 114, pp. 633–641, Jan. 2017, doi: 10.1016/j.matdes.2016.11.090.

[27]   G. K. Sharma and B. Gurumoorthy, "Iso-material contour representation for process planning of heterogeneous object model," *Journal of Computational Design and Engineering*, vol. 7, no. 4, pp. 498–513, Aug. 2020, doi: 10.1093/jcde/qwz001.

[28]   M. A. Velasco, Y. Lancheros, and D. A. Garzón-Alvarado, "Geometric and mechanical properties evaluation of scaffolds for bone tissue applications designing by a reaction-diffusion models and manufactured with a material jetting system," *Journal of Computational Design and Engineering*, vol. 3, no. 4, pp. 385–397, Oct. 2016, doi: 10.1016/j.jcde.2016.06.006.

[29]   A. A. Oshkour, N. A. A. Osman, M. Bayat, R. Afshar, and F. Berto, "Three-dimensional finite element analyses of functionally graded femoral prostheses with different geometrical configurations," *Materials & Design (1980-2015)*, vol. 56, pp. 998–1008, Apr. 2014, doi: 10.1016/j.matdes.2013.12.054.

[30]   J. Park, S.-J. Ahn, H. Lee, and G. Noh, "Implant placement in the removable mandibular advancement device for completely edentulous patients: a finite element study," *Journal of Computational Design and Engineering*, vol. 8, no. 1, pp. 140–148, Jan. 2021, doi: 10.1093/jcde/qwaa067.

[31]   M. A. Bagheri and G. Rouhi, "Design and numerical investigation of an adaptive intramedullary nail with a novel interlocking mechanism," *Journal of Computational Design and Engineering*, vol. 7, no. 6, pp. 722–735, Dec. 2020, doi: 10.1093/jcde/qwaa053.

[32]   W. Kim, A. P. Veloso, D. Araújo, and S. S. Kohles, "Novel computational approaches characterizing knee physiotherapy," *Journal of Computational Design and Engineering*, vol. 1, no. 1, pp. 55–66, Jan. 2014, doi: 10.7315/JCDE.2014.006.

[33]   Y. Yoon, J. Kim, J. Jung, S. Oh, G. Noh, and Y.-D. Kwon, "Effect of mandibular contouring surgery on the stress distribution during various clenching

tasks," *Journal of Computational Design and Engineering*, vol. 8, no. 2, pp. 570–580, Apr. 2021, doi: 10.1093/jcde/qwaa096.

[34] "Hip Dysplasia in Adolescents and Young Adults," *Hospital for Special Surgery*. https://www.hss.edu/conditions_hip-dysplasia-adolescents-young-adults.asp (accessed Dec. 15, 2021).

[35] S. Kurtz, K. Ong, E. Lau, F. Mowat, and M. Halpern, "Projections of Primary and Revision Hip and Knee Arthroplasty in the United States from 2005 to 2030:," *The Journal of Bone & Joint Surgery*, vol. 89, no. 4, pp. 780–785, Apr. 2007, doi: 10.2106/JBJS.F.00222.

[36] K. L. Ong, E. Lau, J. Suggs, S. M. Kurtz, and M. T. Manley, "Risk of Subsequent Revision after Primary and Revision Total Joint Arthroplasty," *Clin Orthop Relat Res*, vol. 468, no. 11, pp. 3070–3076, Nov. 2010, doi: 10.1007/s11999-010-1399-0.

[37] N. N. Mahomed *et al.*, "Rates and Outcomes of Primary and Revision Total Hip Replacement in the United States Medicare Population," *JBJS*, vol. 85, no. 1, pp. 27–32, Jan. 2003.

[38] V. Sansalone *et al.*, "Anatomical distribution of the degree of mineralization of bone tissue in human femoral neck: Impact on biomechanical properties," *Bone*, vol. 50, no. 4, pp. 876–884, Apr. 2012, doi: 10.1016/j.bone.2011.12.020.

[39] H. Ebrahimi *et al.*, "Biomechanical properties of an intact, injured, repaired, and healed femur: An experimental and computational study," *Journal of the Mechanical Behavior of Biomedical Materials*, vol. 16, pp. 121–135, Dec. 2012, doi: 10.1016/j.jmbbm.2012.09.005.

[40] R. Ruben, P. Fernandes, and J. Folgado, "On the optimal shape of hip implants," *Journal of biomechanics*, vol. 45, pp. 239–46, Nov. 2011, doi:

10.1016/j.jbiomech.2011.10.038.

[41]   G. Bergmann *et al.*, "Hip contact forces and gait patterns from routine activities," *Journal of Biomechanics*, vol. 34, no. 7, pp. 859–871, Jul. 2001, doi: 10.1016/S0021-9290(01)00040-9.

[42]   A. J. Wirth, J. Goldhahn, C. Flaig, P. Arbenz, R. Müller, and G. H. van Lenthe, "Implant stability is affected by local bone microstructural quality," *Bone*, vol. 49, no. 3, pp. 473–478, Sep. 2011, doi: 10.1016/j.bone.2011.05.001.

[43]   Y. Haba *et al.*, "Bone Mineral Densities and Mechanical Properties of Retrieved Femoral Bone Samples in relation to Bone Mineral Densities Measured in the Respective Patients," *The Scientific World Journal*, vol. 2012, pp. 1–7, 2012, doi: 10.1100/2012/242403.

[44]   E. N. Ebbesen, J. S. Thomsen, H. Beck-Nielsen, H. J. Nepper-Rasmussen, and Li. Mosekilde, "Lumbar vertebral body compressive strength evaluated by dual-energy X-ray absorptiometry, quantitative computed tomography, and ashing," *Bone*, vol. 25, no. 6, pp. 713–724, Dec. 1999, doi: 10.1016/S8756-3282(99)00216-1.

[45]   N. L. Fazzalari, M. R. Forwood, K. Smith, B. A. Manthey, and P. Herreen, "Assessment of Cancellous Bone Quality in Severe Osteoarthrosis: Bone Mineral Density, Mechanics, and Microdamage," *Bone*, vol. 22, no. 4, pp. 381–388, Apr. 1998, doi: 10.1016/S8756-3282(97)00298-6.

[46]   M. Sanami, "AUXETIC MATERIALS FOR BIOMEDICAL APPLICATIONS," p. 252.

[47]   V. Brailovski, P. Terriault, C. Simoneau, M. Dumas, and B. Jetté, "Development of a Biomimetic Metallic Femoral Stem: Methodological Approach," *MSF*, vol. 879, pp. 1788–1793, Nov. 2016, doi: 10.4028/www.scientific.net/MSF.879.1788.

[48]   R. Huiskes, R. Ruimerman, G. H. van Lenthe, and J. D. Janssen, "Effects of mechanical forces on maintenance and adaptation of form in trabecular bone," *Nature*, vol. 405, no. 6787, Art. no. 6787, Jun. 2000, doi: 10.1038/35015116.

[49]   B. T. Palumbo, K. L. Morrison, A. S. Baumgarten, M. I. Stein, G. J. Haidukewych, and T. L. Bernasek, "Results of Revision Total Hip Arthroplasty with Modular, Titanium-Tapered Femoral Stems in Severe Proximal Metaphyseal and Diaphyseal Bone Loss," *The Journal of Arthroplasty*, vol. 28, no. 4, pp. 690–694, Apr. 2013, doi: 10.1016/j.arth.2012.08.019.

[50]   "NJR 10th Annual Report 2013." https://www.njrcentre.org.uk/njrcentre/News-and-Events/NJR-10th-Annual-Report-2013 (accessed Feb. 05, 2022).

[51]   D. Janssen, J. van Aken, T. Scheerlinck, and N. Verdonschot, "Finite element analysis of the effect of cementing concepts on implant stability and cement fatigue failure," *Acta Orthopaedica*, vol. 80, no. 3, pp. 319–324, Jan. 2009, doi: 10.3109/17453670902947465.

[52]   A. Z. Senalp, O. Kayabasi, and H. Kurtaran, "Static, dynamic and fatigue behavior of newly designed stem shapes for hip prosthesis using finite element analysis," *Materials & Design*, vol. 28, no. 5, pp. 1577–1583, Jan. 2007, doi: 10.1016/j.matdes.2006.02.015.

[53]   A. H. Chern *et al.*, "A review on the fatigue behavior of Ti-6Al-4V fabricated by electron beam melting additive manufacturing," *International Journal of Fatigue*, vol. 119, pp. 173–184, Feb. 2019, doi: 10.1016/j.ijfatigue.2018.09.022.

[54]   A. Darwich and H. Nazha, "Effect of Coating Materials on the Fatigue Behavior of Hip Implants: A Three-dimensional Finite Element Analysis," *Journal of Applied and Computational Mechanics*, vol. 6, Aug. 2019, doi: 10.22055/jacm.2019.30017.1659.

[55] P. Norman, S. Iyengar, I. Svensson, and G. Flivik, "Fatigue Fracture in Dual Modular Revision Total Hip Arthroplasty Stems," *The Journal of Arthroplasty*, vol. 29, no. 4, pp. 850–855, Apr. 2014, doi: 10.1016/j.arth.2013.09.008.

[56] R. Hedayati, H. Hosseini-Toudeshky, M. Sadighi, M. Mohammadi-Aghdam, and A. A. Zadpoor, "Computational prediction of the fatigue behavior of additively manufactured porous metallic biomaterials," *International Journal of Fatigue*, vol. 84, pp. 67–79, Mar. 2016, doi: 10.1016/j.ijfatigue.2015.11.017.

[57] C. E. Pelt, W. Madsen, J. A. Erickson, J. M. Gililland, M. B. Anderson, and C. L. Peters, "Revision Total Hip Arthroplasty With a Modular Cementless Femoral Stem," *The Journal of Arthroplasty*, vol. 29, no. 9, pp. 1803–1807, Sep. 2014, doi: 10.1016/j.arth.2014.04.042.

[58] P. C. Ortega, W. B. Medeiros, A. D. O. Moré, R. F. Vasconcelos, E. da Rosa, and C. R. M. Roesler, "Failure analysis of a modular revision total HIP arthroplasty femoral stem fractured in vivo," *Engineering Failure Analysis*, vol. 114, p. 104591, Aug. 2020, doi: 10.1016/j.engfailanal.2020.104591.

[59] I. Zimmer, "ZMR® Revision Hip System Surgical Technique," p. 68.

[60] K. Rueckl, P. K. Sculco, J. Berliner, M. B. Cross, C. Koch, and F. Boettner, "Fracture risk of tapered modular revision stems: a failure analysis," *Arthroplasty Today*, vol. 4, no. 3, pp. 300–305, Sep. 2018, doi: 10.1016/j.artd.2017.11.002.

[61] M. Esposito, J.-M. Hirsch, U. Lekholm, and P. Thomsen, "Biological factors contributing to failures of osseointegrated oral implants, (II). Etiopathogenesis," *European Journal of Oral Sciences*, vol. 106, no. 3, pp. 721–764, 1998, doi: 10.1046/j.0909-8836..t01-6-.x.

[62] N. F. Al Zoubi, F. Tarlochan, H. Mehboob, and F. Jarrar, "Design of Titanium Alloy Femoral Stem Cellular Structure for Stress Shielding and Stem Stability:

Computational Analysis," *Applied Sciences*, vol. 12, no. 3, Art. no. 3, Jan. 2022, doi: 10.3390/app12031548.

[63]   H. Mehboob, F. Ahmad, F. Tarlochan, A. Mehboob, and S. H. Chang, "A comprehensive analysis of bio-inspired design of femoral stem on primary and secondary stabilities using mechanoregulatory algorithm," *Biomech Model Mechanobiol*, vol. 19, no. 6, pp. 2213–2226, Dec. 2020, doi: 10.1007/s10237-020-01334-3.

[64]   H. Mehboob, F. Tarlochan, A. Mehboob, and S.-H. Chang, "Finite element modelling and characterization of 3D cellular microstructures for the design of a cementless biomimetic porous hip stem," *Materials & Design*, vol. 149, pp. 101–112, Jul. 2018, doi: 10.1016/j.matdes.2018.04.002.

[65]   P. A. Banaszkiewicz, "'Modes of Failure' of Cemented Stem-Type Femoral Components: A Radiographic Analysis of Loosening," in *Classic Papers in Orthopaedics*, P. A. Banaszkiewicz and D. F. Kader, Eds. London: Springer London, 2014, pp. 35–38. doi: 10.1007/978-1-4471-5451-8_8.

[66]   L. Cavalli and M. L. Brandi, "Periprosthetic bone loss: diagnostic and therapeutic approaches," *F1000Res*, vol. 2, p. 266, Jun. 2014, doi: 10.12688/f1000research.2-266.v2.

[67]   K. B. Hazlehurst, "The adoption of laser melting technology for the manufacture of functionally graded cobalt chrome alloy femoral stems," Jul. 2014, Accessed: Feb. 28, 2022. [Online]. Available: https://wlv.openrepository.com/handle/2436/332114

[68]   M. Viceconti, R. Muccini, M. Bernakiewicz, M. Baleani, and L. Cristofolini, "Large-sliding contact elements accurately predict levels of bone–implant micromotion relevant to osseointegration," *Journal of Biomechanics*, vol. 33, no. 12, pp. 1611–1618,

Dec. 2000, doi: 10.1016/S0021-9290(00)00140-8.

[69] S. Yang, K.-F. Leong, Z. Du, and C.-K. Chua, "The Design of Scaffolds for Use in Tissue Engineering. Part I. Traditional Factors," *Tissue Engineering*, vol. 7, no. 6, pp. 679–689, Dec. 2001, doi: 10.1089/107632701753337645.

[70] T. M. Freyman, I. V. Yannas, and L. J. Gibson, "Cellular materials as porous scaffolds for tissue engineering," *Progress in Materials Science*, vol. 46, no. 3–4, pp. 273–282, Jan. 2001, doi: 10.1016/S0079-6425(00)00018-9.

[71] C. J. Boehlert, C. J. Cowen, J. P. Quast, T. Akahori, and M. Niinomi, "Fatigue and wear evaluation of Ti-Al-Nb alloys for biomedical applications," *Materials Science and Engineering: C*, vol. 28, no. 3, pp. 323–330, Apr. 2008, doi: 10.1016/j.msec.2007.04.003.

[72] S. Zameer and M. Haneef, "Fatigue Life Estimation of Artificial Hip Joint Model Using Finite Element Method," *Materials Today: Proceedings*, vol. 2, no. 4–5, pp. 2137–2145, 2015, doi: 10.1016/j.matpr.2015.07.220.

[73] Y.-T. Lin, J. S.-S. Wu, and J.-H. Chen, "The study of wear behaviors on abducted hip joint prostheses by an alternate finite element approach," *Computer Methods and Programs in Biomedicine*, vol. 131, pp. 143–155, Jul. 2016, doi: 10.1016/j.cmpb.2016.04.015.

[74] Y. E. Delikanli and M. C. Kayacan, "Design, manufacture, and fatigue analysis of lightweight hip implants," *Journal of Applied Biomaterials & Functional Materials*, vol. 17, no. 2, p. 228080001983683, Apr. 2019, doi: 10.1177/2280800019836830.

[75] S. Beretta and S. Romano, "A comparison of fatigue strength sensitivity to defects for materials manufactured by AM or traditional processes," *International Journal of Fatigue*, vol. 94, pp. 178–191, Jan. 2017, doi: 10.1016/j.ijfatigue.2016.06.020.

[76] F. J. Quevedo González and N. Nuño, "Finite element modelling approaches for well-ordered porous metallic materials for orthopaedic applications: cost effectiveness and geometrical considerations," *Computer Methods in Biomechanics and Biomedical Engineering*, vol. 19, no. 8, pp. 845–854, Jun. 2016, doi: 10.1080/10255842.2015.1075009.

[77] C.-H. Kim, S. J. Lee, K. Aditya, H. Y. Kim, K. S. Yoon, and P. W. Yoon, "Incidence of a stem sitting proud of a proximally coated cementless tapered wedge stem," *Journal of Orthopaedic Translation*, vol. 19, pp. 118–125, Oct. 2019, doi: 10.1016/j.jot.2019.02.002.

[78] L. Wang, J. Kang, C. Sun, D. Li, Y. Cao, and Z. Jin, "Mapping porous microstructures to yield desired mechanical properties for application in 3D printed bone scaffolds and orthopaedic implants," *Materials & Design*, vol. 133, pp. 62–68, Nov. 2017, doi: 10.1016/j.matdes.2017.07.021.

[79] J. de Krijger, C. Rans, B. Van Hooreweder, K. Lietaert, B. Pouran, and A. A. Zadpoor, "Effects of applied stress ratio on the fatigue behavior of additively manufactured porous biomaterials under compressive loading," *Journal of the Mechanical Behavior of Biomedical Materials*, vol. 70, pp. 7–16, Jun. 2017, doi: 10.1016/j.jmbbm.2016.11.022.

[80] J. de Krijger, "The effect of stress ratio on the fatigue behavior of additively manufactured porous biomaterials," Delft University of Technology, 2016.

[81] S. Amin Yavari *et al.*, "Relationship between unit cell type and porosity and the fatigue behavior of selective laser melted meta-biomaterials," *Journal of the Mechanical Behavior of Biomedical Materials*, vol. 43, pp. 91–100, Mar. 2015, doi: 10.1016/j.jmbbm.2014.12.015.

[82] R. Wauthle *et al.*, "Effects of build orientation and heat treatment on the

microstructure and mechanical properties of selective laser melted Ti6Al4V lattice structures," *Additive Manufacturing*, vol. 5, pp. 77–84, Jan. 2015, doi: 10.1016/j.addma.2014.12.008.

[83] A. Z. Senalp, O. Kayabasi, and H. Kurtaran, "Static, dynamic and fatigue behavior of newly designed stem shapes for hip prosthesis using finite element analysis," *Materials & Design*, vol. 28, no. 5, pp. 1577–1583, Jan. 2007, doi: 10.1016/j.matdes.2006.02.015.

[84] A. A. Oshkour, M. M. Davoodi, N. A. Abu Osman, Y. H. Yau, F. Tarlochan, and W. A. B. W. Abas, "Finite element analysis of circumferential crack behavior in cement–femoral prosthesis interface," *Materials & Design*, vol. 49, pp. 96–102, Aug. 2013, doi: 10.1016/j.matdes.2013.01.037.

[85] U. Holzwarth and G. Cotogno, *Total hip arthroplasty : State of the art, prospects and challenges*. 2012. doi: 10.2788/31286.

[86] I. D. Learmonth, C. Young, and C. Rorabeck, "The operation of the century: total hip replacement," *The Lancet*, vol. 370, no. 9597, pp. 1508–1519, Oct. 2007, doi: 10.1016/S0140-6736(07)60457-7.

[87] B. Jetté, V. Brailovski, C. Simoneau, M. Dumas, and P. Terriault, "Development and in vitro validation of a simplified numerical model for the design of a biomimetic femoral stem," *Journal of the Mechanical Behavior of Biomedical Materials*, vol. 77, pp. 539–550, Jan. 2018, doi: 10.1016/j.jmbbm.2017.10.019.

[88] C. Simoneau, P. Terriault, B. Jetté, M. Dumas, and V. Brailovski, "Development of a porous metallic femoral stem: Design, manufacturing, simulation and mechanical testing," *Materials & Design*, vol. 114, pp. 546–556, Jan. 2017, doi: 10.1016/j.matdes.2016.10.064.

[89] L. E. Murr, "Strategies for creating living, additively manufactured, open-

cellular metal and alloy implants by promoting osseointegration, osteoinduction and vascularization: An overview," *Journal of Materials Science & Technology*, vol. 35, no. 2, pp. 231–241, Feb. 2019, doi: 10.1016/j.jmst.2018.09.003.

[90]   N. F. Al Zoubi, F. Tarlochan, H. Mehboob, and F. Jarrar, "Design of Titanium Alloy Femoral Stem Cellular Structure for Stress Shielding and Stem Stability: Computational Analysis.," 2021.

[91]   G. Ryan, A. Pandit, and D. Apatsidis, "Fabrication methods of porous metals for use in orthopaedic applications," *Biomaterials*, vol. 27, no. 13, pp. 2651–2670, May 2006, doi: 10.1016/j.biomaterials.2005.12.002.

[92]   M. Dumas, P. Terriault, and V. Brailovski, "Modelling and characterization of a porosity graded lattice structure for additively manufactured biomaterials," *Materials & Design*, vol. 121, pp. 383–392, May 2017, doi: 10.1016/j.matdes.2017.02.021.

[93]   G. Bergmann, F. Graichen, and A. Rohlmann, "Hip joint loading during walking and running, measured in two patients," *Journal of Biomechanics*, vol. 26, no. 8, pp. 969–990, Aug. 1993, doi: 10.1016/0021-9290(93)90058-M.

[94]   R. Jain, S. K. Pal, and S. B. Singh, "5 - Numerical modeling methodologies for friction stir welding process," in *Computational Methods and Production Engineering*, J. Paulo Davim, Ed. Woodhead Publishing, 2017, pp. 125–169. doi: 10.1016/B978-0-85709-481-0.00005-7.

[95]   M. Worgull, "Chapter 6 - Modeling and Process Simulation," in *Hot Embossing*, M. Worgull, Ed. Boston: William Andrew Publishing, 2009, pp. 179–225. doi: 10.1016/B978-0-8155-1579-1.50012-4.

[96]   S. Zhang, P. T. Pedersen, and R. Villavicencio, "5 - Collision damage assessment by nonlinear finite element simulations," in *Probability and Mechanics of Ship Collision and Grounding*, S. Zhang, P. T. Pedersen, and R. Villavicencio, Eds.

Butterworth-Heinemann, 2019, pp. 324–368. doi: 10.1016/B978-0-12-815022-1.00005-0.

[97]   V. Mathur and D. Dragomir-Daescu, "Hexahedral vs. Tetrahedral Finite Element Models of the Proximal Femur," p. 1.

[98]   M. A. Bagheri and G. Rouhi, "Design and numerical investigation of an adaptive intramedullary nail with a novel interlocking mechanism," *Journal of Computational Design and Engineering*, vol. 7, no. 6, pp. 722–735, Dec. 2020, doi: 10.1093/jcde/qwaa053.

[99]   C. Lin, "3D Food Printing: A Taste of the Future: 3D food printing…," *Journal of Food Science Education*, vol. 14, no. 3, pp. 86–87, Jul. 2015, doi: 10.1111/1541-4329.12061.

[100]   "Mini 3D printed jet engine can reach 33,000 RPM," *Metal Powder Report*, vol. 70, no. 4, p. 197, Jul. 2015, doi: 10.1016/j.mprp.2015.06.020.

[101]   A. France-Presse, "Dutch startup plans first 3D printed steel bridge to span Amsterdam canal," *The Guardian*, Jun. 17, 2015. Accessed: Mar. 18, 2022. [Online]. Available: https://www.theguardian.com/technology/2015/jun/17/dutch-startup-plans-first-3d-printed-steel-bridge-to-span-amsterdam-canal

[102]   "Additive Manufacturing in an End-to-End Supply Chain Setting | 3D Printing and Additive Manufacturing." https://www.liebertpub.com/doi/abs/10.1089/3dp.2015.0005 (accessed Mar. 18, 2022).

[103]   S. H. Khajavi, J. Partanen, and J. Holmström, "Additive manufacturing in the spare parts supply chain," *Computers in Industry*, vol. 65, no. 1, pp. 50–63, Jan. 2014, doi: 10.1016/j.compind.2013.07.008.

[104]   B. Baufeld, O. V. der Biest, and R. Gault, "Additive manufacturing of Ti–6Al–4V components by shaped metal deposition: Microstructure and mechanical

properties," *Materials & Design*, vol. 31, pp. S106–S111, Jun. 2010, doi: 10.1016/j.matdes.2009.11.032.

[105] N. Serres, D. Tidu, S. Sankare, and F. Hlawka, "Environmental comparison of MESO-CLAD® process and conventional machining implementing life cycle assessment," *Journal of Cleaner Production*, vol. 19, no. 9–10, pp. 1117–1124, Jun. 2011, doi: 10.1016/j.jclepro.2010.12.010.

[106] B. Berman, "3-D printing: The new industrial revolution," *Business Horizons*, vol. 55, no. 2, pp. 155–162, Mar. 2012, doi: 10.1016/j.bushor.2011.11.003.

[107] D. Dimitrov, K. Schreve, and N. de Beer, "Advances in three dimensional printing – state of the art and future perspectives," *Rapid Prototyping Journal*, vol. 12, no. 3, pp. 136–147, Jan. 2006, doi: 10.1108/13552540610670717.

[108] B. Hapuwatte, K. D. Seevers, F. Badurdeen, and I. S. Jawahir, "Total Life Cycle Sustainability Analysis of Additively Manufactured Products," *Procedia CIRP*, vol. 48, pp. 376–381, 2016, doi: 10.1016/j.procir.2016.03.016.

[109] "Global market for 3D printing, materials, services 2025," *Statista*. https://www.statista.com/statistics/315363/global-market-for-3d-priting-and-services/ (accessed Mar. 18, 2022).

[110] B. Dutta and F. H. (Sam) Froes, "The Additive Manufacturing (AM) of titanium alloys," *Metal Powder Report*, vol. 72, no. 2, pp. 96–106, Mar. 2017, doi: 10.1016/j.mprp.2016.12.062.

[111] A. Ben-Ner and E. Siemsen, "Decentralization and Localization of Production: The Organizational and Economic Consequences of Additive Manufacturing (3D Printing)," *California Management Review*, vol. 59, no. 2, pp. 5–23, Feb. 2017, doi: 10.1177/0008125617695284.

[112] A. Emelogu, M. Marufuzzaman, S. M. Thompson, N. Shamsaei, and L. Bian,

"Additive manufacturing of biomedical implants: A feasibility assessment via supply-chain cost analysis," *Additive Manufacturing*, vol. 11, pp. 97–113, Jul. 2016, doi: 10.1016/j.addma.2016.04.006.

[113] E. Sanyé-Mengual *et al.*, "Eco-Designing the Use Phase of Products in Sustainable Manufacturing," *Journal of Industrial Ecology*, vol. 18, Jul. 2014, doi: 10.1111/jiec.12161.

[114] F. L. Bourhis, O. Kerbrat, J.-Y. Hascoet, and P. Mognol, "Sustainable manufacturing: evaluation and modeling of environmental impacts in additive manufacturing," *Int J Adv Manuf Technol*, vol. 69, no. 9, pp. 1927–1939, Dec. 2013, doi: 10.1007/s00170-013-5151-2.

[115] "Full article: Energy consumption model of Binder-jetting additive manufacturing processes." https://www.tandfonline.com/doi/full/10.1080/00207543.2014.937013?casa_token=T 0F8fcONVnUAAAAA%3AEZWyKIJkstfSBrPOWWSDvwIWz9w9vAROO9CtKYE G0OKnldGrggOAs_PT9gaxpp3ygDXcTO2a5vF1 (accessed Mar. 18, 2022).

[116] B. Jetté, V. Brailovski, M. Dumas, C. Simoneau, and P. Terriault, "Femoral stem incorporating a diamond cubic lattice structure: Design, manufacture and testing," *Journal of the Mechanical Behavior of Biomedical Materials*, vol. 77, pp. 58–72, Jan. 2018, doi: 10.1016/j.jmbbm.2017.08.034.

[117] S. E. Alkhatib, F. Tarlochan, H. Mehboob, R. Singh, K. Kadirgama, and W. S. B. W. Harun, "Finite element study of functionally graded porous femoral stems incorporating body-centered cubic structure," *Artif Organs*, vol. 43, no. 7, Jul. 2019, doi: 10.1111/aor.13444.

[118] Y. N. Yeni, B. Wu, L. Huang, and D. Oravec, "Mechanical Loading Causes Detectable Changes in Morphometric Measures of Trabecular Structure in Human

Cancellous Bone," *Journal of Biomechanical Engineering*, vol. 135, no. 5, p. 054505, May 2013, doi: 10.1115/1.4024136.

[119]   M. Miura *et al.*, "Prediction of fracture load and stiffness of the proximal femur by CT-based specimen specific finite element analysis: cadaveric validation study," *BMC Musculoskelet Disord*, vol. 18, no. 1, p. 536, Dec. 2017, doi: 10.1186/s12891-017-1898-1.

[120]   M. O. Heller, G. Bergmann, J.-P. Kassi, L. Claes, N. P. Haas, and G. N. Duda, "Determination of muscle loading at the hip joint for use in pre-clinical testing," *Journal of Biomechanics*, vol. 38, no. 5, pp. 1155–1163, May 2005, doi: 10.1016/j.jbiomech.2004.05.022.

[121]   D. B. Marghitu, C. I. Diaconescu, and B. O. Ciocirlan, "3 - Mechanics of Materials," in *Mechanical Engineer's Handbook*, D. B. Marghitu, Ed. San Diego: Academic Press, 2001, pp. 119–188. doi: 10.1016/B978-012471370-3/50004-8.

[122]   H. T. Ilieş, D. Flanagan, P. T. McCullough, and S. McQuoid, "Determining the Fatigue Life of Dental Implants," *Journal of Medical Devices*, vol. 2, no. 1, p. 011003, Mar. 2008, doi: 10.1115/1.2889058.

[123]   "Prosthesis | Free Full-Text | Evaluation of Fatigue Life for Dental Implants Using FEM Analysis | HTML." https://www.mdpi.com/2673-1592/3/4/28/htm (accessed May 20, 2022).

[124]   S. Kinkel, N. Wollmerstedt, J. A. Kleinhans, C. Hendrich, and C. Heisel, "Patient Activity after Total Hip Arthroplasty Declines with Advancing Age," *Clin Orthop Relat Res*, vol. 467, no. 8, pp. 2053–2058, Aug. 2009, doi: 10.1007/s11999-009-0756-3.

[125]   M. Baumers, C. Tuck, R. Wildman, I. Ashcroft, E. Rosamond, and R. Hague, "Combined build-time, energy consumption and cost estimation for direct metal laser

sintering," *23rd Annual International Solid Freeform Fabrication Symposium - An Additive Manufacturing Conference, SFF 2012*, pp. 932–944, Jan. 2012.

[126] "EOS_System_Data_Sheet_EOSINT_M280.pdf." Accessed: Sep. 27, 2021. [Online]. Available: http://www.bettamachinetools.com.au/media/EOS_System_Data_Sheet_EOSINT_M 280.pdf

[127] "Parts and Materials for Hip Replacement." https://www.hipandknee.com/hip-surgery/about-hip-replacement/parts-materials/ (accessed Mar. 18, 2022).

[128] "Real Discount Rate." https://www.homerenergy.com/products/pro/docs/latest/real_discount_rate.html (accessed Mar. 19, 2022).

[129] E. W. Paxton, C. F. Ake, M. C. S. Inacio, M. Khatod, D. Marinac-Dabic, and A. Sedrakyan, "Evaluation of total hip arthroplasty devices using a total joint replacement registry: EVALUATION OF TOTAL HIP ARTHROPLASTY DEVICES," *Pharmacoepidemiol Drug Saf*, vol. 21, pp. 53–59, May 2012, doi: 10.1002/pds.3228.

[130] K. Hazlehurst, C. J. Wang, and M. Stanford, "Evaluation of the stiffness characteristics of square pore CoCrMo cellular structures manufactured using laser melting technology for potential orthopaedic applications," *Materials & Design*, vol. 51, pp. 949–955, Oct. 2013, doi: 10.1016/j.matdes.2013.05.009.

[131] H. H. Bayraktar, E. F. Morgan, G. L. Niebur, G. E. Morris, E. K. Wong, and T. M. Keaveny, "Comparison of the elastic and yield properties of human femoral trabecular and cortical bone tissue," *Journal of Biomechanics*, vol. 37, no. 1, pp. 27–35, Jan. 2004, doi: 10.1016/S0021-9290(03)00257-4.

[132] D. P. Fyhrie and D. Vashishth, "Bone stiffness predicts strength similarly for

human vertebral cancellous bone in compression and for cortical bone in tension," *Bone*, vol. 26, no. 2, pp. 169–173, Feb. 2000, doi: 10.1016/S8756-3282(99)00246-X.

[133] K. B. Hazlehurst, C. J. Wang, and M. Stanford, "An investigation into the flexural characteristics of functionally graded cobalt chrome femoral stems manufactured using selective laser melting," *Materials & Design*, vol. 60, pp. 177–183, Aug. 2014, doi: 10.1016/j.matdes.2014.03.068.

[134] O. L. A. Harrysson, O. Cansizoglu, D. J. Marcellin-Little, D. R. Cormier, and H. A. West, "Direct metal fabrication of titanium implants with tailored materials and mechanical properties using electron beam melting technology," *Materials Science and Engineering: C*, vol. 28, no. 3, pp. 366–373, Apr. 2008, doi: 10.1016/j.msec.2007.04.022.

[135] S. Arabnejad Khanoki and D. Pasini, "Fatigue design of a mechanically biocompatible lattice for a proof-of-concept femoral stem," *Journal of the Mechanical Behavior of Biomedical Materials*, vol. 22, pp. 65–83, Jun. 2013, doi: 10.1016/j.jmbbm.2013.03.002.

[136] Y. Hirata, Y. Inaba, N. Kobayashi, H. Ike, H. Fujimaki, and T. Saito, "Comparison of Mechanical Stress and Change in Bone Mineral Density Between Two Types of Femoral Implant Using Finite Element Analysis," *The Journal of Arthroplasty*, vol. 28, no. 10, pp. 1731–1735, Dec. 2013, doi: 10.1016/j.arth.2013.04.034.

[137] B. F. Morrey, "Cementless Femoral Fixation in Total Hip Arthroplasty," *Yearbook of Orthopedics*, vol. 2011, pp. 148–149, Jan. 2011, doi: 10.1016/j.yort.2011.04.121.

[138] J. J. Alm, T. J. Mäkinen, P. Lankinen, N. Moritz, T. Vahlberg, and H. T. Aro, "Female patients with low systemic BMD are prone to bone loss in Gruen zone 7 after

cementless total hip arthroplasty: A 2-year DXA follow-up of 39 patients," *Acta Orthopaedica*, vol. 80, no. 5, pp. 531–537, Oct. 2009, doi: 10.3109/17453670903316801.

[139] R. P. Pitto, A. Hayward, C. Walker, and V. B. Shim, "Femoral bone density changes after total hip arthroplasty with uncemented taper-design stem: a five year follow-up study," *International Orthopaedics (SICOT)*, vol. 34, no. 6, pp. 783–787, Aug. 2010, doi: 10.1007/s00264-009-0884-0.

[140] N. Harrison, P. E. McHugh, W. Curtin, and P. Mc Donnell, "Micromotion and friction evaluation of a novel surface architecture for improved primary fixation of cementless orthopaedic implants," *Journal of the Mechanical Behavior of Biomedical Materials*, vol. 21, pp. 37–46, May 2013, doi: 10.1016/j.jmbbm.2013.01.017.

[141] S. M. Ahmadi *et al.*, "Fatigue performance of additively manufactured meta-biomaterials: The effects of topology and material type," *Acta Biomaterialia*, vol. 65, pp. 292–304, Jan. 2018, doi: 10.1016/j.actbio.2017.11.014.

[142] D. M. J. M. Gerhardt, T. G. T. Mors, G. Hannink, and J. L. C. Van Susante, "Resurfacing hip arthroplasty better preserves a normal gait pattern at increasing walking speeds compared to total hip arthroplasty," *Acta Orthopaedica*, vol. 90, no. 3, pp. 231–236, May 2019, doi: 10.1080/17453674.2019.1594096.

[143] M. Morri, E. Natali, and D. Tosarelli, "At discharge gait speed and independence of patients provides a challenges for rehabilitation after total joint arthroplasty: an observational study," *Arch Physiother*, vol. 6, no. 1, p. 6, Dec. 2016, doi: 10.1186/s40945-016-0020-6.

APPENDIX A: LIST OF PUBLICATIONS

- N. F. Al Zoubi, F. Tarlochan, H. Mehboob, and F. Jarrar, "Design of Titanium Alloy Femoral Stem Cellular Structure for Stress Shielding and Stem Stability: Computational Analysis," *Applied Sciences*, vol. 12, no. 3, Art. no. 3, Jan. 2022, doi: 10.3390/app12031548.

- Al Zoubi, N.F.; Tarlochan, F.; Mehboob, H. Mechanical and Fatigue Behavior of Cellular Structure Ti-6Al-4V Alloy Femoral Stems: A Finite Element Analysis. *Appl. Sci.* **2022**, *12*, 4197. https://doi.org/10.3390/app12094197